Experimental Investigation of Graphite/Polyimide

Sandwich Panels in Edgewise Compression

by

Charles Joseph Camarda, LaRC

B.S. June 1974

Polytechnic Institute of Brooklyn

A thesis submitted to

The Faculty of

The School of Engineering and Applied Science

The George Washington University in partial satisfaction

of the requirements for the degree of Master of Science

ABSTRACT

This study experimentally and analytically investigates the local and general buckling behavior of graphite/polyimide sandwich panels simply supported along all four edges and loaded in uniaxial edgewise compression. Material properties of sandwich panel constituents (adhesive and facings) were determined from flatwise tension and sandwich beam flexure tests. An adhesive bond study resulted in the selection of a suitable cure cycle for FM-34 polyimide film adhesive and, a bonding technique using a liquid cell-edge version of that adhesive resulted in considerable mass savings. Tensile and compressive material properties of the facings (quasi-isotropic, symmetric, laminates ($[0,+45,90,-45]_s$) of Celion/PMR-15) were determined at 116, R.T., and 589K (-250, R.T., and 600°F) using the sandwich beam flexure test method. Results indicate that Gr/PI is a usable structural material for short term use at temperatures as high as 589K (600°F). Buckling specimens were 30.5 x 33.0 cm (12 x 13 in.), had quasi isotropic symmetric facings ($[0,\pm45,90]_s$) and a glass/polyimide honeycomb core (HRH-327-3/8-4). Core thicknesses varied (0.635, 1.27, 1.91, and 2.54 cm (0.25, 0.50, 0.75, and 1.0 in.)) and three panels of each thickness were tested in edgewise compression at room temperature to investigate failure modes and corresponding buckling formulas. Specimens 0.635 cm (0.25 in.) thick failed by overall buckling at loads close to the analytically predicted buckling load; all other panels failed by face wrinkling. Results of the wrinkling tests indicate that several buckling formulas were unconservative and therefore not suitable for design purposes; recommended wrinkling equations are presented.

In conclusion, the buckling behavior of Gr/PI sandwich panels, predicted analytically, has been characterized experimentally and results compare favorably.

Acknowledgements

TABLE OF CONTENTS

List of Tables

List of Figures

NOMENCLATURE

A,B,C	Constants defined by equations (C.4)
[A],[B],[D]	Stiffness matrices defined by equations (B.12)
b	Width of plate
C_0, C_1, C_2, C_3	Coefficients of polynomials used in the regression analysis
D_x, D_y	Flexural stiffnesses of orthotropic sandwich plate in x- and y-directions respectively
D_{xy}	Twisting stiffness of sandwich plate
$\bar{D}_x, \bar{D}_y$	Flexural stiffness parameters defined by equations (C.7)
$D_{F_{11}}, D_{F_{22}}$ $D_{F_{12}}, D_{F_{66}}$	Flexural stiffnesses of composite facings as defined by equations (B.12)
D_{Q_x}, D_{Q_y}	Transverse shear stiffness of plate in x- and y-directions respectively
E	Elastic modulus
E_{c_z}	Modulus of core in the z-direction
E_f	Facing modulus
E_{f_x}, E_{f_y}	Facing moduli in x- and y-directions respectively
E_T	Tangent modulus
E_x, E_y	Average elastic moduli of laminate in x- and y-directions respectively
F_c	Lower of flatwise core compressive or tensile strengths, or core-to-facing bond strength
G	Shear modulus
$G_{c_{xz}}$	Core shear modulus in the xz-plane

$G_{f_{xy}}$	Facing shear modulus in the xy-plane
H	Half thickness of facing laminate
h	Depth of sandwich measured between centroids of the facings
j	Total number of points in regression analysis
ℓ	Length of plate
m,n	Number of buckles (half waves) in x- and y-directions respectively
M_x, M_y	Bending moments on plate cross sections perpendicular to x- and y- axes respectively
M_{xy}	Twisting moments on cross sections perpendicular to x- and y- axes
N_x, N_y	Resultant normal forces in the x- and y-directions respectively
N_{xy}	Resultant shearing force in the xy-plane
P	Load
p	Pitch of Moiré grid
Q_x, Q_y	Resultant shearing forces in yz- and xz- planes respectively
q	Lateral loading on plate
$[Q], [\bar{Q}]$	Lamina stiffness matrices defined by eqns. B.2 and B.6 respectively
r	Radius of curvature of plate
S	Standard error of estimate
$s_{\sigma/\epsilon}$	Honeycomb cell size
T	Temperature
T_g	Glass transition temperature
[T]	Transformation matrix defined by equations B.5

t_c	Core thickness
t_f	Average facing thickness
t_{f_1}, t_{f_2}	Thickness of individual facings
u, v, w	Displacements of a point in the middle of a plate in the x-, y-, and z-directions respectively
V_f	Fiber volume fraction
V_v	Void volume fraction
α	Angle of incidence of light source
ε	Strain
ε^o	Midplane strain
σ	Stress
σ_{crimp}	Critical stress associated with shear crimping
σ_{dim}	Critical stress associated with dimpling
σ_{wr}	Critical stress associated with wrinkling
δ	Initial panel waviness
μ	Poisson's ratio
μ_x, μ_y	Poisson's ratios of orthotropic plate associated with bending of plate in x- and y-directions respectively.
μ_{xy}, μ_{yx}	Poisson's ratios of orthotropic plate associated with extension of plate in x- and y- directions respectively
$\bar{\mu}_{xy}, \bar{\mu}_{yx}$	Average Poisson's ratios of composite facings associated with extension of plate in x- and y-directions respectively.
λ	Wavelength
K_x, K_y, K_{xy}	Plate curvatures

Subscripts

ave	Average
i, k	Indices of summation
n	Total number of layers in laminate

1,2   Directions parallel and perpendicular to fiber

       direction respectively

cr   Critical

max   Maximum

ult   Ultimate

CHAPTER I

INTRODUCTION

1.1 General

Structural sandwich construction is defined as a construction consisting of a combination of alternating dissimilar simple or composite materials, assembled and intimately fixed in relation to each other so as to use the properties of each to specific structural advantages for the whole assembly (ref. 1). Some of the many advantages of sandwich construction include: high strength-to-weight ratio, smooth surfaces, good stability, high load carrying capacity, increased fatigue life and high sonic fatigue endurance, and good insulative properties. For these reasons the use of sandwich construction has steadily increased.

Sandwich construction is by no means a novel concept. Although accounts of its origin differ among authors, one of the first records of the use of sandwich structure is that by Fairbairn in 1849 (ref. 2) in the construction of the Britannia Tubular Bridge. The incentive for sandwich development in the aircraft industry came in the early 1900's with the desire to build a true monocoque airplane (ref. 3). In 1919 sandwich structures were used as skin for the pontoons of the Sundstedt airplane, built in the United States, in 1924 a German patent was granted to Th. Von Karman and P. Stock, and in France in 1938, S. E. Mautner designed and built sandwich wings for a small privately owned aircraft (ref. 4). The early 1940's saw the coming of age of sandwich construction with the British World War II de Havilland Mosquito Bomber whose fuselage had a balsa wood core in conjunction with plywood facings. Various cores have been used (ref. 5) but the most successful to date has been the hexagonal-cell honeycomb core which has been used in structural panels for the

1

B-58, B-70, and F-111 series aircraft, as well as in many production helicopter rotor blades and also in the Apollo spacecraft. Aluminum honeycomb sandwich is presently used in the construction of the British Concorde (ref. 6).

The development of new materials such as composites (laminas of high-strength fibers embedded in a resin matrix, oriented at various angles with respect to one another and consolidated to achieve desired directional material properties), and new adhesives and fabrication techniques as well as innovative design concepts (ref. 7) affords limitless applications for sandwich construction and insures increased future usage. Many flight service programs in military and commerical aircraft were begun in the early 1960's to qualify the use of composites in the aerospace industry. One of the first components to achieve flight status was the horizontal stabilizer of the F-111 aircraft (refs. 8 and 9). The first production advanced composite sandwich structure was the F-14 horizontal stabilizer (ref. 10) which consisted of boron/epoxy facings adhesively bonded to a full-depth honeycomb core. Other commerical and military uses of sandwich structures are cited in references 11 and 12. In each instance composite designs resulted in mass savings of approximately 25 percent over metallic designs. Hence, the use of advanced composites in structural sandwich designs will continue to increase as the need for lighter and higher strength structures increases.

With the advent of advanced composite materials (ones which utilize high strength graphite or boron fibers), polyimide resins and adhesives, and thin-gage prepreg development; lightweight composite sandwich panels can be developed for use on space transportation systems such as Space Shuttle (refs. 13 to 15) at temperatures up to 589K (600°F). Considerable reductions in shuttle mass can be realized by the direct replacement of the aluminum

2

sub-structure with graphite/polyimide (Gr/PI) panels; an even greater savings in insulation mass (Reusable Surface Insulation (RSI) in the case of shuttle) is possible because of the higher use temperature of graphite/polyimide material over the aluminum it is replacing. An additional advantage in using graphite fibers in the facings is that the low coefficient of thermal expansion of such panels more closely matches that of RSI and hence could possibly eliminate the need for a strain isolation system (such as the strain isolator pad in the case of shuttle (ref. 16)) between the insulation and the sub-structure. Thus for reusable space transportation systems the use of advanced composites is desireable to save structural mass. Because of predictions of potential mass savings as high as 25 percent (ref. 17), a program was initiated at NASA Langley Research Center entitled Composites for Advanced Space Transportation Systems (CASTS), the purpose of which is to design a composite body flap for the Shuttle Orbiter.

1.2 Objectives and Scope

The purpose of the present study is to experimental., investigate the buckling behavior of Gr/PI sandwich panels which were designed as the skin of the shuttle bodyflap. The sandwich designs must be capable of withstanding temperatures ranging from 116 to 589K (-250 to 600°F). Because of the limited data of bonded Gr/PI honeycomb structures at these temperature extremes, honeycomb sandwich specimens were fabricated and tested to determine adhesive and facing material properties. Gr/PI sandwich panels were then designed, fabricated, and tested at room temperature in uniaxial compression to study buckling of such panels.

Preliminary studies of loads on the body flap of Shuttle indicated that a biaxial state-of-stress exists (ref. 18). Based on the low magnitude and

3

biaxial nature of stresses, minimum gage $[0,\pm45,90]_s$ laminates were chosen for the facings of the sandwich skin of the body flap. The materials chosen for fabrication of the sandwich panels of the present study represents the best choice at the time of selection according to the following peremeters: (1) strength retention at elevated temperature, (2) low density, (3) commercial availability, and (4) ease of fabrication. Celion 3000/PMR-15 Gr/PI was selected as the facing material, FM-34 as the polyimide film adhesive, and Hexel HRH-327-3/8-4 as the glass/polyimide honeycomb core.

Flatwise tensile specimens were tested at 116, R.T., and 589K (-250, R.T., and 600°F) to determine a cure cycle for FM-34 which would produce a high-strength adhesive bond and to investigate the possibility of using a liquid cell-edge version of that adhesive, BR-34, which has a potential for saving considerable mass as noted in reference 13. Sandwich beam flexure specimens were fabricated and tested in four-point bending to determine tensile and compressive material properties of the facings, $[0,+45,90,-45]_s$ laminat $\cdot$ of Celion/PMR-15, at 116, R.T., and 589K (-250, R.T., and 600°F). Honeycomb core material properties were obtained from reference 19.

Buckling specimens 30.5 x 33.0 cm (12 x 13 in.) were designed and fabricated in various core thicknesses to study local and general instability failure modes and to evaluate methods for predicting critical failure loads. Anal tical formulas (refs. 19 to 25) were used to determine upper and lower bounds on critical stresses related to local and general buckling such as: intracellular buckling (dimpling), wrinkling, shear crimping, and overall buckling. To prevent premature end failures of the specimens, techniques such as outting the honeycomb near the ends and tapered end tabs (refs. 25 and 26)

and scalloped doublers (refs. 27 and 28) have been used by other investigators. The specimens in the present study use potted ends and tapered end tabs to prevent local core crushing and end brooming of the composite facings and have scalloped doublers to enhance load diffusion into the panel to prevent stress concentrations near the loaded edges and hence premature failure there. A test rig, similar to that of references 25 and 29, was designed and used to insure a uniform strain distribution across the specimen width. The Moiré fringe method was used to evaluate the buckled mode shapes of the panels and to determine the onset of buckling. The buckling specimens were tested in uniaxial edgewise compression at room temperature and were simply supported about all four edges.

1.3 Brief Review of Pertinent Literature

A good historical review of methods of analysis of sandwich structures can be found in references 22, 24, and 25. Most analysis methods assume an antiplane core, one which possesses no stiffness in the plane of the plate but has a finite shear stiffness in planes normal to the facings. The main difference in the analysis of sandwich plates from regular flat plates is that shear deformation caused by the flexible core material in sandwich panels cannot be neglected. Also, the existence of a flexible core material allows additional instability modes of failure such as wrinkling, dimpling and shear crimping.

Currently there are two methods of analysis of sandwich panels: The general method which includes equations of equilibrium of the separate facings and core and the necessary continuity conditions and can hence determine both

general and possibly local instability modes of failure and the selective method which looks at wrinkling and bending of sandwich panels separately.

Several authors have investigated the general method: Reissner (ref. 30) looked at isotropic panels with very thin faces, Heath (ref. 31) extended an earlier work by Hemp (ref. 32) to include a sandwich with an orthotropic core and Pearce (ref. 25) extended the research of Heath to include anisotropic facings and orthotropic core. Exact (analytical) solutions based on the general method, however, are intractable when applied to sandwich panels; Pearce was only able to obtain an exact solution for wrinkling and overall buckling of panels with effectively orthotropic facings (facings which do not exhibit coupling between normal and shear strains or bending and twisting strains). The general method has, however, been successfully applied to the analysis of sandwich struts and beams as noted in references 33 and 34.

Most analytical work on sandwich panels refers to the selective method. There are three versions of this method with the major differences between each arising from the choice of variables used to express the displacement of the panel. A good account of each stream of thought is given in reference 22. The analysis used in the present study follows from the work of Libove and Batdorf and Stein and Mayers (refs. 35 and 36) and assumes that the materials are elastic, the panel thickness is small compared to its radius of curvature; the facings act as membranes, and the core is antiplane with an infinite transverse normal stiffness. Solutions for simply-supported panels with orthotropic facings and core are obtained using assumed displacement solutions of reference 23. The expressions for overall buckling obtained as such provide a simple solution for effectively orthotropic facings and core.

6

CHAPTER II

DETERMINATION OF MATERIAL PROPERTIES

2.1. Objectives and Scope

Material properties of some constituents (adhesive and facings) of the Gr/PI sandwich panels were experimentally determined by a series of flatwise tensile tests and sandwich beam flexure tests. Properties, such as flatwise adhesive bond strength, facing modulus and Poisson's ratio, μ, and facing strength, were determined at various temperatures (116, R.T., and 589K (-250, R.T. and 600°F)) and used to analytically predict failure modes and loads of the buckling specimens. Research in adhesive bonding was necessary to improve the in-house bonding capability at NASA Langley Research Center using FM-34[1] polyimide film adhesive, Gr/PI facesheets, and glass/polyimide honeycomb core and to verify the capability of fabricating such sandwich panels. In addition, the bond study could determine if potential mass savings are possible by using the liquid version of the FM-34 film adhesive, BR-34, as a cell edge adhesive. FM-34 was chosen because of its good strength retention at 589K (600°F) and its commercial availability.

It was decided that flatwise tensile tests would provide a good measure of adhesive bond strength in a core-to-facing bond situation. Hence, a series of flatwise tensile tests were conducted to determine a suitable bonding procedure and cure cycle for the FM-34 adhesive.

_____

[1]FM-34 film adhesive and BR-34 liquid adhesive: Manufactured by American Cyanamid Company, Bloomingdale Division.

To obtain tensile and compressive material properties of the facing material ($[0,+45,90,-45]_s$ laminates of Celion 6000/PMR-15 Gr/PI composite) at various temperatures, 24 sandwich beam flexure specimens were fabricated and tested in four-point bending. Eight beams were tested, four in tension and four in compression, at each of three temperatures 116, R.T., and 589K (-250°F, R.T., and 600°F). Results of replicate tests were statistically analyzed and stress-and tangent modulus-vs.-strain data are presented.

2.2 Flatwise Tensile Tests

Over thirty 7.62 x 7.62cm (3 x 3 in.) specimens, shown in figure 1, were fabricated using precured $[0,\pm45,90]_s$ laminates of HTS-1/PMR-15 Gr/PI facings, glass/polyimide honeycomb core ([1]HRH-327-3/16-6 or 8) and the desired adhesive. Details of fabrication procedures and cure cycles are given in Appendix A. Steel load blocks were bonded 'o the facings of the specimens and each block has a tapped hole for attaching a loading rod. Universal joints were attached between the testing machine and the loading rods to assure proper alignment of the fixture in the loading machine. The specimens were tested in a universal testing machine operating in a displacement control mode at a constant rate of 0.13 cm/min (0.05 in./min.). Test temperatures other than room temperature were obtained using an environmental chamber positioned within the crossheads and posts of the testing machine. Specimens were held at desired test temperatures for 15 minutes prior to testing to insure thermal equilibrium. Preliminary tests indicated that significant improvements of in-house (NASA Langley) bond strengths could be obtained by abrasively cleaning the edges of the honeycomb and by dipping the core in primer instead of brush or roller coating it on the core (see Appendix A).

---

[1]HRH-327-3/18 - 6 or 8 glass/polyimide honeycomb core: Manufactured by Hexel Corporation.

A series of flatwise tensile tests of specimens, bonded with FM-34 using various cure cycles, aided in the selection of a suitable cure cycle. Two specimens were tested at room temperature for each cure cycle variation listed in Table 1. Specimen failures occurred by either facing delamination or by adhesive bondline rupture. Results of those tests, listed in Table 2, indicate that cure cycles numbered 1 and 5 produced the strongest bonds, having strengths equivalent to or greater than the interlaminar shear strength of the facings. Facing delamination also occurred with cure cycle number 4 but because the bond cure temperature of 616K (650°F) was greater than the facing cure temperature of 603K (625°F) the interlaminar shear strength of the facing was degraded and failure loads were lower. Bonding one face of the specimen at a time with the face to be bonded below the core (cure cycle number 3) provided good nodal filleting but did not enhance the strength of the bond. Instead, bond strengths were lower and failures occurred in the second of the two bonds. Six specimens were tested at 589K (600°F); two specimens were fabricated at each of three cure cycles numbered 1, 5, and cure cycle 1 with a higher cure temperature (603K (625°F)). It was hoped the higher cure temperature would improve the elevated temperature bond strength. Test results of all the flatwise tensile specimens, even those which failed prematurely, are presented to illustrate the success rate of each fabrication method.

Cure cycle number 1 with the elevated cure temperature was chosen because of the higher bond strengths at elevated temperature and because maintaining a vacuum during cure would help eliminate volatiles produced during the cure of the FM-34 adhesive. Although trapped volatiles did not degrade the strengths of the 7.62 x 7.62 cm (3x3 in.) specimens, it would be more difficult to vent the volatiles in large panels. Figures 2 and 3 show the two modes of failure of the flatwise tensile tests.

9

Sixteen flatwise tension specimens were fabricated using cure cycle number 1 with a cure temperature of 603K (625°F). Test results of these specimens are presented in Table 3a. In-house flatwise tensile strengths at room temperature and 116K (-250°F) increased from 1.6 MPa (230 psi) to an average value of 3.2 MPa (470 psi). Failures at this stress level were usually by facing delamination as shown in figure 3. Flatwise tensile strengths at 589K (600°F) were higher than 1.4 MPa (200 psi) with failures occurring in the bondline, similar to the room temperature test shown in figure 2.

Flatwise tensile test results at room temperature of specimens bonded using BR-34 as a cell-edge adhesive are presented in Table 3b. Most of these specimens failed by facing delmination. However, for these specimens the facings delaminated locally about each cell edge as shown in figure 4 and usually resulted in slightly lower strengths. When local facing delamination did not occur, strengths were similar to results of the FM-34 film adhesive. Flatwise tensile strengths using BR-34 were much higher than results presented in reference 13. The mass of the BR-34 adhesive was 0.244 kg/m^2 (0.05 lbm/ft^3) which is a 59 percent reduction in mass compared to FM-34 film adhesive having a mass of 0.586 kg/m^2 (0.12 lbm/ft^2). Thus, the use of Br-34 would result in a mass savings equivalent to 10 percent of the total sandwicn panel mass for a panel consisting of 8 ply Gr/PI facings and a 1.27 cm (0.50 in.) thick core having a density of 64 kg/m^3 (4 lbm/ft^3).

Results of the bond study indicate that a liquid cell-edge adhesive can result in considerable mass savings without necessarily sacrificing bond strength and that further research in this area is warranted. However, since flatwise tensile strengths with BR-34 were not consistent, FM-34 film adhesive was used to fabricate the sandwich beam and buckling specimens.

2.3 Sandwich Beam Flexure Tests

Sandwich beam flexure specimens consisted of Gr/PI facings and glass/polyimide honeycomb core as shown in figure 5. The honeycomb core was HRH 327-3/16-8 glass/polyimide and was cut into strips 2.54 cm (1.00 in.) wide by 55.88cm (22.00 in.) long by 3.175 cm (1.25 in.) high using a diamond tipped saw. The test facing was a $[0,+45,90,-45]_s$ laminate of Celion 6000/PMR-15 which was cured (see appendix A) and cut into 2.54 cm (1.00 in.) by 55.88 cm (22 in.) strips from flat sheets 50.8 cm (20.0 in.) by 58.4 cm (23.0 in.). The opposite facing of the beams were also Gr/PI instead of stainless steel or titanium to prevent bowing of the beams after bonding due to coefficient of thermal expansion mismatch of opposite facings. Additional 0- degree layers were included in the non-test facings ($[0_2,+45,90,-45]_s$, celion 6000/PMR-15) to insure failure would occur in the test facing. The honeycomb core was filled with BR-34 liquid adhesive and glass beads throughout the entire length of the beams except for the 7.62 cm (3.00 in.) test section in the center of the beams. The purpose of the BR-34 adhesive was to increase the adhesive bond area (core-to-facing) and thus help prevent premature adhesive shear failure during the elevated temperature tests. The core surfaces were then ground flat and parallel and the facings were bonded to the core using FM-34 film adhesive. Details of the fabrication of the sandwich beam specimens is presented in Appendix A; a completed beam specimen is shown in figure 6. Each specimen was instrumented with a high temperature Micro-Measurements strain rosette (WK-03-06-WR-350) oriented at 0-, 45-, and 90-degrees with the load axis and bonded in the center of the test facing using a polyimide adhesive (either M-Bond 610 or PLD-700 available from Micro-Measurements and BLH electronics, respectively); a single gage (WK-03-125AD-350) oriented at 0 degrees with the load axis was bonded to the center of the opposite facing.

11

The sandwich beams were placed in a four-point bending test apparatus (fig. 7) which supported the beam on rollers with flat sections 2.54cm (1.00in.) wide machined in them at two points 48.26 cm (19.00 in.) apart. Load was applied by a 222.4 kN (50,000 lbf) capacity hydraulic testing machine which acted at two points on the top flange of the beam spaced 10.16cm (4.00 in.) apart and symmetric about the beam's center. A schematic diagram of a beam specimen loaded in four-point bending is shown in figure 8. Load was applied at a rate of 89 N/sec (20 lbf/sec). For testing at temperatures other than room temperature the specimen was instrumented wit' thermocouple attached to the test facing and the test fixture and sp. m were complutely enclosed in an environmental chamber and either heated or cooled to the desired test temperature. Specimens were allowed to soak at the test temperature for 20 minutes to insure thermal equilibrium.

A data handling system consisting of a 40-channel scanner, digital voltmeter, plotter, printer, clock, and calculator was used to record and reduce data. The load signals from the load cell were connected to one channel of the scanner. Strain signals were initially balanced by a Wheatstone bridge balance (for non room temperature tests strains were set to zero after thermal equilibrium) and during the test were input to selected scanner channels. Strains were corrected for transverse sensitivity of the gages and nonlinearity of the bridge circuit. Thermocouples were connected to the scanner through a 273K (32°F) cold-junction reference.

Beams were tested to failure, data were recorded every three seconds and a stress-strain curve was plotted in real time. Quantities were stored in volts and engineering units on magnetic tape and printed during each test. After each series of replicate tests were completed, a data reduction program used the longitudinal stresses and strains of individual tests as input to a

regression analysis to determine the coefficients of a best fit for all tests, in the series in the least squares sense, of a third-order polynomial relating stress and strain according to the polynomial equation:

$$\sigma = C_0 + C_1\epsilon + C_2\epsilon^2 + C_3\epsilon^3 \tag{1}$$

The third order curve in most cases produced a good fit of data. Two methods were used to calculate the tangent modulus:

Method 1: The polynomial was differentiated.

Method 2: A delta-strain ($\Delta\epsilon$) region was chosen over which average results of the tests were fitted by means of least-squares using a straight line fit. The tangent modulus in each $\Delta\epsilon$ region was the slope of each particular straight line. Higher order polynomial curve fit equations were investigated but in general produced oscillatory tangent modulus-vs-strain curves upon differentiation.

The coefficients of the regression equation are found by solution of the following matrix equations:

$$
\begin{bmatrix}
\sum_i \sigma_i \\[6pt]
\sum_i \epsilon_i \sigma_i \\[6pt]
\sum_i \epsilon_i^2 \sigma_i \\[6pt]
\sum_i \epsilon_i^3 \sigma_i
\end{bmatrix}
=
\begin{bmatrix}
j & \sum_i \epsilon_i & \sum_i \epsilon_i^2 & \sum_i \epsilon_i^3 \\[6pt]
\sum_i \epsilon_i & \sum_i \epsilon_i^2 & \sum_i \epsilon_i^3 & \sum_i \epsilon_i^4 \\[6pt]
\sum_i \epsilon_i^2 & \sum_i \epsilon_i^3 & \sum_i \epsilon_i^4 & \sum_i \epsilon_i^5 \\[6pt]
\sum_i \epsilon_i^3 & \sum_i \epsilon_i^4 & \sum_i \epsilon_i^5 & \sum_i \epsilon_i^6
\end{bmatrix}
\begin{bmatrix}
C_0 \\[6pt]
C_1 \\[6pt]
C_2 \\[6pt]
C_3
\end{bmatrix}
\tag{2}
$$

where the symbol $\sum_i$ implies summation from 1 to j where j is the total number of points recorded during a series of replicate tests for a given test configuration.

13

To assess the magnitude of scatter of experimental points about the regression equation, the standard error of estimate, $S_{\sigma/\epsilon}$, which is a measure of the mean deviation of the sample points from the regression line is determined as follows:

$$S_{\sigma/\epsilon} = \left(\frac{\sum_i \sigma_i^2 - C_0 \sum_i \sigma_i - C_1 \sum_i \epsilon_i \sigma_i - C_2 \sum_i \epsilon_i^2 \sigma_i - C_3 \sum_i \epsilon_i^3 \sigma_i}{j-4} \right)^{1/2} \quad (3)$$

This method of statistical analysis is similar to that presented in reference 37 for the analysis of compressive coupon data.

Results of the sandwich beam flexure tests are presented in Tables 4 and 5 and in figures 9 to 14. As shown in Table 4, the scatter of test data, as determined by the standard error of estimate, was lowest for the room temperature and 116K (-250°F) tensile tests. Maximum scatter occurred for the elevated and room temperature compression tests in which the standard error of estimates, $S_{\sigma/\epsilon}$, were 10.67 MPa (1547 psi) and 11.10 MPa (1610 psi) as compared to respective average ultimate strengths of 567.7 MPa (82.34 ksi) and 334 MPa (48.44 ksi). Average ultimate strengths of the laminate were slightly higher in compression than tension for each test temperature. Ultimate strengths of the Celion 6000/PMR-15 [0,+45,90,-45]$_s$ laminates were higher than results for HTS/PMR-15 as reported in references 37 and 38 except for tensile strength at 589K (600°F (ref. 38)). Average room temperature tensile and compressive ultimate strengths for the HTS/PMR-15 laminates were 450.6 and 532.4 MPa (65.36 and 77.23 ksi) respectively as compared to 565.2 and 567.7 MPa (81.98 and 82.34 ksi) for Celion 6000/PMR-15. Average tensile ultimate

strengths at 116K (-250°F) increased by 8.5 percent over room temperature values and strengths at 589K (600°F) decreased by 43 percent. Average compressive ultimate strengths at 116K (-250°F) and 589K (600°F) increased and decreased respectively by 13.8 and 41.2 percent over room temperature values.

Modulus values of the Celion/PMR-15 laminates were higher for all test temperatures than values reported in references 37 and 38 for HTS/PMR-15 laminates. This is probably due to the higher fiber volume fraction of the Celion/PI laminates, 72 percent, compared to 43-55 percent for the HTS/PMR-15 laminates of references 37 and 38. Modulus values at 0.2 percent strain and 116K (-250°F) were about ten percent higher than values at room temperature; modulus values at 589K (600°F) were about the same as room temperature values. Stress-and tangent-modulus as a function of strain for various temperatures are presented in figures 9 to 14. Table 4 lists the coefficients of the regression equation used in the reduction of the experimental data. The data in the figures represent experimental points of all replicate tests; the solid line in the figures is the best fit third-order polynomial obtained from the regression analysis. The solid tangent-modulus curves were plotted using method 1 and the x- symbols were obtained by method 2. Tensile modulus values were fairly linear throughout the usable strain region (ϵ < .35 percent) as shown by figures 9, 11, and 13. Compressive modulus values tended to be nonlinear at room temperature and became linear at 589K (600°F) as shown by figures 10 and 14. The two methods used to predict tangent modulus as a function of strain agreed well.

Representative tensile and compressive failures are shown in figures 15 and 16 respectively. Most tensile failures occured in the center of the beam while most compressive failures occured near the edge of the potted section of the honeycomb next to the load tabs.

15

CHAPTER III

BUCKLING OF SANDWICH PANELS

3.1 Objectives and Scope

Flat, rectangular, honeycomb sandwich panels were simply-supported about all four edges and tested in uniaxial edgewise compression to experimentally study local and general instability modes of failure. Facings of all sandwich panels were similar and core thicknesses, t_c, were varied to determine the failure envelope of such panels resulting from local and general failure modes. Specimen length, width, and core thicknesses were chosen to allow the investigation of wrinkling and overall buckling modes of instability. Specimens were 30.5 x 33.0 cm (12 x 13 in.) with core thicknesses of 0.635, 1.27, 1.91, and 2.54 cm (0.25, 0.50, 0.75, and 1.00 in.). A test fixture was designed which simply-supported the panel along all four edges and allowed alignment of the panel during loading to insure uniform strain across the width of the panel during testing. The simply-supported boundary condition was chosen for experimental testing because it more closely represents conditions actual shuttle bodyflap panels will experience. At least three panels of each core thickness were tested at room temperature and results were compared with analytical predictions of failure mode and load. Panels were instrumented with strain gages on each facing to monitor strain uniformity across the width of the panel and to determine the onset of overall buckling and, if possible, facing wrinkling. The "Moiré fringe method was also used to help predict the onset of buckling and wrinkling and to determine the buckled mode shape of the panels. Knowledge of the mode shape could help assess how well the test fixture simulated the desired simply-supported boundary conditions. Quality-control standards for fabrication of the panels were very

16

high to minimize scatter in experimental data. A complete description of procedures used to fabricate the buckling specimens, including quality control and inspection procedures, is presented in Appendix A.

3.2 Specimen Design

A computer program was written to determine the elements of the $[A]$, $[B]$, and $[D]$ matrices for the quasi-isotropic, symmetric Gr/PI facings and sandwich based on laminate theory presented in Appendix B. The program used overall buckling equations of Appendix C, minimizing with respect to m and n, to predict overall panel buckling load (assuming both infinite and finite core shear stiffness); the local instability equations of Appendix D were used to predict local instability modes and associated loads. Results were computed for various ply thicknesses, core thicknesses, and operating temperatures.

Laminate material properties and property variation with respect to temperature, used in the design of the buckling specimens, were obtained from references 39 and 40. Honeycomb core material properties were obtained from reference 19. Various cores and core thicknesses (0.635 to 2.54 cm (0.25 to 1.00 in.)) and panel lengths and widths (10.2 to 122 cm (4.0 to 48.0 in.)) were analytically investigated at various temperatures (room temperature to 589K (600°F)) and design envelopes, typified by figure 17, were determined. Preliminary studies of structural loads on the shuttle bodyflap (ref. 18) indicate that a biaxial state-of-stress is present. Based on the low magnitude and biaxial nature of stresses, minimum gage, symmetric laminates of $[0,\pm45, 90]_s$ Gr/PI were chosen for the facings of the sandwich skin of the bodyflap. Since the laminate orientation of the facings is quasi-isotropic, the average elastic modulus, E_x or E_y as calculated in Appendix B, was used for the facing modulus, E_f, in equations in Appendix D. Results of critical stress as a function of core thickness and an assumed ply thickness of 0.0076

17

cm (0.003 in.) are shown in figure 17. Only balanced-symmetric laminates were considered in the present investigation to prevent laminate warpage during the cure cycle caused by bending-stretching coupling terms (nonzero ⌐B] matrix of the material). Non-symmetric laminates such as [0,±45, 90] could be fabricated and forced flat and bonded symmetrically with respect to the centerline of the core. This would reduce the mass of the panel and could possibly be sufficient to accomodate the low loads predicted for the bodyflap. Analysis techniques would have to be generalized to include anisotropic facings as was done in reference 25. Because of fabrication uncertainties, however, non-symmetric laminates were not considered for experimental study. Thin-gage Celion 3000 material would present a substantial mass savings over the Celion 6000 material and, hence, was used to fabricate the buckling specimens. Average thickness-per-ply of the Celion 3000 laminates was 0.007 cm (0.0028 in.) as compared to 0.0166 cm (0.0065 in.) for Celion 6000. The lowest density commercially available core which could function structurally at 589K (600°F) is either Hexel HRH-327-3/16-4 or HRH -327-3/8-4 Glass/PI which has a mass of 64 kg/m^3 (4 lbm/ft^3) and either a 0.48 cm (3/16 in.) or a 0.95 cm (3/8 in.) cell size respectively. Critical dimpling stresses of the honeycomb core with the larger cell size were lower and, hence, design envelope curves indicate that overall buckling, dimpling, laminate strength, or wrinking could be critical failure modes depending on scatter in material properties and different analysis techniques. Since it is desirable to verify as many analytical predictions for various failure modes as possible, the honeycomb core with the 0.95 cm (3/8 in.) cell size was chosen. A panel size of 30.5 x 30.5 cm (12 x 12 in.) was adequate to investigate several failure modes.

End failures in composite compression specimens are common because of the very stiff and highly directional nature of composite material which can lead

18

to large local stress concentrations. In addition, a phenomenon known as end brooming can occur because of uneven fiber lengths at the loaded end which causes a local fanning-out of the edges. The honeycomb core near the loaded ends of the specimens was potted with BR-34 liquid polyimide adhesive and tapered end tabs of $[\pm45]_s$ glass/PI were bonded at each end to prevent local end failures such as core crushing or end brooming; scalloped doublers were bonded beneath the end tabs to enhance load diffusion into the panel and help reduce stress concentrations. A stainless-steel sheet was embedded in the BR-34 potting at each end to align the specimens in the knife edges. Laminates were bonded to the core and end tabs and doublers were secondary bonded using FM-34 film adhesive. Figure 18 shows a completed buckling specimen; details of specimen manufacture are given in Appendix A; details of significant panel parameters are listed in Table 6.

3.3 Test Apparatus and Procedures

3.3.1 Apparatus

It was decided that simply-supported edges would be a more realistic boundary condition for the test panels since it represents conditions actual panels on the shuttle bodyflap will probably experience. Simulating simply-supported edge conditions in the laboratory, however, is a difficult task as noted in references 25 and 29. A test fixture, similar to that of reference 25, was fabricated to simply-support all four edges of the sandwich panel and allow alignment of a loaded panel to insure uniform strain across the panel during testing. The stainless-steel strips, which were embedded in each of the potted ends of the panel, fit into stainles steel supports which fit in V-groove blocks as shown in figure 19a; side supports are illustrated in figure 19b. The V-groove blocks fit into adjustable end loading heads which were attached to the hydraulic load machine. The end loading heads

contained a flat stainless-steel bar which was used to align the specimen laterally with the aid of aligning screws as shown in figure 20. The sides of the panel were simply supported by knife edges which were supported by Z-section steel beams as shown in figures 19b and 20. The side supports maintained a relatively snug fit against the panel because of the high degree of flatness of the panels as discussed in Appendix A. However, because of the raised scalloped doublers the side supports could not extend the complete length of the panel. The Z-section beams were braced so that motion of the side supports was restrained. The knife-edges of the side supports were bolted snuggly in place at two locations on two sides as shown in the schematic of figure 19b and as partially shown in figure 20. The side supports were positioned 1.27 cm (0.5 in.) from each side edge making the simply supported panel dimensions 30.5 x 30.5 cm (12 x 12 in.).

A 222KN (50 Kip) MTS hydraulic load machine was used to compress the panels. A mercury vapor light source was used in conjunction with a photographic line grid having a pitch, p, of 17.7 lines/cm (50 lines/in.) to determine out-of-plane panel displacements, w, and mode shapes using the Grid-Shadow Moiré technique as discussed in references 41 and 42 and in section 3.3.3. A Nikon F2AS camera was used to photograph the panels during loading. The camera was positioned perpendicular to the sandwich panel and the light source formed on angle of 30 degrees with that perpendicular.

3.3.2 Instrumentation and test procedure

The panel was instrumented with 12 single, foil-type strain gages and two 45-degree strain rosettes, micro-measurements WK-03-125AD-350 and WK-03-060-WR-350 respectively, as shown schematically in figure 21. The positioning of the gages allowed measurement of longitudinal strain distributions across the panel width, on each facing, and along the length of

the panel. Back-to-back longitudinal strain gages were positioned at five points on the panel (four corner points and one centrally located one). The purpose of the back-to-back gages was to detect bending of the panel and to determine the buckling load and possibly the wrinkling load. The data acquisition system used to reduce and store data is identical to that mentioned in section 2.3.

The hydraulic testing machine was operated in a displacement control mode at a rate of approximately 0.020 cm/sec (0.008 in./sec.) and strain gages were scanned approximately every three seconds. Raw data was converted to engineering units, printed in real time and storeu on disk. Gages were balanced prior to testing using Wheatstone bridge circuits as in section 2.3. Panels were loaded up to approximately 50 percent of failure load, strains across the panel width were monitored and necessary adjustments in alignment were made using the adjustable screws shown in figure 20. The panel was then unloaded and the Moiré grid positioned in front of the specimen. Strain gages were then zeroed and load was applied to the specimen.

3.3.3 The Shadow - Moiré method

The shadow Moire method is a technique for measuring the out-of-plane deformations, w, of a specimen. A reference line grid is positioned in front of a specimen and either a collimated or point light source is shown through the reference grating, producing a shadow grid on the specimen. The shadow or specimen grid will be distorted by the out-of-plane depth of the surface, and when it is viewed together with the reference grid by eye or camera, Moiré fringes are created which represent the topology of the surface.

In the present study a reference grid having a pitch, p, of 19.7 lines/cm (50 lines/in.) was positioned about 0.31b cm (0.125 in.) from the front face of the panel and parallel to it with lines running in the lengthwise direction. The front face of each panel was painted white to enable the

21

shadow grid to be visible. A mercury vapor light source was positioned at an angle of 30 degrees to the normal of the reference grid. This angle of incidence of the light source was governed by the side simple supports which caused large shadows over the specimen at higher angles of incidence. The approximate sensitivity of the technique can be calculated using the following equation

$$w = p/\tan \alpha \qquad (4)$$

where p is the pitch of the reference grid, α is the angle of incidence of the light source, and the minimum fringe order is assumed to be 1. This equation assumes the camera to be positioned perpendicular to the plane of the specimen. With the arrangement of the present apparatus the sensitivity is approximately 0.088 cm (0.035 in.). A more detailed description of the Moiré technique can be found in references 41 and 42.

CHAPTER IV

RESULTS OF BUCKLING TESTS

Two modes of panel failure were discernable from experimental results: wrinkling and overall buckling. Specimens with a core thickness, t_c, of approximately 0.635 cm (0.25 in.) failed by overall buckling and all other specimens, having nominal core thicknesses of 1.27, 1.91, and 2.54 cm (0.5, 0.75, and 1.00 in.), failed by wrinkling. None of the panels tested failed by either laminate strength, dimpling, or shear crimping. The shadow-Moiré method was useful in determining mode shapes of the overall buckling specimens but was not able to determine wrinkling mode shapes because of the high stiffness and brittle nature of the Gr/PI facings and hence, the relatively small out-of-plane displacements. A reference grid with a smaller pitch, p, could increase the sensitivity of the Moiré method and thus possibly enable smaller deflections to be discernable but this was not attempted in the present investigation.

4.1 Wrinkling Specimens

Significant panel parameters, related to the fabrication and quality of the wrinkling and overall buckling specimens, are presented in Table 6. Facing and total sandwich panel thickness measurements were made at various panel locations and initial panel waviness, δ, was measured as explained in Appendix A. Because of good fabrication and quality control procedures the panels were consistent in dimensional and material properties. Average thickness-per-ply of all wrinkling specimens was 0.0071 cm (0.0028 in.) with maximum variations in total laminate (8 plies) thicknesses averaging only 0.00451 cm (0.00178 in.); average variation in total sandwich panel thicknesses was only 0.0059 cm (0.0023 in.). Maximum panel waviness, δ_{max}, averaged only 0.0097 cm (0.0038 in.).

23

Results of longitudinal strain uniformity across specimen width are presented in figures 22a and b for two values of applied load. The adjustable test fixture was useful in eliminating large strain variations caused by lateral misalignment, similar to test fixtures used in references 25 and 29. Strains were fairly uniform across the width of the panel as shown in figure 22. However, slightly higher strains and strain variations do occur at the edges of the panels as was also noted in reference 25. Trends in strain distributions at the low load level, 44,480N (10,000 lbf), were similar to trends at the higher load level of 88,960N (20,000 lbf). There were no consistent trends in strain distributions from panel to panel, however, most of the wrinkling specimens did fail near the end of the side simple supports where slightly higher strains were recorded.

Longitudinal back-to-back strains as a function of stress were calculated for each position on the panel as shown in figure 21. Results of several tests (panel numbers 75010 and 75012) are presented in figures 23a and b. Back-to-back strain variation was usually lowest in the center of the panels (X=Y=0). Irregularities in slopes were noted in some specimens as shown in figure 23b for panel number 75012. These irregularities in slope occur at too low a load to be considered to be an indication of wrinkling or some form of local instability as mentioned in reference 25. The irregularities in the present study were possibly caused by some inteference or interaction of the test fixture. Material behavior was slightly nonlinear to failure, similar to results of the four-point flexure tests as noted in Chapter 2. Back-to-back stress -vs.- strain data could not predict the onset of local buckling

(wrinkling); an attempt to use the force stiffness method of reference 43 to predict wrinkling was unsucccessful, all panel failures were abrupt with no indication of local instability. It would probably be necessary to instrument both sides of a facing extensively prior to bonding to the core in order to calculate facing bending strains and predict local buckling using the force stiffness met' .d. Modulus values at 0.2 percent strain, maximum back-to-back strain variation at 0.6 percent strain, theoretical wrinkling stress, and experimental ultimate stress and strain values of each panel are presented in Table 7. Maximum back-to-back strain variation was fairly low considering the size and complexity of the sandwich panels. Compressive modulus values at 0.2 percent strain of the sandwich panels which used Celion 3000 material were slightly higher than results of beam tests which used the Celion 6000 material; the average modulus of all wrinkling specimens is 53.9 GPa (7.82 x 10^6 psi) as compared to 48.95 GPa (7.10 x 10^6 psi) obtained using the four-point beam flexure test method. Since the fiber volume fraction of the beam specimens was higher than the buckling specimens (72 percent compared to approximately 61 percent) it appears that the thinner gage Celion 3000 material did not experience any degradation in modulus.

Results of replicate tests indicate that scatter was low. Scatter in critical wrinkling stress ranged from a minimum of 7.6 Mpa (1.1 ksi) for the 1.27 cm (0.5 in.) specimens to a maximum of 89 Mpa (13 ksi) for the 2.54 cm (1.00 in.) specimens. This amounts to a range from minimum to maximum of 1.7- to 29- percent respectively when compared to average critical stress values. From Tables 6 and 7 some trends in results are evident:

1) average failure stresses of the wrinkling specimens decrease as core height, t_c, increases. This is characteristic of a wrinkling or local buckling type of instability. Average failure stresses were 452, 354, and 311 MPa (65.6, 51.4, and 45.1 ksi) for the 1.27, 1.91, and 2.54 cm (0.5, 0.75, and 1.0 in.) thick cores respectively.

25

2) specimens with higher total facing thicknesses had higher failure
   loads, however, these specimens did not necessarily have higher
   failure stresses. This is because the thicker facings had a lower
   fiber volume fraction, V_f, because not enough excess resin was
   removed during the consolidation phase of laminate fabrication. That

3) average failure strains were 0.87, 0.71 and 0.63 percent for the
   1.27, 1.91, and 2.54 cm (0.5, 0.75, 1.0 in.) thick core panels,
   respectively.

4) panels with the largest value of initial waviness, δ_{max}, had the
   lowest ultimate load.

5) ultimate strains of the wrinkling specimens were well below ultimate
   laminate strains as calculated from the beam tests.

As mentioned earlier, most of the wrinkling specimens failed close to the
end of one of the side simple-supports. Failure of a 1.27 cm (0.50 in.) panel
is illustrated in figures 24a and b; the failure extends across the panel
to the top of the left side simple support. The failures were perpendicular
to the direction of load. Wrinkling failure was most noticeable in the 1.27
cm (0.50 in.) specimens in which the facings separated from the core due to a
tensile failure of the adhesive. Failed panel number 7508, figure 25a,
illustrates the outward buckling of the facing; the panel was cut along the
dashed line of that figure to further illustrate the tensile failure of the
adhesive which was precipitated by wrinkling (fig. 25b). Figure 26 is a side
view of two different panels (t_c = 1.27 cm (0.50 in.)). It is not conclusive
from the side views whether the failures were symmetric or antisymmetric,
however, laminate failures on either facing were similar which suggests that
failures were symmetric. This agrees with results of references 25 and 44
which indicate that for honeycomb cores, where the modulus of the core in the

26

direction of the load is much less than the modulus of the core in the direction perpendicular to the facings, symmetric wrinkling will occur at a lower load than that for antisymmetric wrinkling.

4.2 Overall Buckling Specimens

Experimental results of overall buckling specimens are presented in Table 8 and figures 27a, b, c, and d. The experimental method used to predict the critical overall buckling stress was to determine the stress associated with the maximum extreme fiber strain on the convex side of the buckled panel. This method was chosen, as was done in reference 25, over other methods such as stress -vs.- bending strain and stress -vs.- average compressive strain. The specimens exhibited a very short post buckling region as evidenced from the experimental results of P_{cr} and P_{ult} as shown in Table 8. Average values of P_{cr}, P_{ult}, σ_{cr}, and σ_{ult} were 95.43 kN (21,453. lbf), 100.4 kn (22,574. lbf), 251.5 MPa (36.48 ksi), and 264.8 MPa (38.4 ksi) respectively. Scatter in P_{cr}, P_{ult}, σ_{cr}, and σ_{ult} was 40-, 36-, 33-, and 28- percent respectively when compared to average values. However, during instrumentation of panel number 7251 the temperature controller of the oven which was used to cure the polyimide strain gage adhesive caused a temperature overshoot to occur. This panel, therefore, experienced temperatures in excess of the laminate cure temperature which probably resulted in considerable material property degradation, hence, the low critical and ultimate loads and stresses. If this test is neglected in the results, average values of P_{cr}, P_{ult}, σ_{cr}, and σ_{ult} are 101.9 kN (22,903. lbf), 106.3 kN (23,897. ibf), 264.1 MPa (38.3 ksi), and 275.5 MPa (39.96 ksi) respectively and corresponding scatter is 21-, 20-, 21-, and 20-percent. Comparison of experimental and analytical results is presented in the next section.

27

Similar to results of reference 25, all of the overall buckling specimens failed on the concave side of the specimen in a typical compressive failure mode. Most of the specimens failed in the center, all the failures were perpendicular to the direction of load as shown in figure 28. The Moire method was useful in visualizing the deflected mode shapes of the specimens and determining how effective the mechanism for simply supporting the panels was. Panel number 7256 was the only specimen which failed near a simple support. Photographs of Moiré fringe patterns of panel 7256 indicated that it did not deform symmetrically in half sine waves in the length and width directions as expected. The out-of-plane deformation of panel 7256 with icnreasing load is illustrated in figures 29a, b, c, and d. As shown, the peak out-of-plane deformation occurs in the upper right hand portion of the specimen. This panel eventually failed near the lower left hand simple support. Moiré fringe patterns of specimen 7251 are shown in figures 30a through d for increasing load. As shown, the maximum out-of-plane displacement does occur in the center of the panel. Displacements seem to be symmetric in the longitudinal direction, however, non-zero displacments appear to occur near the right handside simple support. Since the panel was clamped snugly at this support it was thought that this discrepancy could possibly be explained by some sort of panel or reference grid motion relative to one another. Displacements do occur at the corners of the panel, however, since the simple supports do not extend the total panel length. As the panel approaches failure, mode shapes tend to be nonsymmetric (fig. 30d). As mentioned in reference 25, it is very difficult to simulate true simply-supported boundaries when the buckled mode shape occurs at m=n=1 or the buckled shape is half a sine wave in the length and width direction. The

28

higher tne number of waves in thc buckled pattern the lower the effect the exactness of the boundary conditions has on the behavior of the specimen.

4.3 Comparison of Analytical and Experimental Results

The analysis assumes the fcllowing room temperature unidirectional material properties:

E_{11} = 133 GPa (19.3 x 10^6 psi)

E_{22} = 9.10 GPa (1.32 x 10^6 psi)

μ_{12} = 0.37

μ_{21} = 0.025

G_{12} = 5.58 GPa (0.81 x 10^6 psi)

E_{c_z} = 0.345 GPa (50 x 10^3 psi)

$G_{c_{xz}}$ = 0.200 GPa (29 x 10^3 psi)

$G_{c_{yz}}$ = 0.083 GPa (12 x 10^3 psi)

F_c = 3.45 MPa (500 psi)

From the laminate theory presented in Appendix B, $\bar{E}_x = \bar{E}_y$ = 51.97 GPa (7.538 x 10^6 psi) and $\bar{\mu}_{xy}$ = 0.3075. These results agree with experimental results from the sandwich beam flexure tests in which the average modulus, $\bar{E}_x$ = 48.95 GPa (7.1 x 10^6 psi) and $\bar{\mu}_{xy}$ = 0.347. Since facing laminates were quasi-isotropic, symmetric ($[0,\pm45, 90]_s$), A_{16} and A_{26} coupling terms were identically zero; the D_{16} and D_{26} coupling terms were negligible. Analytical results, assuming a lamina thickness of 0.0076 cm (0.003 in.), are presented in Table 7 and 8 and in figure 31 and are compared with experimental results. The overall buckling analysis described in Appendix C, which included the core shear flexibility, agreed well with experimental overall buckling results.

29

Average experimental overall buckling stress (neglecting results of panel 7251) was 264 MPa (38.3 ksi) com. ed exactly with the analytically predicted overall buckling stress. From experimental wrinkling results it appears that equations D.5 and D.8 were unconservative and impractical to use from a design standpoint. Equation D.4 was conservative in its prediction of symmetric wrinkling loads and is useful for design purposes, however, if panel imperfections can be measured accurately equation D.6 would give a closer approximation to maximum wrinkling loads. Wrinkling results using equation D.6 and assuming δ_{max}= 0.01 cm (0.004 in.) were 7-,26-, and 32- percent higher than experimental results for the 1.27, 1.91, and 2.54 cm (0.5, 0.75, and 1.0 in.) thick cores respectively.

CHAPTER V

SUMMARY AND CONCLUSIONS

5.1 General

The potential economic gain from structural-mass savings in the design of reentry spacecraft with thermally insulated surfaces and of high speed aircraft is great due to the high operating cost and weight sensitivity of such vehicles. Considerable reductions in the mass of a reusable space transportation system such as space shuttle can be realized by the direct replacement of its aluminum sub-structure with an advanced composite such as graphite/polyimide (Gr/PI); an even greater savings in insulation mass is possible because of the higher use temperature of Gr/PI. Predictions in mass savings as high as 25-percent prompted a study, the purpose of which was to design a composite bodyflap for the shuttle orbiter.

The purpose of the present study was to investigate the buckling behavior, local and general, of Gr/PI sandwich panels capable of use at temperatures ranging from 116 to 589K (-250 to 600°F) as the sandwich skin of the shuttle bodyflap. The study investigated adhesive and facing material properties and evaluated buckling formulas for predicting local and general sandwich panel instabilities. Flatwise tensile specimens were tested at 116, R.T., and 589K (-250, R.T., and 600°F) to determine a cure cycle for FM-34 which would produce a high-strength adhesive bond and to investigate the possibility of using a liquid cell-edge version of that adhesive, BR-34, which could save additional adhesive mass. Results of the bond study include a fabrication technique for adhesively bonding sandwich structures and an adhesive cure cycle which produced flatwise tensile strengths in excess of 3.4

31

MPa (500 psi) at 116K and R.T. (-250°F and R.T.) and 1.4 MPa (200 psi) at 589K (600°F). Results also indicated that a liquid cell edge adhesive can result in considerable panel mass savings (10 percent) without necessarily sacrificing bond strength, however, further research is necessary since flatwise tensile strengths using BR-34 were not consistent. Sandwich beam specimens were tested in four-point bending to determine facing tensile and compressive material properties at 116 R.T., and 589K (-250 R.T., and 600°F). The test facing of the beam was a $[0,+45,90,-45]_s$ laminate of Celion/PMR-15 and the opposite face was the same material with additional 0-degree layers $[0_2,+45,90,-45]_s$. Average ultimate strengths were slightly higher in compression than tension for each test temperature. Average room temperature tensile ultimate strength is 450.6 MPa (55.36 ksi). Average tensile ultimate strengths at 116K (-250°F) increased by 8.5-percent over room temperature values and strengths at 589K (600°F) decreased by 43 percent. Average compressive ultimate strengths at 116 and 589K (-250 and 600°F) increased and decreased respectively by 13.8- and 41.2-percent over room temperature values. Modulus values of 0.2-percent strain did not vary much with temperature and remained about 52 GPa (7.5×10^6 psi). Results of the sandwich beam flexure tests indicate that Celion/PI is a usable structural material for short-term use at temperatures from 116 to 589K (-250 to 600°F).

Flat rectangular honeycomb sandwich panels were simply-supported about all four edges (30.5 x 30.5 cm (12 x 12 in.) in size) and tested in edgewise compression. Core thickness was varied to determine the failure envelope of such panels resulting from either a local or general failure mode and to evaluate buckling formulas used to predict failure. Two modes of panel failure were discernable from experimental results, wrinkling and overall

32

buckling. As predicted analytically, specimens with a core thickness of 0.635 cm (0.25 in.) failed by overall buckling and all other specimens, having nominal core thicknesses of 1.27, 1.91, and 2.54 cm (0.5, 0.75, and 1.00 in.), failed by wrinkling. The shadow Moiré method was useful in determining mode shapes of the overall buckling specimens but was not able to detect wrinkling.

Results of the wrinkling tests indicated that several analytical methods were unconservative and therefore not suitable for design purposes. Most of the wrinkling specimens failed near side-simple supports. The failure mode appeared to be symmetric wrinkling with faiures occuring because of tensile rupture of the adhesive. Some trends in wrinkling results are:

1. average failure stresses of the wrinkling specimens decrease as core thickness increases and are 452,354, and 311 MPa (65.6, 51.4, and 45.1 ksi) for the 1.27, 1.91, and 2.54 cm (0.5, 0.75, and 1.0 in.) thick cores respectively.

2. facings with the highest fiber volume fraction had the highest modulus.

3. panels with the largest value of initial waviness had the lowest ultimate load.

The average experimental buckling stress of the 1.27 cm (0.25 in.) thick specimens was 265 MPa (38.4 ksi) and compared exactly with analysis. All of the overall buckling specimens except one failed in the center on the concave facing by compression.

5.2 Suggested Further Research

Additional work, both experimental and analytical, is necessary to evaluate wrinkling and overall buckling of sandwich panels which are symmetric about the core centerline but whose facings are anisotropic in nature. This would be necessary, for instance, to analyze unsymmetric four-ply facings ([0,±45,90]) which are bonded symmetrically about the honeycomb centerline. Manufacture of such a sandwich might satisfy bodyflap loads and result in considerable mass savings. Development of a liquid cell-edge adhesive, such as BR-34, has the potential for reducing panel mass by 10-percent and should be also investigated further. In addition, buckling analysis of sandwich panels subjected to biaxial mechanical and thermal loads is necessary.

APPENDIX A

FABRICATION OF TEST SPECIMENS

A.1 Flatwise Tensile and Sandwich Beam Specimens

In order to insure that the fabrication procedures could be used to
manufacture full-scale structures in existing aerospace industry facilities,
limits of 2.1 MPa (300 psi) and 6K/min (10°F/min.) were imposed on the maximum
pressure and heat-up rate that could be used.

A.1.1 Laminate fabrication

The Gr/PI material is precompacted prior to cure to remove excess solvent
and resin. The prepreg is laid up into the proper laminate orientation,
weighed to the nearest 0.1g (0.0002 lbm), and a perforated teflon coated
fiberglass release cloth is placed on the top and bottom of the laminate as
shown in figure 32. Bleeder paper is then applied to each side of the
assembly. A thin film of nylon is applied to an aluminum caul plate and the
laminate assembly is placed on the nylon. A 0.305 cm (0.12 in.) thick mild
steel upper caul sheet is then placed on top of the laminate to provide a
smooth upper mold surface during precompaction. Two layers of bleeder paper
are placed unto the steel caul plate and the assembly is vacuum bagged with a
0.01 cm (0.004 in.) thick film of nylon. The seal between the vacuum bag and
the aluminum caul plate is provided with a conventional low temperature
polybutadiene strip sealant. The assembly is then placed under vacuum to
ascertain the integrity of the vacuum bag and seals.

Laminates were B-staged by pulling a vacuum of 25.4 cm of Hg (10 in. of
Hg) and holding a temperature of 483 K (410°F) for two hours. The vacuum
pressure was maintained and the laminate was cooled to 339 K (150°F) after
which the vacuum was released and the laminate allowed to cool to room

35

temperature. Following B-staging the laminates were vacuum bagged and, as shown in figure 33, subjected to a vacuum of 71 cm of Hg (28 in. of Hg) which was maintained throughout the cure cycle. An initial external pressure of 1.03 MPa (150 psi) was applied to the bagged laminate during which the temperature was raised to 522 K (480°F) at a rate of 1.7 K/min (3°F/min.). The external pressure was then increased to 1.72 MPa (250 psi) and held for 30 minutes. After thirty minutes the temperature was raised to 603 K (625°F) and held for three hours. The laminate was cooled, under combined vacuum and pressure, at a rate of 2.8 K/min (5°F/min) to 339 K (150°F). The vacuum and pressure were released and the laminate allowed to cool to room temperature. All laminates were fabricated in an autoclave. After fabrication, all laminates were ultrasonically C-scanned for defects. For quality assurance all laminates were scanned at frequencies from 80 to 20 Hz. Below 20 Hz cross ply laminations become visible. Laminates had an average fiber volume fraction, V_f, of about 72 percent.

A.1.2 <u>Assembly and bonding procedures for flatwise tensile specimens</u>

1. Surface preparation

    1.1 Solvent clean the composite face sheets, honeycomb core, and steel end blocks by wiping with clean cloths saturated with MEK solvent. After wiping, dip cleaned parts in clean MEK. Blow dry with clean dry air.

    1.2 Abrasive clean the bonding surfaces of the facings and end blocks by grit blasting using 120 aluminum oxide grit. Set air pressure at 0.55 to 0.62 MPa (80 to 90 psi) for the steel end blocks and 0.28 to 0.31 MPa (40 to 45 psi) for the composite face sheets.

    1.3 Repeat 1.1.

    1.4 Abrasive clean bonding surfaces and edges of honeycomb. Abrasive clean down inside of each cell 0.318 to 0.476 cm (1/8 to 3/16 in.) all four directions.

    Type of blasting equipment:

    > Pennwalt SS White-Industrial Products
    > Abrasive Jet machining Unit, - Model K

36

Abrasive:
                          Airabrasive Powder No. 1
                          Pressure:
                          0.28 MPa (40 psi)

1.5   Repeat 1.1.

1.6   Weigh out and mix thoroughly 3 parts of BR-34 primer and 1 part
      of BR-34 thinner by weight.

1.7   Using a medium bristled brush, prime bonding surfaces of the
      face sheet and end blocks, brushing primer in both directions.

1.8   In a clean container (pan) pour primer to a depth of
      approximately 0.318 cm (0.125 in.). Set honeycomb (bonding
      surface down) in the primer, remove and shake off excess primer.

1.9   Dry primer as follows:
                  Room temperature for 30 min.
                  378K (220°F) for 30 min., and
                  483K (410°F) for 45 min.

2. Assembly
    2.1   Remove the FM-34 adhesive from the freezer, allow package to
          warm up to room temperature before opening.

    2.2   Cut four pieces of adhesive 7.6 cm (3 in.) square (to match end
          blocks and facings).

    2.3   Remove the protective backing from one side of each piece.

    2.4   Position the adhesive squares on primed surfaces of each end
          block, and on one side of each facing.

    2.5   Press the adhesive into intimate contact with its substrate.
          Remove remaining protective film.

    2.6   Assemble the specimens using 0.154 x 7.6 x 7.6 cm (1/16 x 3 x
          3 in.) silicone sheet rubber on top and bottom of specimen, and
          bonding fixtures designed to maintain proper component
          alignment.

    2.7   During assembly insert a thermocouple (30 or 36 gauge) in the
          bond line between the end block and the facing at the bottom
          of the specimen. This thermocouple is to be used to control the
          bondline temperature.

    2.8   Enclose the fixture in a vacuum bag.

    2.9   Position the vacuum bag assembly on the press platen.

    2.10 Draw a full vacuum on the assembly.

2.11 Close the press to obtain upper platen contact with assembly, but only lowest possible positive pressure.

2.12 Set temperature controller to 589 K (600°F) bond line temperature.

2.13 Start heating specimen.

2.14 When bond line reaches 405 K (270°F) apply 0.34 MPa (50 psi) pressure and continue heating.

2.15 When bond line reaches 589 K (600°F) hold at this temperature for two hours.

2.16 Cool to room temperature, 305 K (90°F) under pressure and vacuum.

2.17 Remove specimen from bag and fixture.

A.1.3 Assembly and bonding procedures for sandwich beam flexure specimens

1. Honeycomb preparation

   1.1 Spray honeycomb with liquid detergent inside and out. Leave to soak 2-4 minutes, rinse with running warm water 2-4 minutes and oven dry at 278 K (220°F) for 30 minutes.

   1.2 Vapor degrease 3-5 minutes in Freon.

   1.3 Mix BR-34 Adhesive as furnished (81% solids) with 0.0076-0.013 cm (3-5 x 10^{-3} in.) glass beads, 1 part BR-34 to 1 part beads.

   1.4 Using putty knife, completely fill all honeycomb cells, except the center 7.62 cm (3 in.), by blading mixture through cells from a single side.

   1.5 Clamp honeycomb to hold flat while curing BR-34.

   1.6 After clamping securely, allow filled honeycomb to air dry 1 hour minimum. Place in oven at room temperature and raise temperature to 378 K 220°F. Hold for 2 hours. Slowly raise temperature 1.1-2.8 K (2-5°F)/minute to 589 K (600°F) and hold for 2 hours. Let cool and remove from fixture.

   1.7 Remove excess BR-34/beads from honeycomb by sawing from edges and ends to obtain original dimensions. Grind top and bottom to expose core ends. Top and bottom surfaces shall be flat and parallel +0.003 cm (+0.001 in.).

2. Cleaning and priming

   2.1 Record measurement of thickness taken from center of each facing

2.2   Hand wipe facings using clean cloth saturated with MEK solvent.

2.3   Vapor degrease and rinse in Freon, facings and filled honeycomb.

2.4   Abrasive clean bonding surfaces of facings and honeycomb with
      120 grit aluminum oxide grit. Set air pressure at
      (0.276-0.345 MPa (40-50 psi). Abrasive clean unfilled honeycomb
      cells by direction grit from four (4) directions (both sides) so
      as to clean (0.318 to 0.476 cm (1/8 to 3/16 in.) down into
      cells. Do not blast excessively so as to erode honeycomb.
      (0.276-0.345 MPa (40-50 psi). Abrasive clean unfilled honeycomb
      cells by direction grit from four (4) directions (both sides) so
      as to clean (0.318 to 0.476 cm (1/8 to 3/16 in.) down into
      cells. Do not blast excessively so as to erode honeycomb.

2.5   Repeat Step 2.3.

2.6   Remove primer from freezer and allow closed container to warm to
      room temperature before opening. Weigh out and mix thoroughly 3
      parts BR-34 Primer to 1 part thinner, by weight. Continue to
      mix primer during application to prevent settling.

2.7   Using a medium bristled brush, prime bonding surfaces of facings
      and honeycomb. Apply primer 0.318 cm (1/8 in.) down into cells
      or unfilled portion of honeycomb.

2.8   Dry primer as follows:

      Room temperature for 30 minutes,
      378K (220°F) for 30 minutes
      483K (410°F) for 45 minutes

2.9   The cumulative time period from cleaning to bonding shall not
      exceed 72 hours. Parts shall be handled with white gloves after
      Step 2.2.

3. Assembly and cure

    3.1   Remove FM-34 Adhesive from freezer and allow package to warm to
          room temperature before opening.

    3.2   Peel back protective backing and position primed surface of face
          sheets onto adhesive film. Cut around facings with razor blade.

    3.3   Place a strip of 0.159 cm (1/16 in.) silicone rubber sheet to
          match size of facing in bottom of cleaned and sprayed
          (Frekote-33) fixture.

    3.4   Place facing, honeycomb, facing (spacer strip if needed), and
          top of fixture into press. NOTE: Insert thermocouple bead at
          one end between bottom face sheet and honeycomb.

39

3.5 Bring platens up to touch. Set controllers to 600K (620°F) and apply heat until bondline temperature reaches 405K (270°F). Apply 0.345 MPa (50 psi) and continue heat rise until bondline reaches 589K (600°F). Reset controllers to 589K (600°F) and hold for 2 hours. (Pack Q-felt or equal around fixture to limit heat loss.)

3.6 Cool to below 339K (150°F) under pressure.

3.7 Remove specimen from press and fixture.

A.2 Buckling Specimens

To minimize the mass of the buckling specimens and still maintain the balanced symmetric quasi-isotropic nature of the facings it was decided to use the thinnest prepreg of Celion/PI commercially available which is Celion 3000/PMR-15. Celion 3000/PMR-15 has an average thickness per ply of about 0.007 cm (0.0028 in.) as compared to C.0166 cm (0.0065 in.) for Celion 6000/PMR-15. The average fiber volume fraction of the Celion 3000 laminates is 61.6 percent as compared to 72 percent for the Celion 6000 laminates.

A.2.1 Laminate fabrication

Laminates of $[0,\pm45,90]_s$ Celion 3000/PMR-15 Gr/PI were B-staged by pulling a vacuum of 25.4 cm (10 in.) of Hg and holding a temperature of 491 K (425°F) for one hour. The vacuum pressure was maintained and the laminate was cooled to 339K (150°F) after which the vacuum was released and the laminate allowed to cool to room temperature. Following B-staging the laminates were vacuum bagged, two at a time as shown in figure 34, and cured according to the cycle shown in figure 35. Laminate sheets were approximately 38 x 76 cm (15 x 30 in.) and were trimmed to 33 x 30.5 cm (13 x 12 in.) sizes. Trimmed pieces of material were used to calculate T_g, V_f, V_v, specific gravity, and percent weight loss.

A.2.2 Assembly and bonding procedures

Glass/Polyimide honeycomb core (Hexel HRH-327-3/8-4) of various thicknesses (0.635, 1.27, 1.91, and 2.54 cm (0.25, 0.50, 0.75, and 1.00 in.)) were cut to buckling specimen dimensions (33 x 30.5 cm (13 x 12 in.)) and perforated at node bond lines as shown in figure 36. Perforating the core would allow the escape of any volatiles produced during the cure of the FM-34 polyimide adhesive and prevent otherwise trapped volatiles from producing weak bonds. The honeycomb core was potted at each ··d (2.54 cm (1.0 in.) in

41

length) with BR-34 liquid adhesive as shown in figure 37. The vacuum bag
schematic and cure cycle for the end potting is shown in figure 38. After
cure the filled ends of the honeycomb were machined flat and parallel as shown
in figure 39. Tapered end tabs were machined from Glass/PI laminates 0.635 cm
(0.25 in.) thick and scalloped doublers were machined from 3 ply Glass/PI
laminates. Figure 40 gives a view of the honeycomb core, scalloped doublers,
tapered end tabs, stainless steel sheet, and Gr/PI facesheet. Faying surfaces
of the assembly were primed with Br-34 and bonded using FM-34 film adhesive
$(0.059 \text{ kg/m}^2 (0.135 \text{ lbm/ft}^2))$. The cure and post cure cycles used for
secondary bonding are given in figures 41 and 42. After cure, slots were
machined in the potted ends of the specimens and alignment sheets were
inserted and bonded. Figure 43 gives an end view of a fabricated buckling
specimen and figure 44 gives a view of the entire panel. Dimensions of the
panels are given in the schematic diagram shown in figure 45.

A.3 Quality Control

Quality control of prepreg and processing technique is necessary to
insure manufacture of laminates and sandwich panels with repeatable
properties. Nondestructive evaluation of the laminates and bonded specimens
is also necessary to insure structural integrity. A discussion of the
extensive quality control procedures for composite structural elements for the
CASTS program is given in reference 17. In addition to quality control
procedures for prepreg, resin, and adhesive and nondestructive evaluation of
laminates, the bonded specimens were also ultrasonically scanned to check
honeycomb core-to-facing bonds. The thickness of each individual facing and
completed sandwich panel was measured at six panel locations (as shown in
figure 45) and average values and maximum deviations are noted in Table 6.

42

Digitized readouts of 45 points over each face of every panel were recorded and a curve fit routine used to plot surface waviness of each panel. Figure 46 is a typical plot of the waviness of a sandwich panel; the maximum displacement or irregularity, δ_{max}, was recorded for each panel.

APPENDIX B

LAMINATE THEORY

Laminate theory is used to predict the average elastic material behavior of the facings and compare results with experimental calculations. The theory assumes that individual lamina behave orthotropically, on a macroscopic level, and that material properties of laminate composed of several lamina oriented at various angles with respect to one another can be determined using Kirchholf plate assumptions. The theory is presented briefly below; a more detailed description can be found in references 45 and 46.

Lamina and laminate geometries and coordinate systems are shown in figure 47. The lamina coordinate system (fig. 47a) is aligned with the principle material directions of lamina, parallel (1) and perpendicular (2) to the fibers. The laminate coordinate system (fig. 47b), however, usually corresponds to loading directions and does not often correspond with the principle material directions of a ply or lamina. Since each lamina is asusmed to be homogenuous, orthotropic, and loaded in a state of plane stress, the stress-strain relations in the natural coordinate system are

$$\left\{ \begin{array}{c} \sigma_1 \\ \sigma_2 \\ \sigma_{12} \end{array} \right\} = \left[\begin{array}{ccc} Q_{11} & Q_{12} & 0 \\ Q_{12} & Q_{22} & 0 \\ 0 & 0 & Q_{66} \end{array} \right] \left\{ \begin{array}{c} \varepsilon_1 \\ \varepsilon_2 \\ \varepsilon_{12} \end{array} \right\} \tag{B.1}$$

where
$$
\begin{aligned}
Q_{11} &= E_{11}/(1-\mu_{12}\,\mu_{21}) \\
Q_{22} &= E_{22}/(1-\mu_{12}\,\mu_{21}) \\
Q_{12} &= \mu_{21}\,E_{11}/(1-\mu_{12}\,\mu_{21}) = \mu_{12}E_{22}/(1-\mu_{12}\,\mu_{21}) \\
Q_{66} &= G_{12} \\
Q_{16} &= Q_{26} = 0
\end{aligned}
\tag{B.2}
$$

where from the reciprocal relation

$$\mu_{21}E_{11} = \mu_{12}E_{22} \tag{B.3}$$

In any other coordinate system in the plane of the lamina the stresses can be expressed as

$$\begin{Bmatrix} \sigma_x \\ \sigma_y \\ \sigma_{xy} \end{Bmatrix} = \begin{bmatrix} \bar{Q}_{11} & \bar{Q}_{12} & \bar{Q}_{16} \\ \bar{Q}_{12} & \bar{Q}_{22} & \bar{Q}_{26} \\ \bar{Q}_{16} & \bar{Q}_{26} & \bar{Q}_{66} \end{bmatrix} \begin{Bmatrix} \varepsilon_x \\ \varepsilon_y \\ \varepsilon_{xy} \end{Bmatrix} \tag{B.4}$$

where the transformed stiffness matrix $[\bar{Q}]$, is calculated from the reduced stiffness matrix and transformation matrix $[T]$

$$[T] = \begin{bmatrix} \cos^2\theta & \sin^2\theta & 2\sin\theta\,\cos\theta \\ \sin^2\theta & \cos^2\theta & -2\sin\theta\,\cos\theta \\ -\sin\theta\cos\theta & \sin\theta\cos\theta & \cos^2\theta-\sin^2\theta \end{bmatrix} \tag{B.5}$$

as

$$[\bar{Q}] = [T]^{-1} [Q] [T]^{-T} \tag{B.6}$$

where θ is the angle between the fiber direction and the laminate x-axis taken as positive as shown in figure 47a.

$$\bar{Q}_{11} = Q_{11}\cos^4\theta + 2(Q_{12} + 2Q_{66})\sin^2\theta\cos^2\theta + Q_{22}\sin^4\theta$$

$$\bar{Q}_{12} = (Q_{11} + Q_{22} - 4Q_{66})\sin^2\theta\cos^2\theta + Q_{12}(\sin^4\theta + \cos^4\theta)$$

$$\bar{Q}_{22} = Q_{11}\sin^4\theta + 2(Q_{12} + 2Q_{66})\sin^2\theta\cos^2\theta + Q_{22}\cos^4\theta \tag{B.7}$$

$$\bar{Q}_{16} = (Q_{11} - Q_{12} - 2Q_{66})\sin\theta\cos^3\theta + (Q_{12} - Q_{22} + 2Q_{66})\sin^3\theta\cos\theta$$

$$\bar{Q}_{26} = (Q_{11} - Q_{12} - 2Q_{66})\sin^3\theta\cos\theta + (Q_{12} - Q_{22} + 2Q_{66})\sin\theta\cos^3\theta$$

$$\bar{Q}_{66} = (Q_{11} + Q_{22} - 2Q_{12} - 2Q_{66})\sin^2\theta\cos^2\theta + Q_{66}(\sin^4\theta + \cos^4\theta)$$

The resultant forces and moments acting on a laminate are obtained by the integration of the stresses in each lamina through the thickness laminate as

$$\begin{Bmatrix} N_x \\ N_y \\ N_{xy} \end{Bmatrix} = \int_{-H}^{H} \begin{Bmatrix} \sigma_x \\ \sigma_y \\ \sigma_{xy} \end{Bmatrix} dz$$

(B.8)

$$\begin{Bmatrix} M_x \\ M_y \\ M_{xy} \end{Bmatrix} \int_{-H}^{H} \begin{Bmatrix} \sigma_x \\ \sigma_y \\ \sigma_{xy} \end{Bmatrix} zdz$$

the stresses, σ, can be expressed in each lamina as a function of laminate middle surface strains and curvatures using the Kirchhof-Love hypothesis as

$$\{\sigma\}_k = [\bar{Q}]_k \left\{ \begin{Bmatrix} \varepsilon_x^o \\ \varepsilon_y^o \\ \varepsilon_{xy}^o \end{Bmatrix} + z \begin{Bmatrix} \kappa_x \\ \kappa_y \\ \kappa_{xy} \end{Bmatrix} \right\}$$

(B.9)

Since the state of stress is assumed constant over each lamina equation (3.8) can be rewritten for an n-ply laminate as

$$\begin{Bmatrix} N_x \\ N_y \\ N_{xy} \end{Bmatrix} = \sum_{k=1}^{n} \int_{z_{k-1}}^{z_k} \begin{Bmatrix} \sigma_x \\ \sigma_y \\ \sigma_{xy} \end{Bmatrix}_k dz$$

$$\begin{Bmatrix} M_x \\ M_y \\ M_{xy} \end{Bmatrix} = \sum_{k=1}^{n} \int_{z_{k-1}}^{z_k} \begin{Bmatrix} \sigma_x \\ \sigma_y \\ \sigma_{xy} \end{Bmatrix}_k zdz$$

(B.10)

substituting equations B.9 and B.10 into eq. B.8 gives

$$\{N\} = \sum_{k=1}^{n} \int_{z_{k-1}}^{z_k} [\bar{Q}]_k \left\{ \{\varepsilon^o\} + z \{\kappa\} \right\} dz$$

$$\{M\} = \sum_{k=1}^{n} \int_{z_{k-1}}^{z_k} [\bar{Q}_k] \left\{ \{\varepsilon^o\} + z \{\kappa\} \right\} zdz$$

(B.11)

or

$$\{N\} = [A] \{\varepsilon^o\} + [B] \{\kappa\}$$

$$\{M\} = [B] \{\varepsilon^o\} + [D] \{\kappa\}$$

where

$$[A] = \sum_{k=1}^{n} [\bar{Q}]_k (z_k - z_{k-1})$$

$$[B] = \frac{1}{2}\sum_{k=1}^{n} [\bar{Q}]_k (z_k^2 - z_{k-1}^2) \qquad\qquad (B.12)$$

$$[D] = \frac{1}{3}\sum_{k=1}^{n} [\bar{Q}]_k (z_k^3 - z_{k-1}^3)$$

For the case of a symmetric laminate with no applied bending moment, such as the case of this study, the average elastic properties of the laminate can be expressed as

$$\bar{E}_x = \frac{1}{2Ha_{11}} \qquad\qquad \bar{\mu}_{xy} = \frac{-a_{12}}{a_{11}}$$

$$\bar{E}_y = \frac{1}{2Ha_{22}} \qquad\qquad\qquad\qquad (B.13)$$

$$\bar{G}_{xy} = \frac{1}{2Ha_{66}} \qquad\qquad \bar{\mu}_{yx} = \frac{-a_{12}}{a_{22}}$$

where $[a] = [A]^{-1}$

since only a quasi-isotropic laminate is considered in the present study and because its balanced symmetric $A_{16} = A_{26} = 0$ and the matrix $[a]$ is:

$$[a] = \begin{bmatrix} \dfrac{A_{22}}{A_{11}A_{22}-A_{12}^2} & \dfrac{-A_{12}}{A_{11}A_{22}-A_{12}^2} & 0 \\[4mm] \dfrac{-A_{12}}{A_{11}A_{12}-A_{12}^2} & \dfrac{A_{11}}{A_{11}A_{22}A_{12}^2} & 0 \\[4mm] 0 & 0 & \dfrac{1}{A_{66}} \end{bmatrix} \qquad (B.14)$$

and therefore:

$$E_x = \frac{1}{2H} \left[\frac{A_{11}A_{22}-A_{12}^2}{A_{22}} \right] \qquad \bar{\mu}_{xy} = \frac{A_{12}}{A_{22}}$$

$$\bar{E}_y = \frac{1}{2H} \left[\frac{A_{11}A_{22}-A_{12}^2}{A_{11}} \right] \qquad \bar{\mu}_{yx} = \frac{A_{12}}{A_{11}} \qquad\qquad (B.15)$$

$$\bar{G}_{xy} = \frac{1}{2H} A_{66}$$

since the laminate is quasi-isotropic $A_{11} = A_{22}$, hence

$$\bar{E}_x = \bar{E}_y \text{ and } \bar{\mu}_{xy} = \bar{\mu}_{yx}$$

APPENDIX C

FUNDAMENTAL EQUATIONS OF SMALL-DEFLECTION SANDWICH PLATE THEORY USED IN THE PRESENT STUDY

The overall or general buckling analysis uses the small-deflection theory for orthotropic sandwich plates and shells presented in references 35 and 36. The theory assumes that the materials are elastic, deflections are small compared to the panel thickness and that the thickness is small compared to the other dimensions of the panel (see figure 48). The analysis also assumes an antiplane core (modulus of elasticity of core in planes parallel to the facings is assumed zero but the shear modulus in planes perpendicular to the facings is finite) having an infinite stiffness normal to the planes of the facings.

Five equations relating force equilibrium in the x-, y-, and z-directions and moment equilibrium in the x- and y-directions and six equations relating middle surface forces and moments with middle surface strains are presented in reference 36 and reduced to three equations in three unknowns Q_x, Q_y and w as shown below:

$$Q_x + \frac{D_x}{1-\mu_x\mu_y}\left[\frac{\partial^3 w}{\partial x^3} - \frac{1}{D_{Q_x}}\frac{\partial^2 Q_x}{\partial x^2} + \mu_y\frac{\partial^3 w}{\partial x\partial y^2} - \frac{\mu_y}{D_{Q_y}}\frac{\partial^2 Q_y}{\partial x\partial y}\right] +$$

$$\frac{1}{2}D_{xy}\left[2\frac{\partial^3 w}{\partial x\partial y^2} - \frac{1}{D_{Q_x}}\frac{\partial^2 Q_x}{\partial y^2} - \frac{1}{D_{Q_y}}\frac{\partial^2 Q_x}{\partial x\partial y}\right] = 0 \tag{C.1}$$

$$Q_y + \frac{D_y}{1-\mu_x\mu_y}\left[\frac{\partial^3 w}{\partial y^3} - \frac{1}{D_{Q_y}}\frac{\partial^2 Q_y}{\partial y^2} + \mu_x\frac{\partial^3 w}{\partial x^2\partial y} - \frac{\mu_y}{D_{Q_x}}\frac{\partial^2 Q_x}{\partial x\partial y}\right] +$$

$$\frac{1}{2}D_{xy}\left[2\frac{\partial^3 w}{\partial x^2\partial y} - \frac{1}{D_{Q_x}}\frac{\partial^2 Q_x}{\partial x\partial y} - \frac{1}{D_{Q_x}}\frac{\partial^2 Q_y}{\partial x^2}\right] = 0 \tag{C.2}$$

and assuming the radius of curvature $r = \infty$ as it does for flat plates and that only in-plane biaxial normal loads are applied, the third equation is:

$$\frac{D_x}{1-\mu_x\mu_y} \frac{\partial^4 w}{\partial x^4} + \left(\frac{\mu_y D_x}{1-\mu_x\mu_y} + 2D_{xy} + \frac{\mu_x D_y}{1-\mu_x\mu_y}\right) \frac{\partial^4 w}{\partial x^2 \partial y^2} + \frac{D_y}{1-\mu_x\mu_y} \frac{\partial^4 w}{\partial y^4}$$

$$- \left[N_x \frac{\partial^2 w}{\partial x^2} + N_y \frac{\partial^2 w}{\partial y^2} + 2N_{xy} \frac{\partial^2 w}{\partial x \partial y}\right]$$

$$- \frac{1}{D_{Q_x}}\left[\frac{D_x}{1-\mu_x\mu_y} \frac{\partial^3 Q_x}{\partial x^3} + \left(\frac{\mu_x D_y}{1-\mu_x\mu_y} + D_{xy}\right) \frac{\partial^3 Q_x}{\partial x \partial y^2}\right]$$

$$- \frac{1}{D_{Q_y}}\left[\frac{D_y}{1-\mu_x\mu_y} \frac{\partial^3 Q_y}{\partial y^3} + \left(\frac{\mu_y D_y}{1-\mu_x\mu_y} + D_{xy}\right) \frac{\partial^3 Q_y}{\partial x^2 \partial y}\right] = 0 \tag{C.3}$$

For simply supported boundary conditions along all four edges in which all points in the boundary (not just those on the middle plane) are prevented from moving parallel to the edges the boundary conditions $x = 0$ or $x = \ell$ are $w = M_x = V = N_x = Q_y = 0$ and at a boundary $y = 0$ or $y = b$ are $w = M_y = u = N_y = Q_x = 0$ (refs. 35 and 36). Assumed trigonometric solutions for w, Q_x, and Q_y which satisfy these boundary conditions are, from reference 28

$$w = A \sin \frac{m\pi x}{\ell} \sin \frac{n\pi y}{b}$$

$$Q_y = B \sin \frac{m\pi x}{\ell} \cos \frac{n\pi y}{b} \tag{C.4}$$

$$Q_x = C \cos \frac{m\pi x}{\ell} \sin \frac{n\pi y}{b}$$

If equations (C.4) are substituted into equations (C.1), (C.2), and (C.3) and the symmetry relationship

$$\mu_x D_y = \mu_y D_x \tag{C.5}$$

which was derived in reference 35 using Maxwell-Betti's reciprocal theorem is used, you obtain the following expression (ref. 28)

50

$$N_x \left(\frac{m\pi}{\ell}\right)^2 + N_y \left(\frac{n\pi}{b}\right)^2 = W_{11} - \frac{W_{22}W_{13}^2 + W_{33}W_{12}^2 - 2W_{12}W_{13}W_{23}}{W_{22}W_{33} - W_{23}^2} \tag{C.6}$$

where

$$W_{11} = \bar{D}_x \left(\frac{m\pi}{\ell}\right)^4 + D_{12} \left(\frac{m\pi}{\ell}\right)^2 \left(\frac{n\pi}{b}\right)^2 + \bar{D}_y \left(\frac{n\pi}{b}\right)^4$$

$$W_{12} = \bar{D}_y \left(\frac{n\pi}{b}\right)^3 + \frac{D_{12}}{2} \left(\frac{m\pi}{\ell}\right)^2 \left(\frac{n\pi}{b}\right)$$

$$W_{13} = \bar{D}_x \left(\frac{m\pi}{\ell}\right)^3 + \frac{D_{12}}{2} \left(\frac{m\pi}{\ell}\right)\left(\frac{n\pi}{b}\right)^2$$

$$W_{22} = D_{Q_y} + \bar{D}_y \left(\frac{n\pi}{b}\right)^2 + \frac{D_{xy}}{2} \left(\frac{m\pi}{\ell}\right)^2 \tag{C.7}$$

$$W_{23} = \frac{D_{12} - D_{xy}}{2} \left(\frac{m\pi}{\ell}\right) \left(\frac{n\pi}{b}\right)$$

$$W_{33} = D_{Q_x} + \bar{D}_x \left(\frac{m\pi}{\ell}\right)^2 + \frac{D_{xy}}{2} \left(\frac{n\pi}{b}\right)^2$$

and

$$D_{12} = 2 D_{xy} + \mu_x D_y + \mu_y \bar{D}_x$$

$$\bar{D}_x = \frac{D_x}{1-\mu_x\mu_y} \quad , \quad \bar{D}_y = \frac{D_y}{1-\mu_x\mu_y}$$

The buckling load of a plate is obtained from equations C.6 and C.7 by minimizing with respect to m and n, the number of half waves in the buckle pattern in the length and width directions of the plate, respectively. The smallest n consistent with the assumption of simply supported plates is n = 1.

APPENDIX D

LOCAL BUCKLING FORMULAS USED IN THE PRESENT STUDY

There are several instability modes which can cause failure of a sandwich structure; as shown in figure 49 they are: intracellular buckling (face dimpling), face wrinkling (either symmetric or antisymmetric), and shear crimping. Intracellular buckling is a localized mode of instability which occurs only when the core is not continuous, as in the case of honeycomb or corrugated cores. As shown in figure 49a, the facings buckle in a plate-like fashion directly above core cells, with cell edges acting as edge supports. These buckles can deform sufficiently to cause permanent, plastic deformations and can eventually lead to the face wrinkling instability mode (fig. 49b). The face wrinkling mode is a localized buckling of the facings in which the wavelengths of the buckles is of the same order as the thickness of the core. Depending on the nature of the material properties of the core the facings can buckle symmetrically or antisymmetrically. For the case of honeycomb cores, in which the elastic modulus parallel to the facings is very low compared to the modulus in the direction perpendicular to the facings, failure is usually by symmetric wrinkling (ref. 44). Depending on the tensile and compressive strengths of the core material in the z-direction and the flatwise tensile strength of the bond between the facings and the core, the sandwich panel can fail in several ways as shown in figure 50.

Shear crimping (fig. 49c) is considered to be a special form of general instability for which the buckle wavelength is very short due to a low transverse shear modulus of the core. This mode occurs suddenly and usually causes the core to fail in shear, however, it may also cause a shear failure in the core-to-facing bond.

There are many references concerning the analysis and prediction of local instability modes of failure of sandwich structures (refs. 20 to 22, 24, 25, and 47 to 49). Formulas for predicting local instability vary among references and for that reason several methods were used to predict local failure loads an upper and lower bound were calculated for various failure modes and sandwich panel thicknesses. The formulas for local buckling of a sandwich panel subject to uniaxial compression and appropriate references are given as follows:

Intracellular buckling

from references 21, and 47 to 49 for istoropic facings:

$$\sigma_{dim} = \frac{2E_f}{(1-\mu^2)} \left(\frac{t_f}{s}\right)^2 \tag{D.1}$$

where E_f is the facing modulus, t_f is the facing thickness, and s is the honeycomb cell size, from reference 24

$$\sigma_{dim} = 3E_f \left(\frac{t_f}{s}\right)^2 \tag{D.2}$$

from reference 25, assuming orthotropic faces

$$\sigma_{dim} = 0.825 \frac{\pi^2}{3} \left[\left(\frac{2\sqrt{E_{f_x}E_{f_y}} + \bar{\mu}_{yx}E_{f_x} + \bar{\mu}_{xy}E_{f_y}}{4(1-\bar{\mu}_{xy}\bar{\mu}_{yx})}\right) + G_{f_{xy}}\right]\left(\frac{t_f}{s}\right)^2 \tag{D.3}$$

where E_{f_x} and E_{f_x} are the facing shear moduli in the x- and y-direction respectively and $G_{f_{xy}}$ is the facing shear modulus in the xy plane

For isotropic faces equation (D.3) reduces to

$$\sigma_{dim} = 0.825 \frac{\pi^2}{3} \left[\frac{E_f(1+\mu)}{2(1-\mu^2)} + G_{f_{xy}}\right]\left(\frac{t_f}{s}\right)^2$$

Facing Wrinkling (Symmetric)

From references 21 and 48 lower and upper bounds on wrinkling stress are respectively

$$\sigma_{wr} = 0.33 \ E_f \left(\frac{E_{c_z} t_f}{E_f t_c} \right)^{1/2} \qquad \text{(lower bound)} \qquad (D.4)$$

and

$$\sigma_{wr} = 0.82 \ E_f \left(\frac{E_{c_z} t_f}{E_f t_c} \right)^{1/2} \qquad \text{(upper bound)} \qquad (D.5)$$

where E_{c_z} is the modulus of the core in the direction normal to the facings and t_c is the thickness of the core from reference 48 accounting for initial facing imperfections

$$\sigma_{wr} = \frac{0.82 \ E_f \left(\dfrac{E_{c_z} t_f}{E_f t_c} \right)^{1/2}}{1 + 0.64 \delta \left(\dfrac{E_{c_z}}{t_c F_c} \right)} \qquad (D.6)$$

where F_c is the flatwise sandwich strength and δ is the amplitude of initial waviness in the facings.

from reference 24

for $t_c/t_f < 50$

$$\sigma_{wr} = 0.5 \ (G_{c_{xz}} E_{c_z} E_f)^{1/3}$$

and for $t_c/t_f > 50$

$$\sigma_{wr} = 0.76 \ (G_{c_{xz}} E_{c_z} E_f)^{1/3} \qquad (D.7)$$

from reference 18

$$\sigma_{wr} = \frac{\pi^2}{t_f \ell^2} \left\{ D_{F_{11}} m^2 + 2 \left(D_{F_{12}} + 2 D_{F_{66}} \right) \left(\frac{\ell}{b}\right)^2 + \frac{D_{F_{22}}}{m^2} \left(\frac{\ell}{b}\right)^4 \right\}$$

$$+ \frac{E_{c_z} \ell^2}{t_f m^2 \pi^2 h}$$

(D.8)

Shear Crimping

From reference 21

$$\sigma_{crim} = \left(\frac{h^2}{2 t_f t_c}\right) G_{c_{xz}}$$

(D.9)

and from reference 47

$$\sigma_{crim} = \left(\frac{t_c}{2 t_f}\right) G_{c_{xz}}$$

(D.10)

REFERENCES

1. Dietz, A. G. H.: Composite Materials. Edgar Marlburg Lecture, Am. Soc. for Testing and Materials, Philadelphia, PA, 1965.

2. Fairbairn, W.: An Account of the Construction of the Britannia and Conway Tubular Bridges. John Weale, 1849.

3. Hoff, N. J.; and Mautner, S. E.: Sandwich Construction. Presented at the National Light Aircraft Meetings, I.A.S., Detroit, April 27-28, 1944.

4. Hoff, N. J.; and Mautner, S. E.: The Buckling of Sandwich-Type Panels. J. Aero. Sci., 12, 3 July, 1945, pp. 285-297.

5. Bert, Charles W.: Analysis of Plates. Composite Materials, Vol. 7, Structural Analysis and Design Part I, edited by Christos Chamis, 1975.

6. Hamer, J.: Honeycomb Structure and Its Application to the Concorde Rudder. Composites, Vol. 2, No. 4, Dec., 1971, pp. 242-245.

7. Stein, Manual; and Williams, Jerry: Buckling and Structural Efficiency of Sandwich-Blade Stiffened Composite Compression Panels. NASA TP-1269, Sept. 1978.

8. Salkind, M.; and Holister, G., eds.: Applications of Composite Materials. STP 524, ASTM, Philadelphia, Pa., 1973.

9. Rogers, C.: Structural Design with Composites. Fundamental Aspects of Fiber Reinforced Plastics, ed. by Schwartz, R. and Schwartz, H., Wiley, N.Y., 1968, pp. 141-160.

10. Lubin, G.; and Dastin, S. First Boron Composite Structural Production Part. 26th SPI Conference Proceedings, Society for the Plastics Ind., N.Y., 1971, Sec. 17-C.

11. Salkind, Michel J.: Fiber Composite Structures. Proceedings of the 1975 International Conference on Composite Materials.

12. Braybrook, Roy: Fighters for the 1990's; Building on Today's Technology. Interavia, Jan. 1978.

13. Poesch, Jon G.: Development of Lightweight Graphite-Polyimide Sandwich Panels. Non-Metallic Materials Selection Processing and Environmental Behavior. Proceedings of the 4th National Technical Conference and Exhibition, sponsored by the Society of Aerospace Material and Process Engineers, Palo Alto, Calif., October 17-19, 1972.

14. Stein, Bland A.; and Pride, Richard A.: Effects of 450 and 600°F Exposures on the Mechanical Properties of Polyimide/Glass-Fiber Honeycomb Sandwiches Laminated Beams. J. Aircraft, Vol. 5, No. 1, Jan-Feb., 1968.

15. Stone, R. H.: Development of Graphite/Polyimide Honeycomb Core Materials. NASA CR-158921, Sept., 1978.

16. Strouhal, George; and Tillian, Donald J.: Testing the Shuttle Heat-Protection Armor. Aeronautics and Astronautics, Jan. 1976, pp. 57-65.

17. Composites for Advanced Space Transportation Systems (CASTS). Technical Report for Period July 1, 1975 through April 1, 1978. NASA TM-80038. 1979.

18. Anon.: Design and Test Requirements for the Application of Composites to Space Shuttle Orbiter. Vol. I. Summary, Rockwell International Report SD 75-SA-0178-1, Dec. 3, 1975.

19. Anon.; Mechanical Properties of Hexel Honeycomb Materials. Hexel Report TSB 120, 1975.

20. Smith, R. H. Luckin; and Thomas, D. J.: Intercell Buckling of Honeycomb Core Sandwich Pandels. Unviersity of Bristol Report No. 174.

21. Sullins, R. T.; Smith, G. W.; and Spier, E. E.; Manual For Structural Stability Analysis of Sandwich Plates and Shells. NASA CR-1457, Dec., 1969.

22. Allen, Howard G.: Analysis and Design of Structural Sandwich Panels. Pergamon Press, 1969.

23. Peterson, James P.: Plastic Buckling of Plates and Shells Under Biaxial Loading. NASA TND-4706, Aug., 1968.

24. Plantema, Fredrik J.: Sandwich Construction. John Wiley and Sons, 1966.

25. Pearce, T. R. A.: The Stability of Simply-Supported Sandwich Panels with Fibre Reinforced Faceplates. University of Bristol Thesis Submitted for the Degree of Ph.D., Sept. 1973.

26. Ishai, Ori; and Soggi, Aharon: Instability of Sandwich Beam and Columns with FRP Facings. From the Proceedings of the 1975 International Conference on Composite Materials.

27. Peterson, J. P.; Influence of Specimen Design and Test Procedure on Results of Buckling Tests of Shell Structures. ASTM, STP 419.

28. Anderson, M.S.; and Updegraff, R.G.: Some Research Results on Sandwich Structures. NACA TN 4009, 1957.

29. Hoff, N. J.; Boley, Bruno A.; and Coan, John M.: The Development of a Technique for Testing Stiff Panels in Edgewise Compression. Experimental Stress Analysis. Vol. 5, No. 2, P. 14, 1948.

30. Reissner, E.: Finite Deflections of Sandwich Plates. Journal of the Aeronautical Sciences, Vol. 15, No. 7, July, 1948 pp 435-440.

31. Heath, W. G.: Sandwich Construction. Correlation and Extension of Existing Theory of Flat Panels Subjected to Lengthwise Compression. Aircraft Engineering, Vol. 32 Parts I and II, 1960.

32. Hemp, W. S.: On a Theory of Sandwich Construction. A.R.C. R & M 2778, Mar., 1949.

33. Williams, D.; Leggett, D.M.A; and Hopkins, H.G.: Flat Sandwich Panels Under Compressive End Loads. A.R.C. R&M 2/43, 1946.

34. Cox, H.L.; and Riddell, J. R.: Sandwich Construction and Core Mateials, Part III. Instability of Sandwich Struts and Beams. A.R.C., R&M 2125, 1945.

35. Stein, M.; and Mayers, J.: A Small Deflection Theory for Curved Sandwich Plates. NACA Report 1008, 1951 (Supersedes NACA TN 2017).

36. Libove, Charles; and Batdorf, S. B.: A General Small-Deflection Theory for Flat Sandwich Plates. NACA Report 899, 1948.

37. Raju, B. Basava; Camarda, Charles J.; and Cooper, Paul A.: Elevated Temperature Applications of the IITRI Compression Test Fixture for Graphite-Polyimide Filamentary Composites. NASA TP 1496, 1979.

38. Shuart, Mark J.: An Evaluation of the Sandwich Beam as a Compressive Test Metod for Composites. NASA TM 78783, Sept. 1978.

39. Hanson, Morgan P.; ad Chamis, Christos C.: Graphite-Polyimide Composites for Application to Aircraft Engines. NASA TN D-7698, June 1974.

40. Anon.: Advanced Composites Design Guide. Air Force Materials Laboratory, Wright-Patterson Air Force Base, Vol. IV, 1973.

41. Dykes, B. C.: Analysis of Displacement in Large Plates by the Grid-Shadow Moire' Technique Exp. Stress Analysis and its Influence on Design, M.L. Meyer, ed., Inst. Mech. Eng., C. 1971, pp. 125-134.

42. Chiang, Fu-Pen: Moire Methods of Strain Analysis. Experimental Mechanics, Chapter VI, pp. 290-308, Aug., 1979.

43. Jones, Robert E.; and Greene, Bruce E.: The Force/Stiffness Technique for Nondestructive Buckling Testing. Presented at the AIAA/ASME/SAE 15th Structures, Structural Dynamics, and Materials Conference, Las Vegas, Nevada, April 17-19, 1974.

44. Norris, C. B.; Ericksen, W.S.; March, H. W.; Smith, C.B.; and Boller, K.H.: Wrinkling of the Facings of Sandwich Construction Subjected to Edgewise Compression. FPL Report No. 1810, March 1956.

45. Jones, Robert M.: Mechanics of Composite Materials. Scripta Book Company, 1975.

46. Ashton, J. E.; Halpin, J. C.; and Petit, P. H.: Primer on Composite Materials: Analysis. Technomic Publishing Co., Inc., 1969.

47. Anon.: Sandwich Construction for Aircraft. ANC-23, Parts I and II. Munitions Board, Aircraft Committee. U. S. Gov. Printing Office, 1955.

48. Anon.: Honeycomb and Prepreg in Sandiwch Construction. Hexel Report TSB-100, 1974.

49. U.S. Department of Defense: Structural Sandwich Composites. MIL-HDBK-23, 20 Dec., 1968.

TABLE 1 - CURE CYCLES OF FLATWISE TENSILE SPECIMENS

CURE CYCLE NUMBER	DESCRIPTION
1	Vacuum + 0.34 MPa (50 psi) at R. T. Cure to 589K (600^{0}F) @ 5 K/min. (9^0/min) hold for 2 hours No post cure
2	Vacuum +0.34 MPa (50 psi) at R. T. Cure to 450K (350^{0}F) @ 5 K/min. (9^{0}F/min.) hold for 2 hours Post cure at 589 K (600^{0}F) hold at temp. for 2 hours with clamps
3	Same as cure #1 but bond top and bottom facings separately with facings to be bonded on bottom
4	Vacuum + 0.34 MPa (50 psi) at R. T. Cure to 616 K (650^{0}F) @ 5 K/min. (9^{0}F/min.) hold for 1.5 hours
5	Same as cure #1 but don't apply vacuum

TABLE 2. - FLATWISE TENSILE TEST RESULTS OF CURE CYCLE BOND STUDY
(Core density = 96 kg/m³ (6 lbf/ft³)
A) Room Temperature

Specimen Number	Cure Cycle Number	P_{ult} kN (lbf)	σ_{ult} MPa (psi)	Description of Failure
32078-1	1	18.90 (4250)	3.25 (472)	Failed between facing and core. Facing delaminated also.
32078-2	1	23.35 (5250)	4.02 (583)	Failed between facing and core. Facing delaminated.
32178-1	2	16.24 (3650)	2.80 (406)	Facing delamination
32178-2	2	19.79 (4450)	3.41 (494)	Failed between facing and core
32278-1	4	13.57 (3050)	2.34 (339)	Facing delamination
32278-2	4	17.70 (3980)	3.05 (442)	Facing delamination
32378-1	5	21.13 (4750)	3.64 (528)	Failed between facing and core
32378-2	5	23.22 (5220)	4.00 (580)	Facing delamination
32778-1	3	16.90 (3800)	2.91 (422)	Failed second bond between facing and core
32778-2	3	16.01 (3600)	2.76 (400)	Failed second bond between facing and core

B) 589 K (600°F)

Specimen Number	Cure Cycle Number	P_{ult} kN (lbf)	σ_{ult} MPa (psi)	Description of Failure
40578-1	1	7.918 (1780)	1.37 (198)	Failed between facing and core
40578-2	1	8.363 (1880)	1.44 (209)	Failed between facing and core
40778-1	1[a]	11.23 (2525)	1.94 (281)	Failed between facing and core
40778-2	1[a]	7.451 (1675)	1.28 (186)	Failed between facing and core
41 8-1	5	4.938 (1110)	0.848 (123)	Failed between facing and core
41378-2	5	6.139 (1380)	1.05 (153)	Failed between facing and core

[a] same as cure cycle #1 but cure to 603 K (625°F)   60

TABLE 3. - FLATWISE TENSILE TEST RESULTS
a) FM-34 film adhesive, cure cycle #1 with cure temp. = 603K (625°K)

Specimen Number	Temp. K (°F)	Core Density kg/m³ (lbm/ft³)	P_{ult} kN (lbf)	q_{ult} MPa (psi)	Description of Failure
41011	R.T.	96 (6)	13.12 (2950)	2.26 (328)	Facing delamination
41213	R.T.		21.80 (4900)	3.75 (544)	Facing delamination
41819	589 (600)		8.80 (1980)	1.52 (220)	Failed between facing and core
42021	589 (600)		7.784 (1750)	1.33 (194)	Failed between facing and core
42223	589 (600)		3.38 (760)	0.58 (84)	Failed between end-block and facing
42425	116 (-250)		1.11 (250)	1.92 (278)	Failed between end-block and facing
42627	116 (-250)	↓	4.448 (1000)	0.765 (111)	Facing delamination
CG12	R.T.	128 (8)	18.24 (4100)	3.14 (456)	Failed between facing and core
CG34	116 (-250)		18.46 (4150)	3.18 (461)	Facing delamination
CG56	R.T.		13.34 (3000)	2.30 (333)	Failed between facing and core
CG78	R.T.		22.24 (5000)	3.83 (556)	Facing delamination
CG910	589 (600)		7.651 (1720)	1.32 (191)	Failed between facing and core
CG1112	589 (600)		8.451 (1900)	1.46 (211)	Failed between facing and core
CG1314	589 (600)		8.051 (1810)	1.39 (201)	Failed between facing and core
CG1516	116 (-250)		18.90 (4250)	3.25 (472)	Facing delamination
CG1718	116 (-250)	↓	24.24 (5450)	4.18 (606)	Failed between facing and core

61

TABLE 3. - FLATWISE TENSILE TEST RESULTS
b) Br-34 cell edge adhesive, cure cycle #1, R.T.

Specimen Number	Core Density kg/M³ (lbm/ft³)		P_{ult} kN (lbf)	σ_{ult} MPa (psi)	Description of Failure
1	96 (6)		9.186 (2065)	1.58 (229)	Failed between block and facing
2			5.627 (1265)	0.97 (141)	Failed between block and facing
3			5.783 (1300)	0.99 (144)	Failed between ock and facing
4			11.30 (2540)	1.94 (282)	Facing delamination (localized around cell edges)
5			3.09 (695)	0.53 (77)	Facing delamination (localized around cell edges)
6			11.23 (2525)	1.94 (281)	Facing delamination (localized around cell edges)
7			12.41 (2790)	2.14 (310)	Facing delamination (localized around cell edges)
8			12.86 (2890)	2.21 (321)	Facing delamination (localized around cell edges)
9	↓		17.68 (3975)	3.05 (442)	Failed between facing and core
10	128 (8)		16.22 (3647)	2.79 (405)	Facing delamination (not localized)
11			--	--	Failed immediately at very low load between block and facing
12			--	--	Failed immediately at very low load between block and facing
13	↓		20.68 (4650)	3.57 (517)	Facing delamination
14	96 (6)		19.48 (4380)	3.31 (487)	Facing delamination

TABLE 4. - COEFFICIENTS OF POLYNOMIALS USED TO CURVE FIT DATA

$$\sigma = C_0 + C_1\epsilon + C_2\epsilon^2 + C_3\epsilon^3$$

Standard Numbers	C_0 Pa (psi)	C_1 Pa (psi)	C_2 Pa (psi)	C_3 Pa (psi)	Standard Error of Estimate	
					psi	MPa
Room Temp. Tension 3,4,5, & 19	-3.695 E+4 (-5.359 E+0)	5.012 E+10 (7.269 E+6)	2.293 E+12 (3.325 E+8)	-2.327 E+14 (-3.375 E+10)	792.187	5.46
Room Temp. Compression 14,18,20 & 27	1.964 E+6 (2.848 E+2)	5.047 E+10 (7.320 E+6)	-2.900 E+11 (-4.200 E+7)	-3.330 E+13 (-4.830 E+9)	1609.543	11.10
Low Temp. Tension 6,13,15 & 23	-2.944 E+5 (-4.270 E+1)	6.194 E+10 (8.983 E+6)	3.924 E+10 (5.692 E+6)	-7.619 E+13 (-1.105 E+11)	980.474	6.76
Low Temp. Compression 8,21,25 & 26	-2.450 E+6 (-3.553 E+2)	5.887 E+10 (8.538 E+6)	-5.273 E+11 (-7.648 E+7)	-1.549 E+13 (-2.247 E+9)	1271.968	8.77
High Temp. Tension 7,9,16 & 22	-4.360 E+5 (-6.324 E+1)	5.291 E+10 (7.674 E+6)	8.894 E+11 (1.290 E+8)	-1.430 E+14 (-2.074 E+10)	1399.392	9.65
High Temp. Compression 10,11,12 & 28	4.613 E+6 (6.691 E+2)	4.648 E+10 (6.741 E+6)	7.660 E+11 (1.111 E+8)	-2.372 (-3.441 E+9)	1546.977	10.67

TABLE 5. - SUMMARY OF SANDWICH BEAM FLEXURE TESTS OF $[0,+45,90,-45]_s$ Celion 6000/PMR-15
a) SI UNITS

Specimen Number	Test Condition	Temp. (K)	σ_{ult} (MPa)	$\sigma_{ult_{ave}}$ (MPa)	ε_{ult} (%)	$\varepsilon_{ult_{ave}}$ (%)	$E_{\varepsilon=.002}$ (GPa)	μ (ε=.002)	μ_{ave} ε=.002
3	Tension	R.T.	539.2	565.2	*	*	56.54	0.343	0.333
4			569.2		*			0.312	
5			595.9		*			0.354	
19			556.6		*			0.322	
14	Compression	R.T.	599.0	567.7	-1.391	-1.381	48.95	0.350	0.347
18			590.5		-1.579			0.313	
20			557.9		-1.328			0.356	
27			523.3		-1.227			0.368	
6	Tension	116	579.1	613.5	*	*	61.36	*	0.329
13			*		*			0.343	
15			661.3		*			0.332	
23			600.0		*			0.312	
8	Compression	91.5	666.1	646.2	-1.368	-1.285	56.54	0.334	0.337
21		136	618.9		-1.249			0.345	
25		116	679.2		*			0.313	
26			620.5		-1.237			0.356	
22	Tension	589	318.7	322.8	0.626	0.608	54.47	0.289	0.344
9			317.5		0.580			0.366	
16		597	346.2		0.653			0.354	
7			308.7		0.573			0.367	
10	Compression	589	296.5	334.0	-0.644	-0.657	48.95	0.388	0.382
11			423.0		-0.690			0.376	
12			338.4		-0.696			0.376	
28			278.0		-0.657			0.388	

* - Gage malfunction

Specimen Number	Test Condition	Temp. (°F)	σ_{ult} (ksi)	σ_{ult} (ksi)	ϵ_{ult} (%)	ϵ_{ult} (%)ave	$E_{\epsilon = .002}$ (psi)	μ (ϵ=.002)	μ_{ave} (ϵ=.002)
3	Tension	R.T.	78.20		*			0.343	
4			82.55	81.98	*	*	8.2×10^6	0.312	0.333
5			86.42		*			0.354	
19			80.73		*			0.322	
14	Compression	R.T.	86.87		-1.392			0.350	
18			85.65	82.34	-1.579	-1.381	7.1×10^6	0.313	0.347
20			80.92		-1.328			0.356	
27			75.90		-1.227			0.368	
6	Tension	-250	83.99		*			*	
13			*	88.97	*	*	8.9×10^6	0.343	0.329
15			95.91		*			0.332	
23			87.02		*			0.312	
8	Compression	-295	96.60		-1.368			0.334	
21		-215	89.77	93.72	-1.249	-1.285	8.2×10^6	0.345	0.337
25		-250	98.51		*			0.313	
26			90.00		-1.237			0.356	
22	Tension	600	46.22		0.626			0.289	
9			46.05	46.81	0.580	0.608	7.9×10^6	0.366	0.344
16		615	50.21		0.653			0.354	
7			44.77		0.573			0.367	
10	Compression	600	43.00		-0.644			0.388	
11			61.35	48.44	-0.690	-0.657	7.1×10^6	0.376	0.382
12			49.08		-0.696			0.376	
28			40.33		-0.599			0.388	

* - Gage malfunction

TABLE 6. – SIGNIFICANT PANEL PARAMETERS

a) S.I. Units

Panel No.	V_f (%)	V_v (%)	T_g (cm)	t_h (K)	t_c (cm)	t_{f_1} (cm)	t_{f_2} (cm)	$t_{f_1} + t_{f_2}$ (cm)	t_{ave} per ply (cm)	δ_{max} (cm)	Δt_f (cm)	Δt_h (cm)
7251	62.2	4.3	611	0.77724	0.66944	0.05362	0.05419	0.10781	0.00673	0.00889	0.0051	0.003
7254	61.2	.3	592	0.78344	0.66632	0.05955	0.05757	0.11712	0.00732	0.00940	0.0025	0.003
7256	60.7	.1	605	0.78260	0.66576	0.05814	0.05870	0.11684	0.00732	0.00813	0.0051	0.005
7255	60.3	0	611	0.78402	0.66751	0.05786	0.05870	0.1166	0.00729	0.0109	0.0025	0.005
	(61.1)	(1.175)	(605)	(.78184)	(.66726)	(.05729)	(.11456)	(.0940)	(.00716)	(.00940)	(.00381)	(.004)
7508	63.6	2.5	601	1.3984	1.2923	0.05362	0.05249	0.10612	0.00663	0.00711	0.0025	0.005
75010	58.4	2.4	589	1.4087	1.2969	0.05701	0.05475	0.11176	0.00699	0.00711	0.0051	0.013
75912	63.9	1.9	606	1.4052	1.2972	0.05390	0.05419	0.10809	0.00676	0.01190	0.0051	0.005
	(62)	(2.27)	(599)	(1.4041)	(1.2954)	(.05433)	(.05433)	(.10866)	(.00653)	(.00864)	(.00592)	(.008)
77516	61	.2	614	2.0368	1.9208	0.05786	0.05814	0.11600	0.00724	--	0.0025	0.005
77517	59.3	.4	607	2.0360	1.9174	0.05926	0.05926	0.11852	0.00742	--	0.0025	0.005
77518	63.1	.9	611	2.0317	1.9169	0.05842	0.05644	0.11486	0.00719	0.01118	0.0051	0.005
	(61.1)	(.5)	(611)	(2.0348)	(1.9184)	(.05824)	(.05824)	(.11646)	(.00728)	(.01118)	(.00338)	(.005)
710019	59.5	.4	612	2.6883	2.5719	0.05814	0.05842	0.11656	0.00728	0.00711	0.0051	0.005
710020	60.6	0	600	2.6838	2.5686	0.05786	0.05729	0.11514	0.00720	0.00940	0.0025	0.005
710021	63.5	.2	622	2.6839	2.6839	0.05786	0.05842	0.11628	0.00727	0.01067	0.0051	0.005
	(61.2)	(.2)	(611)	(2.6465)	(2.5694)	(.05795)	(.05804)	(.00724)	(.00724)	(.00914)	(.0042)	(.005)

( ) – average of replicate specimens

66

TABLE 6. - SIGNIFICANT PANEL PARAMETERS

b) U.S. Customary Units

Panel No.	v_f (%)	v_v (%)	T_g (°F)	t_h (in)	t_c (in)	t_{f_1} (in)	t_{f_2} (in)	$t_{f_1} + t_{f_2}$ (in)	t_{ave} per ply (in)	δ_{max} (in)	Δt_f (in)	Δt_h (in)
7251	62.2	4.3	640	0.30600	0.26357	0.02111	0.02133	0.04244	0.00265	0.0035	0.002	0.001
7254	61.2	.3	606	0.30844	0.26233	0.02344	0.02267	0.04611	0.00288	0.0037	0.001	0.001
7256	60.7	.1	630	0.308111	0.26211	0.02289	0.02311	0.04600	0.00288	0.0032	0.002	0.002
7255	60.3	0	640	0.30867	0.26280	0.02278	0.02311	0.04589	0.0043	0.00287	0.001	0.002
	(61.1)	(1.175)	(629)	(.30781)	(.26270)	(.02256)	(.02256)	(.04510)	(.00282)	(.0037)	(.0015)	(.0015)
7508	63.6	2.5	622	0.55056	0.50878	0.02111	0.02067	0.041778	0.002611	0.0028	0.001	0.002
75010	58.4	2.4	600	0.55460	0.51060	0.02244	0.02156	0.04406	0.00275	0.0028	0.002	0.005
75912	63.9	1.0	631	0.55322	0.51070	0.02122	0.02133	0.042556	0.00266	0.0047	0.002	0.002
	(62)	(2.27)	(618)	(.55280)	(0.510)	(.02139)	(.02139)	(.042778)	(.00257)	(.0034)	(.00233)	(.003)
77516	61	.2	646	0.30189	0.75622	0.02278	0.02289	0.04567	0.00285	--	0.001	0.002
77517	59.3	.4	633	0.30156	0.75489	0.02333	0.02333	0.04666	0.00292	--	0.001	0.002
77518	63.1	.9	640	0.7999	0.57467	0.02300	0.02222	0.04522	0.00283	0.0044	0.002	0.002
	(61.1)	(.5)	(640)	(.80112)	(0.02293)	(.02293)	(.02293)	(.04585)	(.002867)	(.0044)	(.00133)	(.002)
710019	59.5	.4	642	1.0584	1.01256	0.02289	0.02300	0.04589	0.002868	0.0028	0.002	0.002
710020	60.6	0	621	1.0566	1.01127	0.02278	0.02256	0.04533	0.002833	0.0037	0.001	0.002
710021	63.5	.2	660	1.05667	1.05667	0.02278	0.02300	0.04578	0.002861	0.0042	0.002	0.002
	(61.2)	(.2)	(641)	1.01158	(1.01158)	.022815	.022852	(.04567)	(.00285)	(.0036)	(.00167)	(.002)

( ) - average of replicate specimens

TABLE 7. - SUMMARY OF ROOM TEMPERATURE WRINKLING PANEL RESULTS

$([0,\pm 45,90]_s$ Celion 3000/PMR-15 facings and HRH-327-3/8-4 Glass/PI core)

Panel No.	Core Thickness t_c cm (in)	$E_{\epsilon=.002}$ GPa (psi)	Max. Back-to-Back Strain Variation $\left(\dfrac{\Delta\epsilon}{\epsilon}\right)$ (%) $\epsilon=.006$	Theoretical Wrinkling Stress			Experimental		
				eq.D.4	MPa (ksi) eq.D.5	eq.D.6 (δ=.004in)	σ_{ult} MPa (ksi)	$\epsilon_y]t$ (%)	Pult kN (lb)
7508	1.27 (0.50)	53.4 (7.75x10⁶)	16.7	292.3 (42.4)	723.9 (105.)	484.0 (70.2)	454.7 (65.95)	0.89	159.3 (35820)
7510	→	54.0	11.0	→	→	→	447.5 (64.90)	0.88	165.1 (37120)
7512		58.6 (8.5x10⁶)	15.0				455.1 (66.00)	0.83	161.3 (36270)
77516	1.91 (0.75)	52.9 (7.67x10⁶)	25.0	240.6 (34.9)	597.1 (86.6)	446.1 (64.7)	356.1 (51.66)	0.70	136.4 (30670)
77517	→	52.9 (7.67x10⁶)	16.7	→	→	→	374.6 (54.33)	0.78	146.6 (32960)
77518		53.8 (8.00x10⁶)	20.0				332.2 (48.18)	0.66	126.0 (28320)
710019	2.54 (1.00)	50.5 (7.33x10⁶)	18.0	207.5 (30.1)	515.7 (74.8)	411.6 (59.7)	365.8 (53.06)	0.77	141.0 (31650)
710020	→	54.0 (7.83x10⁶)	40.0	→	→	→	276.5 (40.11)	0.54	105.1 (23640)
710021		54.0 (7.83x10⁶)	27.0				289.9 (42.05)	0.57	111.3 (25020)

Theoretical Dimpling Stress Range: 409.7 MPa (59.42 ksi) to 641.2 MPa (93.0 ksi)
Laminate Strength: 576 MPa (82.3 ksi)
Ultimate Strain: 1.4 percent

TABLE 8. - SUMMARY OF ROOM TEMPERATURE RESULTS OF OVERALL BUCKLING PANELS

$(T_c \quad 0.635 \text{ cm } (0.25 \text{ in.}))$

Panel No.	Experimental Results				Theoretical
	P_{cr} kN (lbf)	P_{ult} kN (lbs)	σ_{cr} MPa (ksi)	σ_{ult} MPa (ksi)	σ_{cr} MPa (ksi)
7251[1]	76.09 (17,105)	82.75 (18,600)	213.7 (31.00)	232.4 (33.72)	264.7 (38.39)
7254	93.33 (20,981)	97.64 (21,950)	241.3 (35.00)	252.5 (36.62)	
7255	97.92 (22,013)	102.50 (23,040)	254.4 (36.90)	266.3 (38.63)	
7256	114.38 (25,714)	118.76 (26,700)	296.5 (43.00)	307.8 (44.65)	

[1]Panel exposed to excessive temperature during instrumentation

69
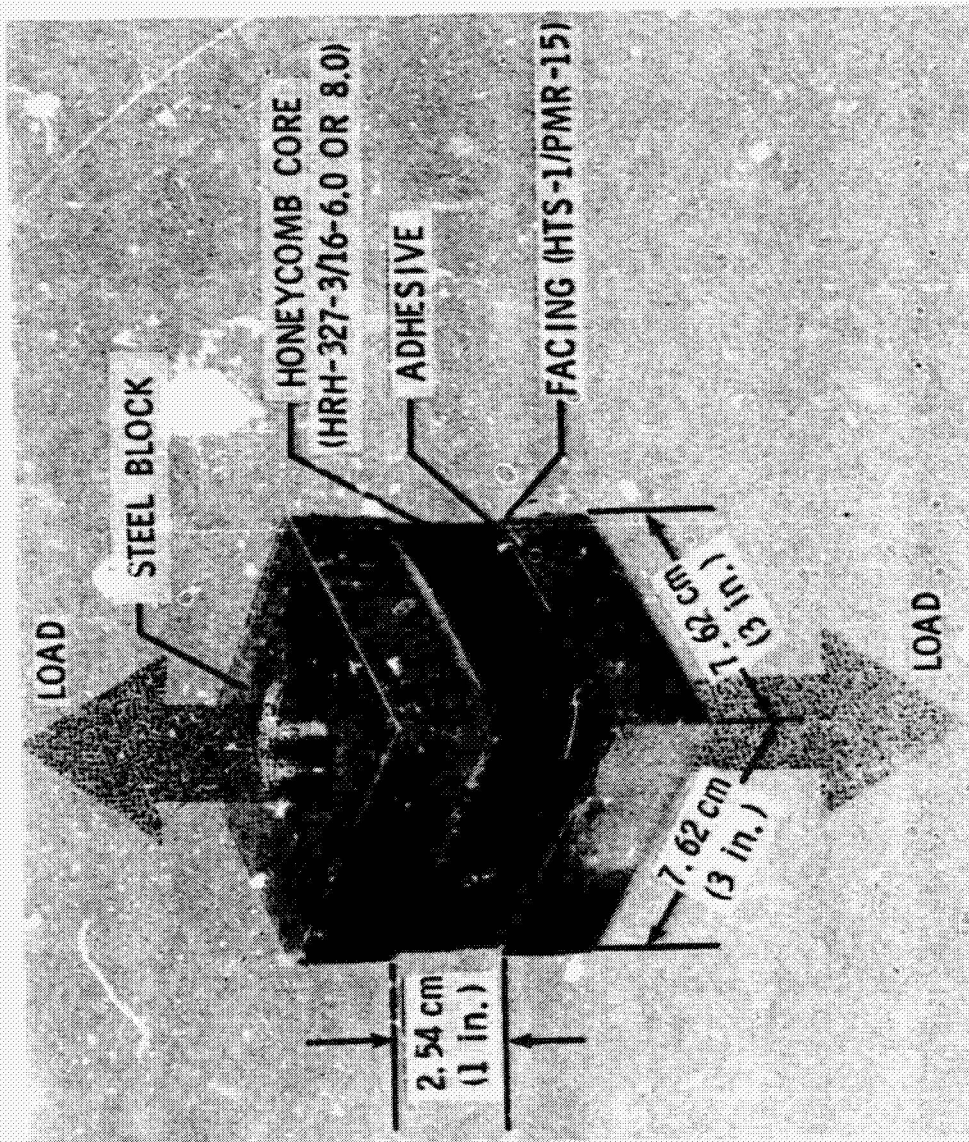
Figure 1.- Schematic diagram of flatwise tensile specimen.
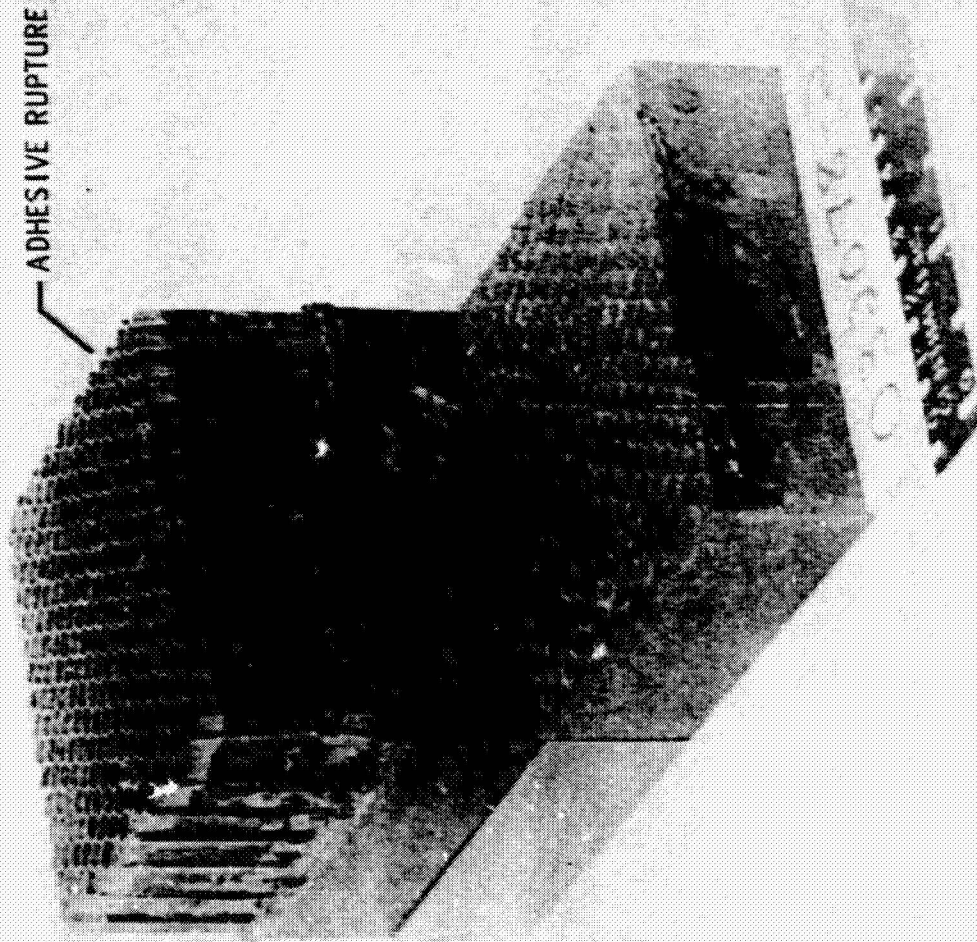
Figure 2.- Failed flatwise tensile specimen; failure occurs between facing and core: (Room temperature, σ_{cr} = 4.02 MPa (583 psi), FM-34 film adhesive).

71

FACING DELAMINATION
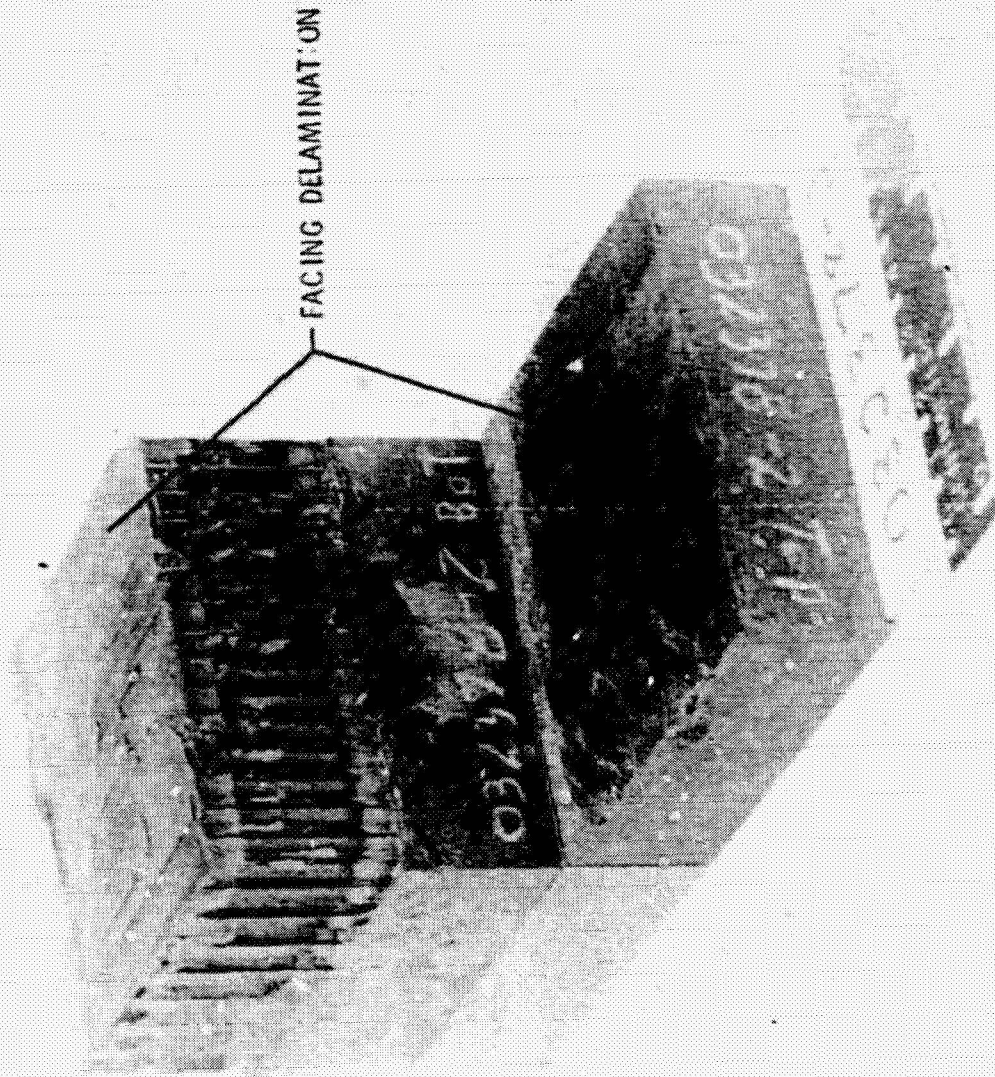
Figure 3.- Failed flatwise tensile specimen; failure occurs by facing delamination. (Room temperature, $\sigma_{cr} = 4.00$ MPa (580 psi), FM-34 film adhesive).

LOCAL FACING
DELAMINATION
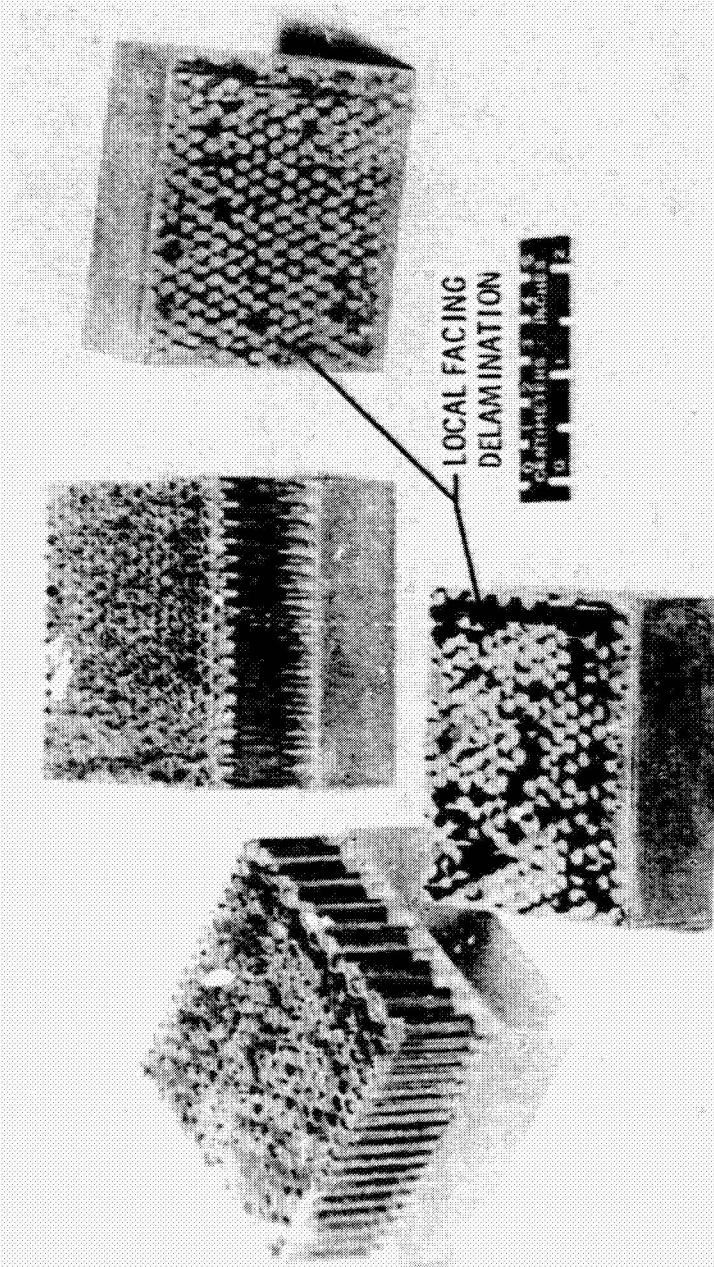
Figure 4.- Failed flatwise tensile specimens; failure occurs by local facing delamination about honeycomb cell edges. (Room temperature, BR-34 liquid cell-edge adhesive).

73

HRH-327-3/16-8
Glass/PI Honeycomb

[0, +45, 90, -45]$_s$
Celion 6000/PMR-15

[0$_2$, +45, 90, -45]$_s$
Celion 6000/PMR-15
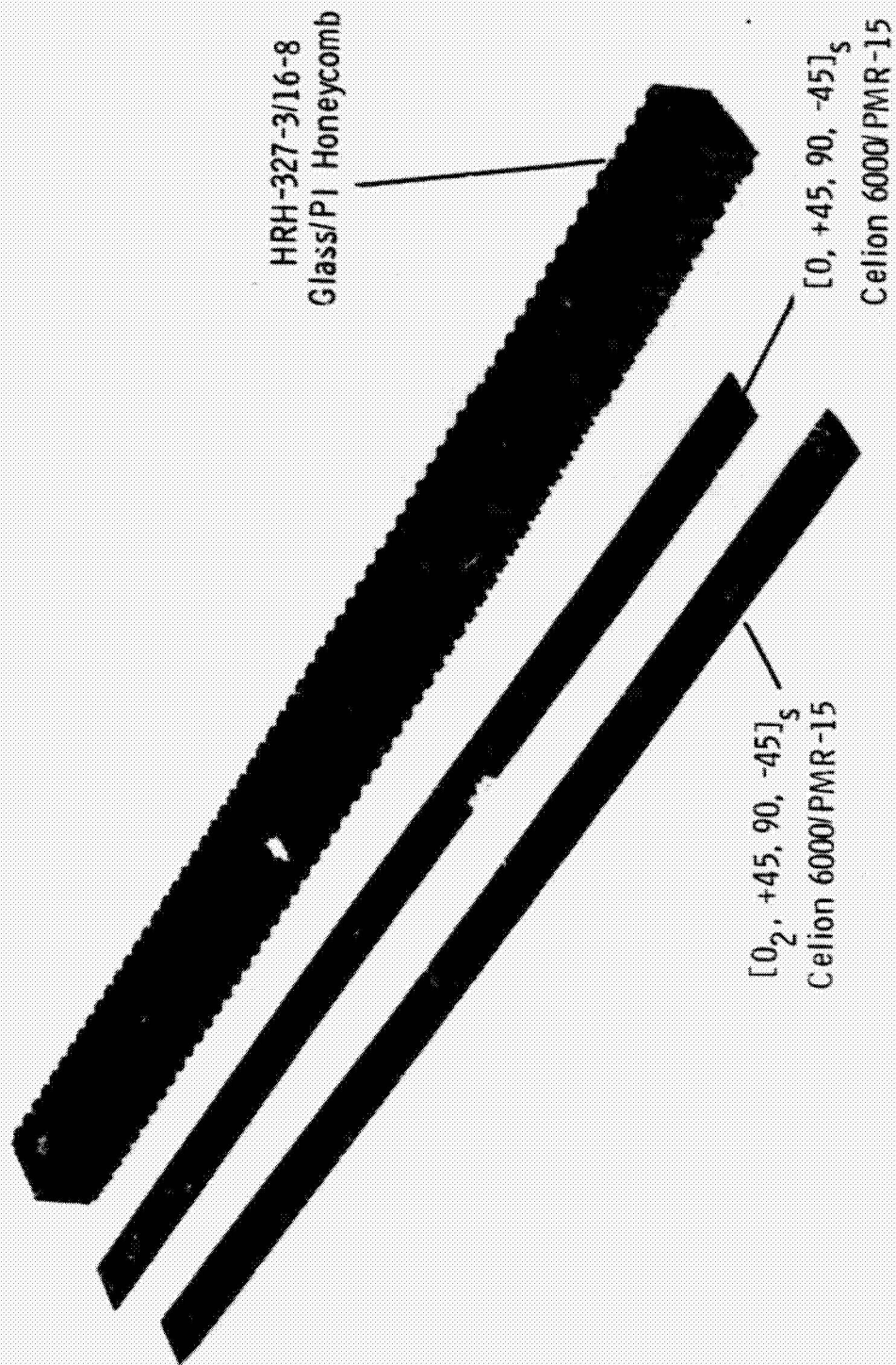
Figure 5.- Sandwich beam constituents.

Figure 6. - Sandwich beam flexure specimen.
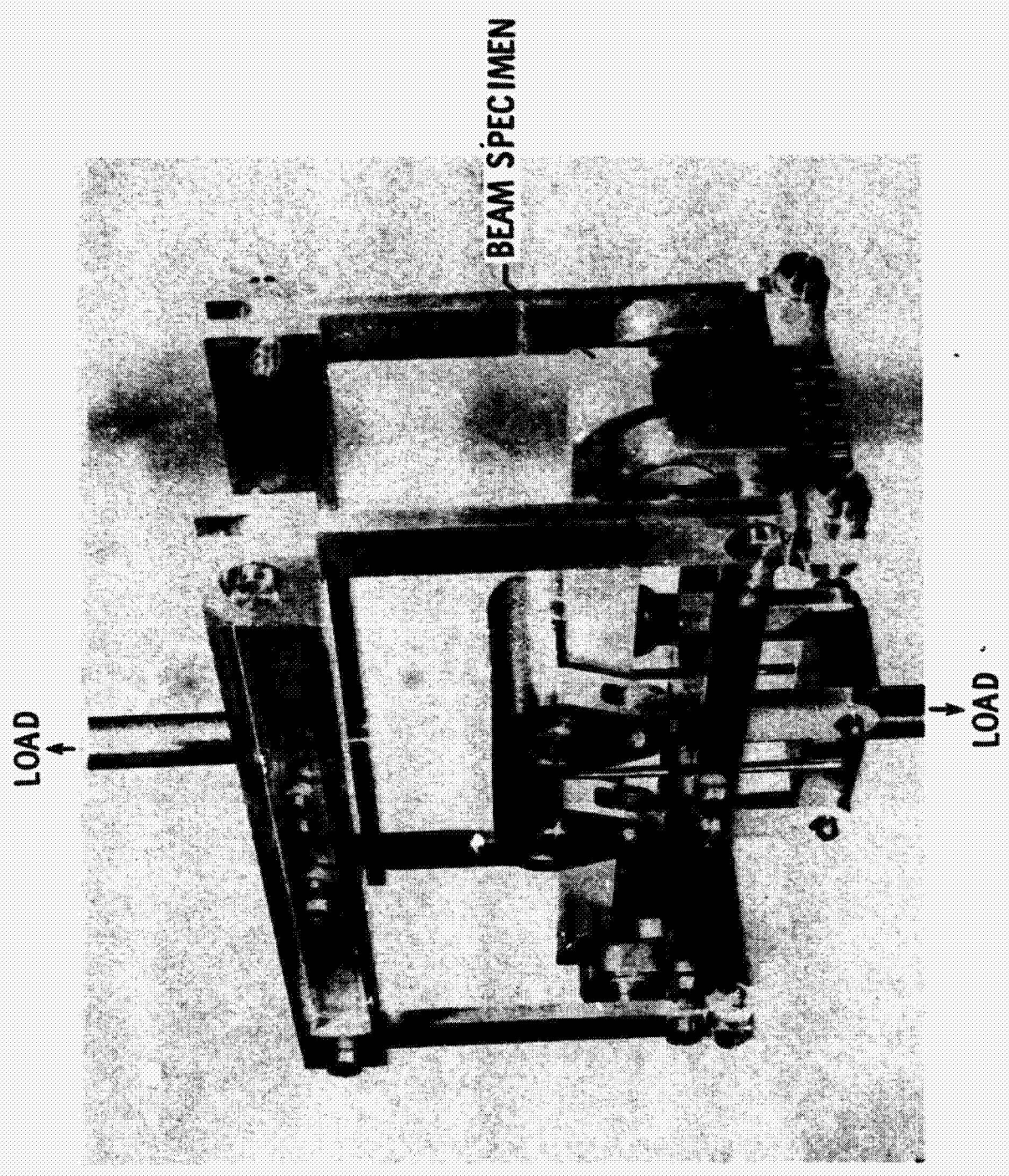
Figure 7.- Four-point bending test apparatus.
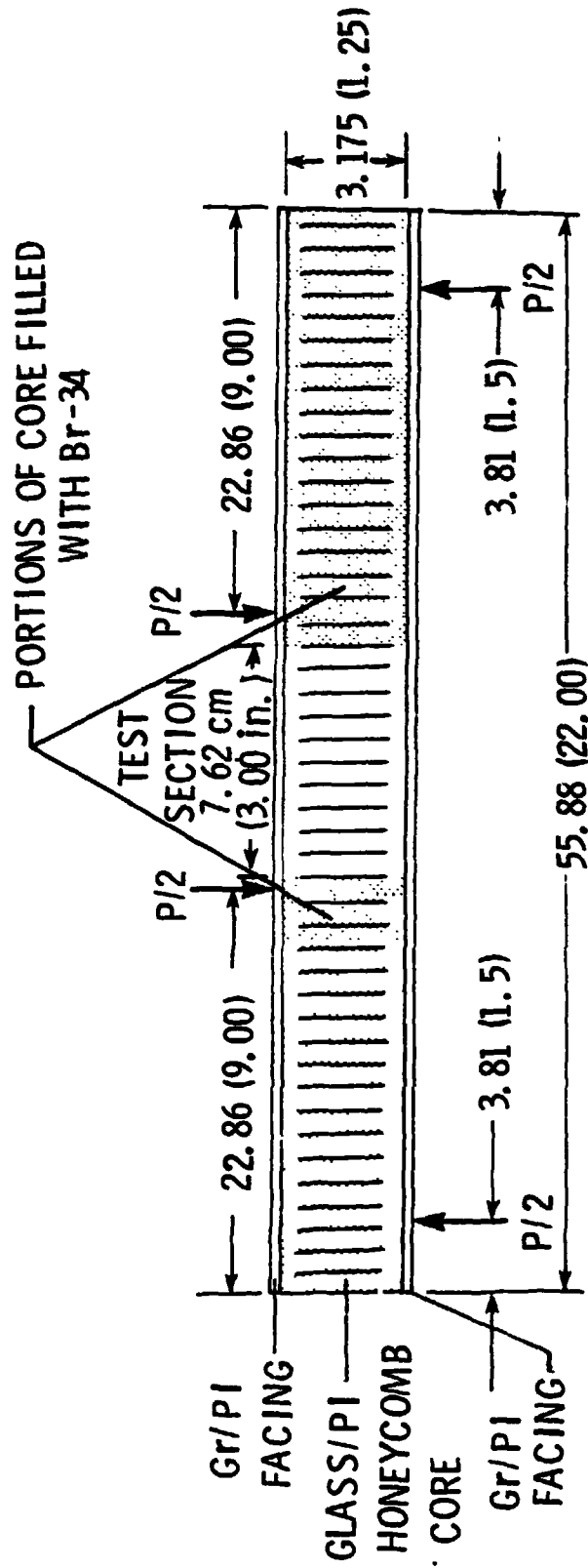
Figure 8. – Sandwich beam in four-point bending.

ALL UNITS IN cm (in.)

PORTIONS OF CORE FILLED WITH Br-34

TEST SECTION 7.62 cm (3.00 in.)

P/2

P/2

P/2

P/2

22.86 (9.00)

22.86 (9.00)

3.175 (1.25)

3.81 (1.5)

3.81 (1.5)

55.88 (22.00)

Gr/PI FACING

GLASS/PI HONEYCOMB CORE

Gr/PI FACING

77
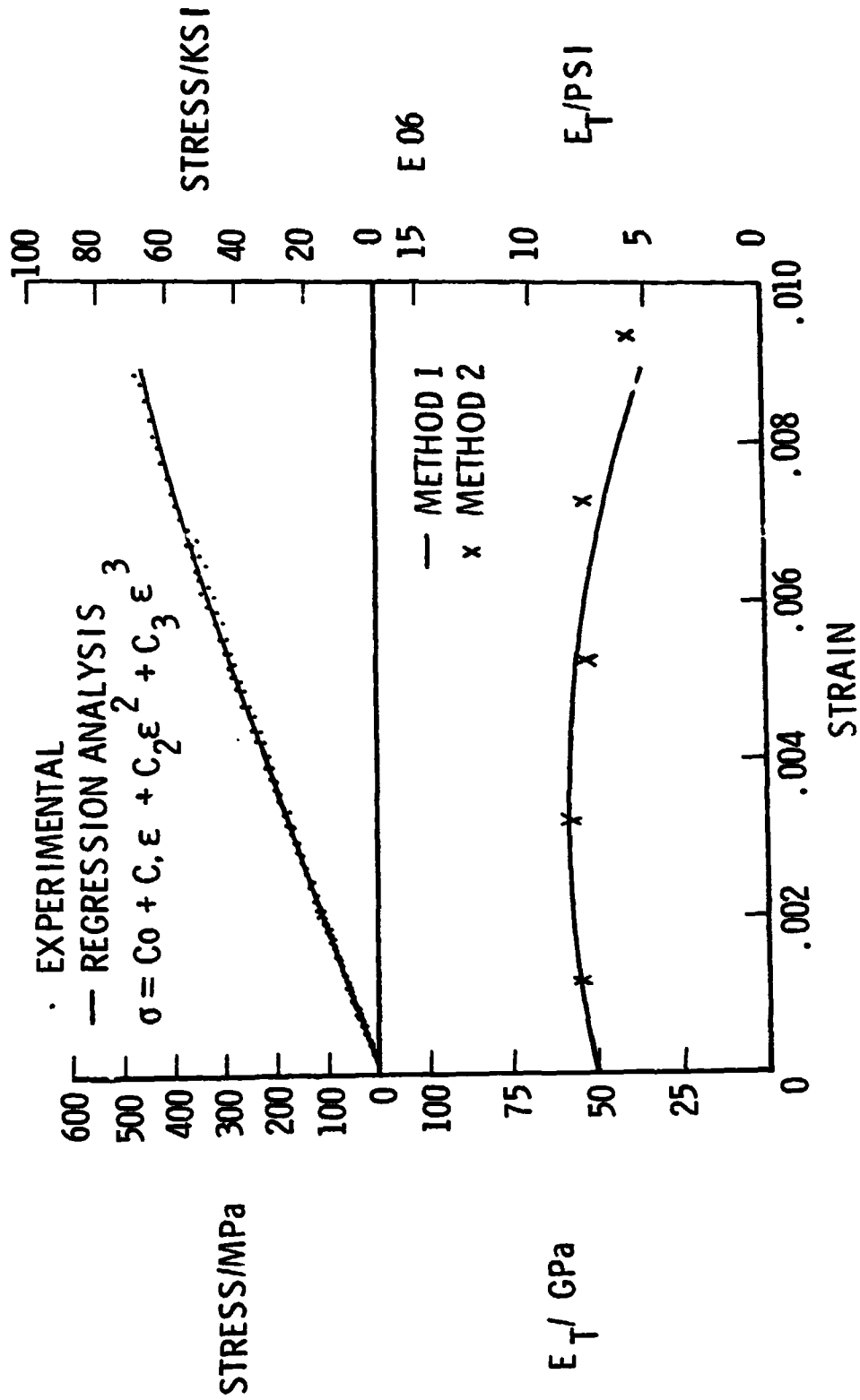
Figure 9.- Tensile stress - and tangent modulus - vs. - strain behavior of [0, +45, 90, -45]s Celion 6000/PMR-15 at room temperature (tests 3, 4, 5, and 19).
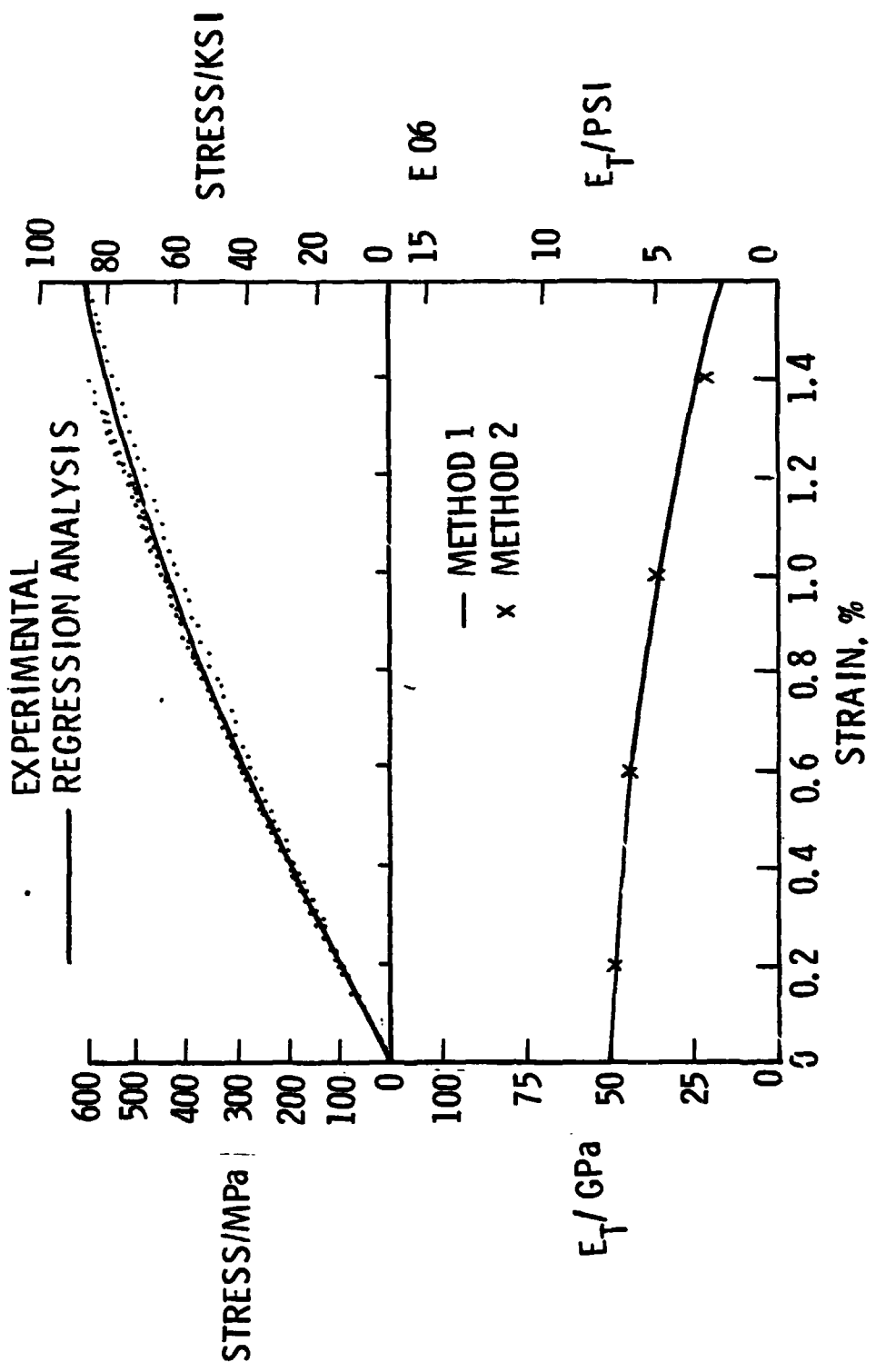
Figure 10.- Compressive stress-and tangent modulus-vs.-strain behavior of $[0,+45,90,-45]_s$ Celion 6000/PMR-15 at room temperature (tests 14,18,20, and 27).
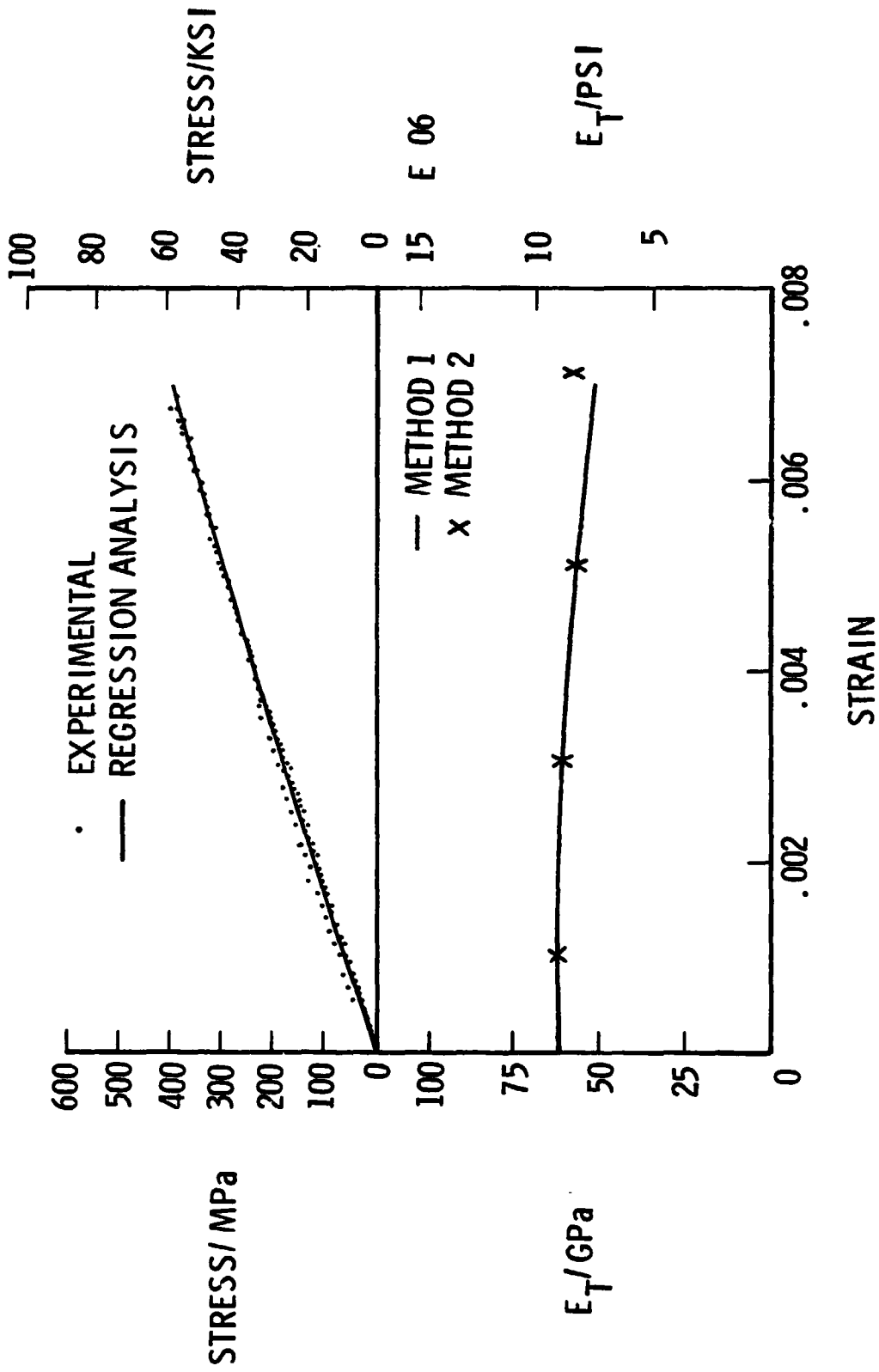
Figure 11.- Tensile stress - and tangent modulus - vs. - strain behavior of [0, +45, 90, -45]s Celion 6000/PMR-15 at 116K ¦ (-250° F) (tests 6, 13, 15, and 23).
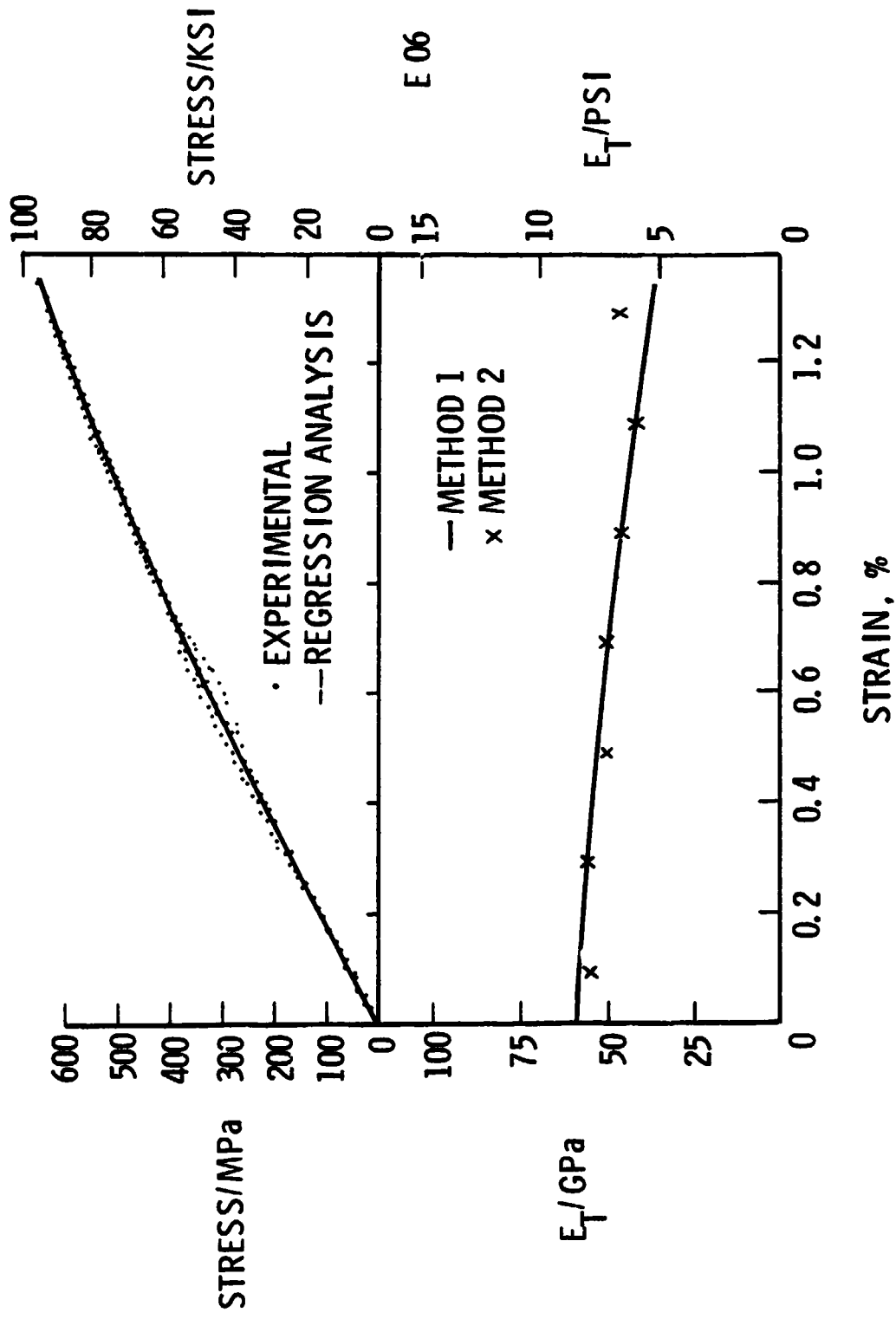
Figure 12.– Compressive stress–and tangent modulus–vs.–strain behavior of $[0,+45,90,-45]_s$ Celion 6000/PMR–15 at 116K (–250°F) (tests 8,21,25, and 26).
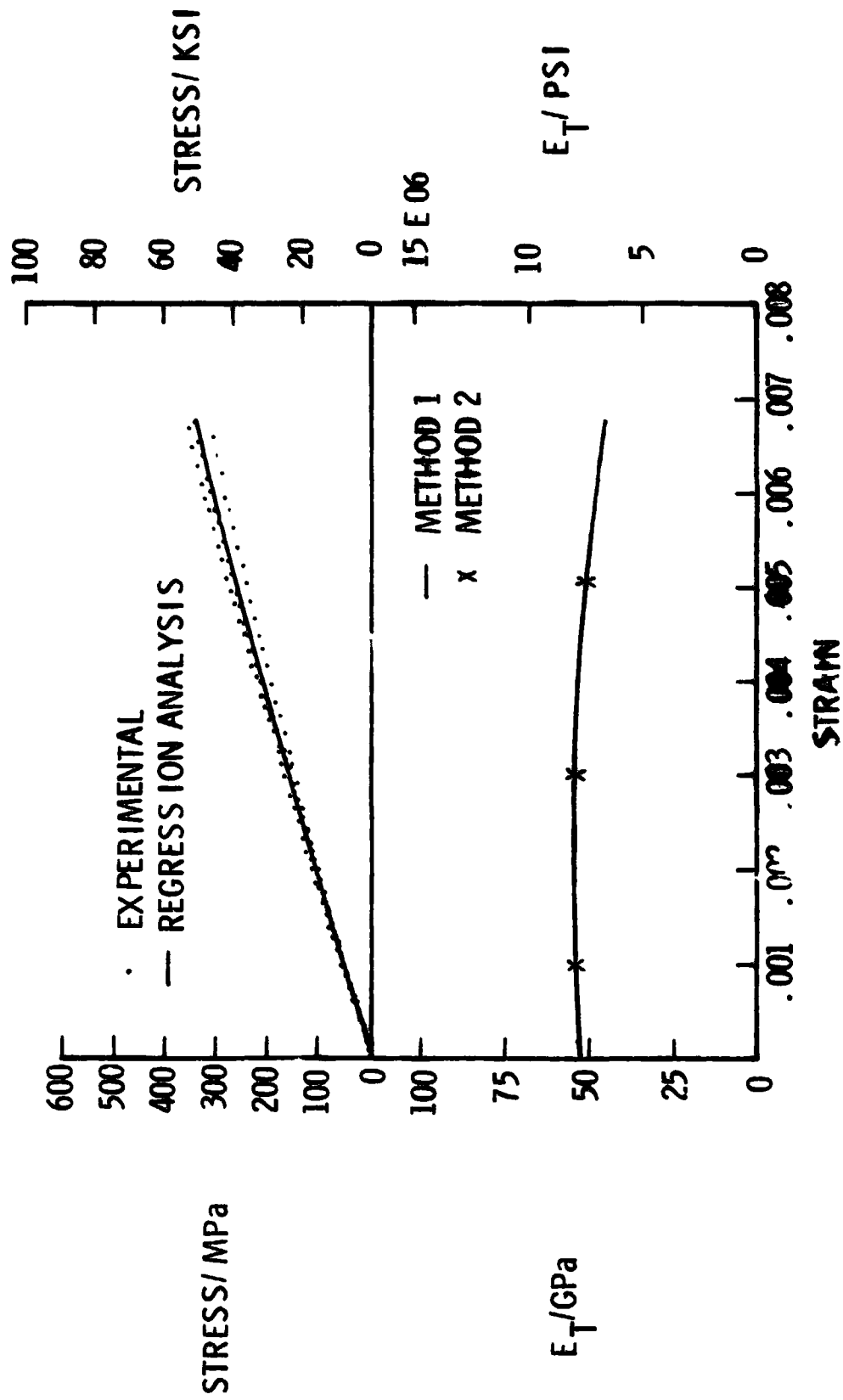
Figure 13.- Tensile stress - and tangent modulus - vs. strain behavior of [0, +45, 90, -45]s Celion 6000/PMR-15 at 589K. (600° F) (tests 22, 9, 16, and 7).
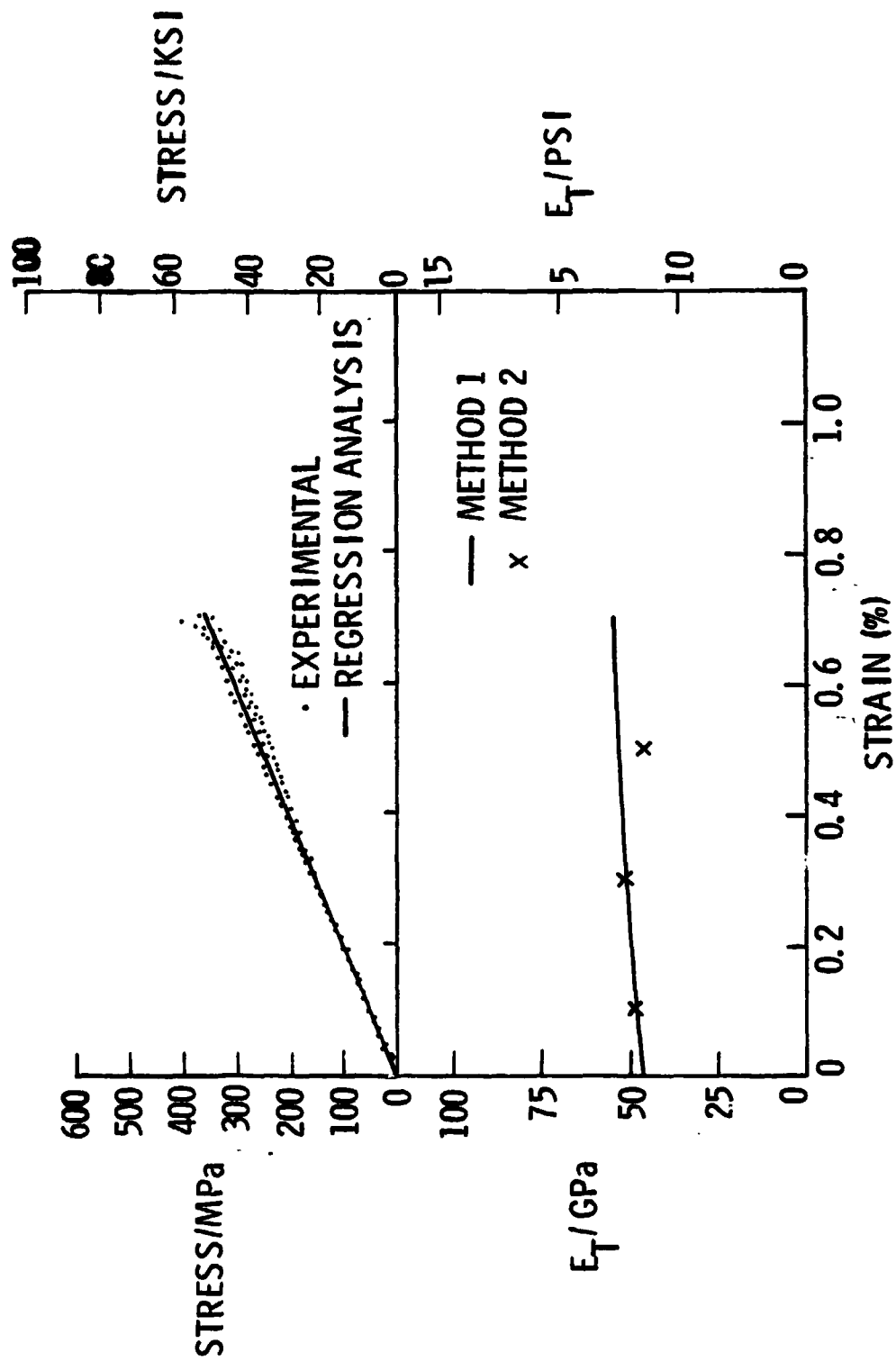
Figure 14. - Compressive stress-and tangent modulus-vs. strain behavior of [0,+45,90,-45]$_s$ Celion 6000/PMR-15 at 589K (600°F) (tests 10,11,12, and 28).

[0, +45, 90, -45]$_s$
Celion 6000/PMR-15

[0$_2$, +45, 90, -45]$_s$
Celion 6000/PMR-15

Figure 15.- Failed sandwich beam flexure specimen, tensile test.

84

C - 2
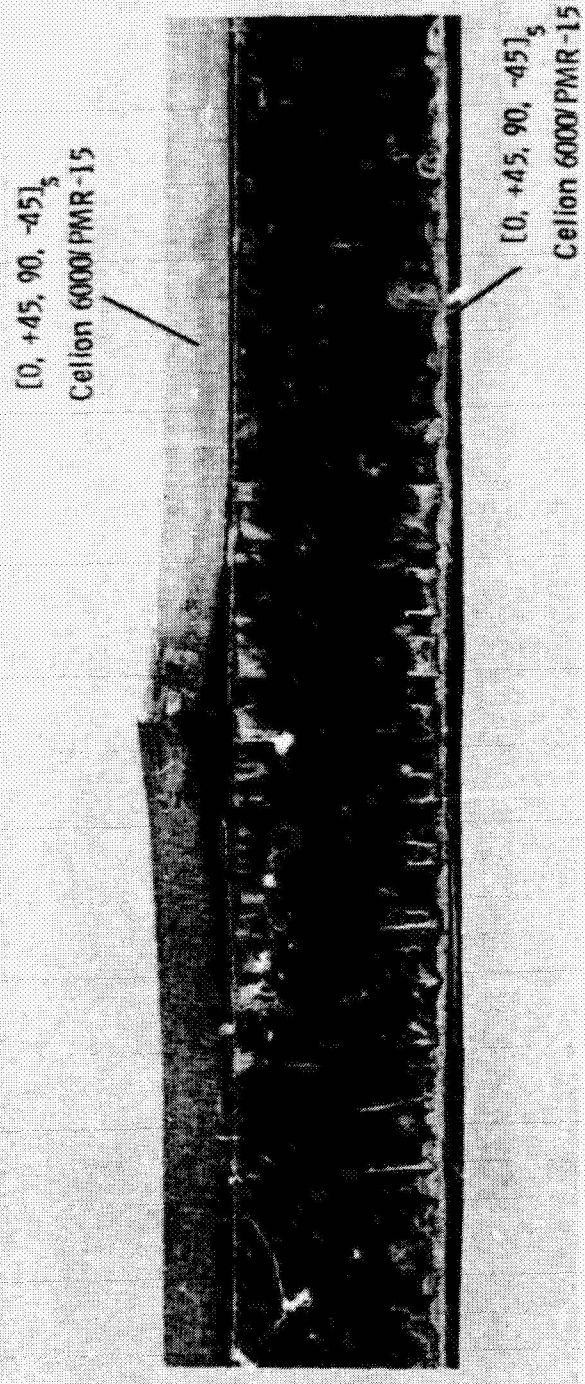
Figure 16.- Failed sandwich beam flexure specimen, compressive test.

85
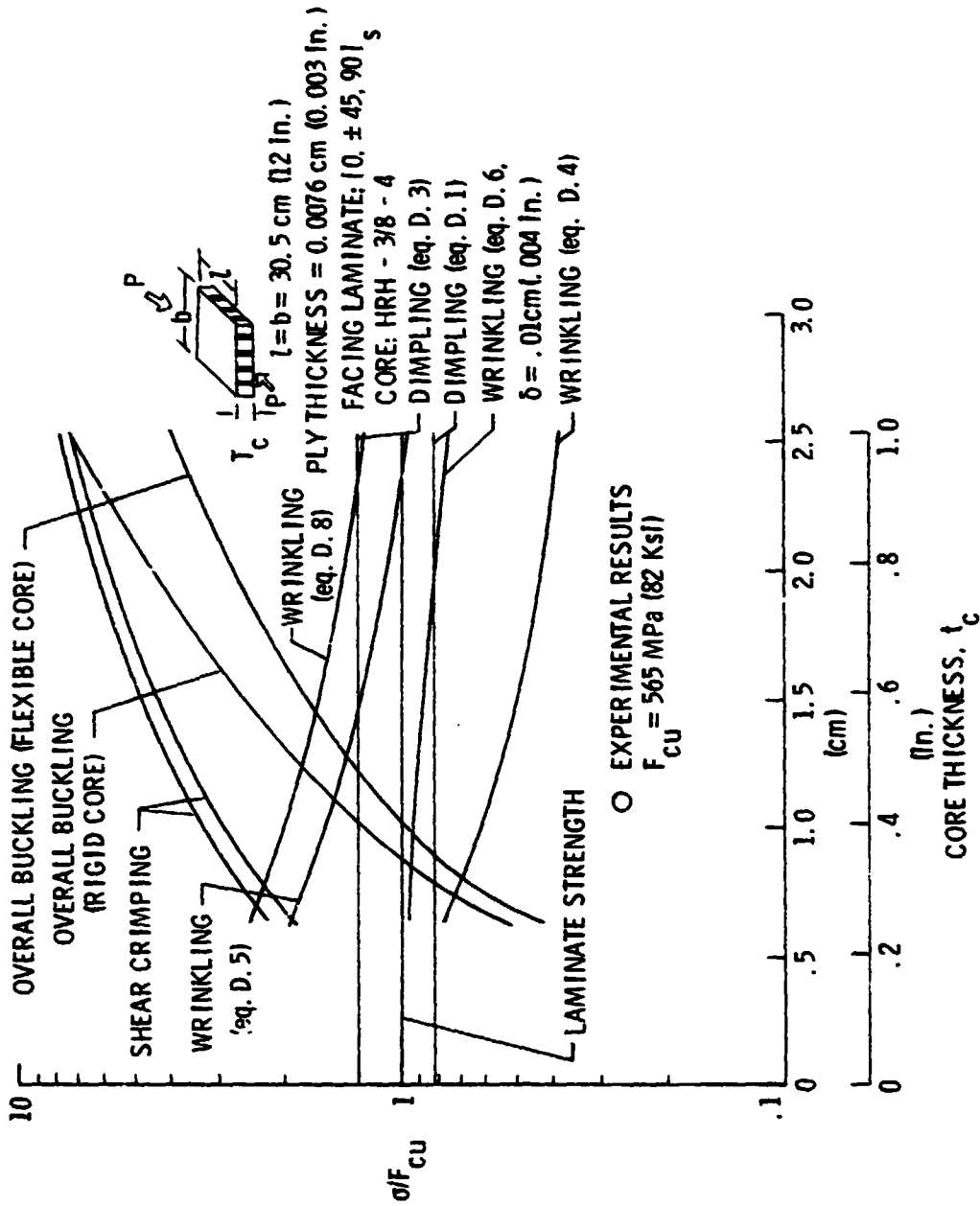
Figure 17.- Design envelope for graphite/polyimide sandwich panel with glass/polyimide honeycomb core simply-supported along all edges and subject to an edgewise compressive load.
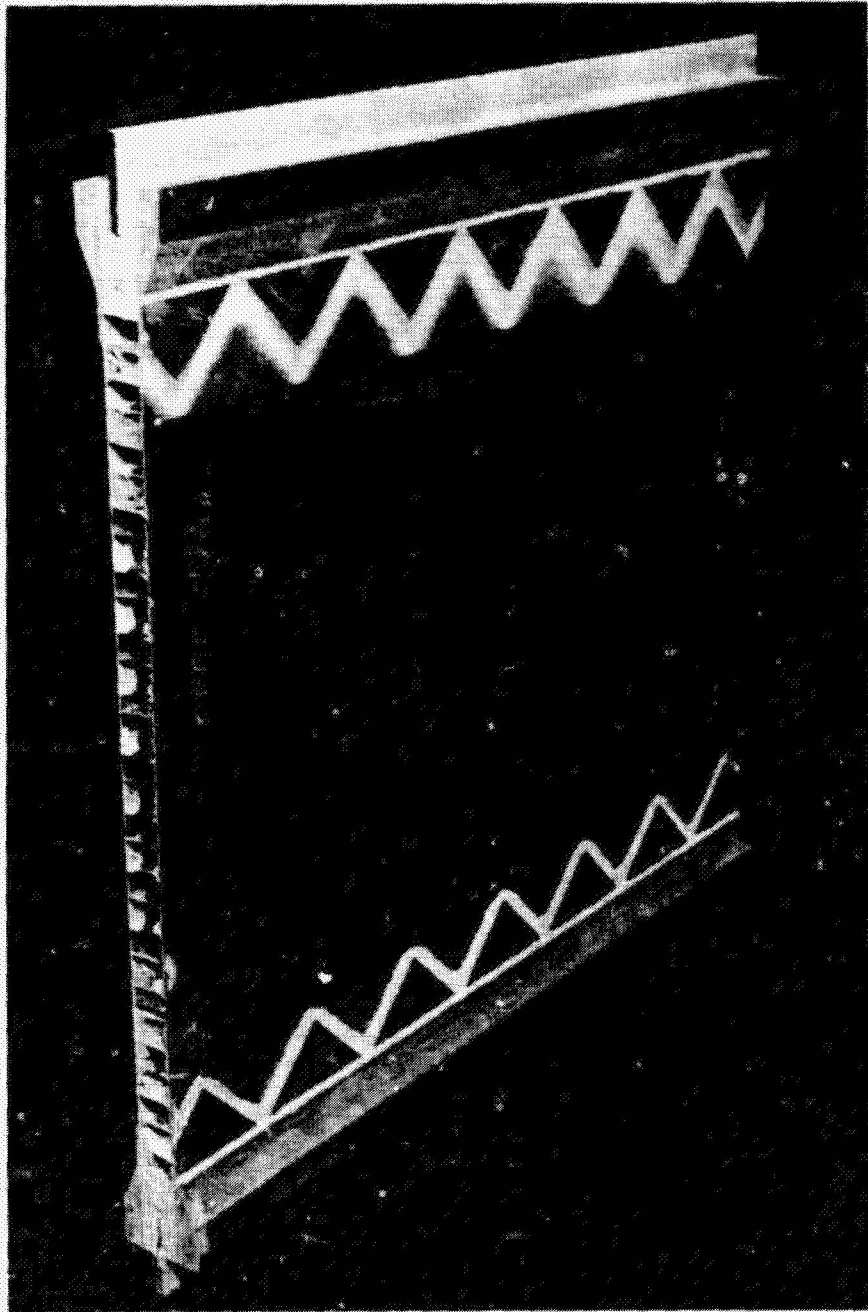
Figure 18.- Buckling specimen.

LOAD BLOCK

R=1.91 cm (0.75 In.)

R=0.79 cm (.313 In.)

KNIFE EDGE

ALIGNMENT SHEET

END TAB

Br-34 POTTING

GLASS/PI HONEYCOMB
CORE

SCALLOPED DOUBLER

Gr/PI FACING

C_L
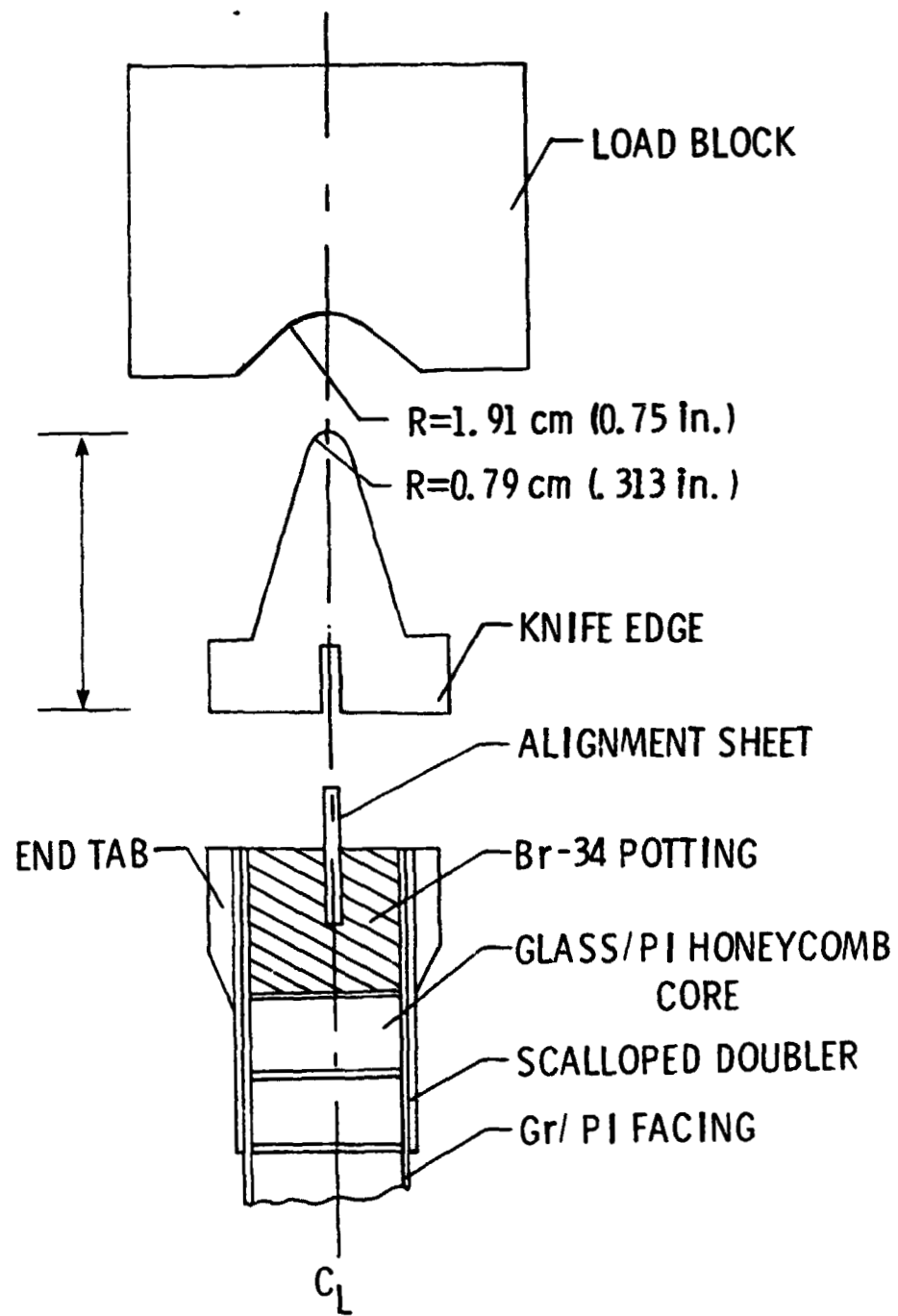
(a) End supports.

Figure 19.- Technique for simply-supporting panel.

88

Z-SECTION BEAM
SUPPORT

KNIFE EDGE
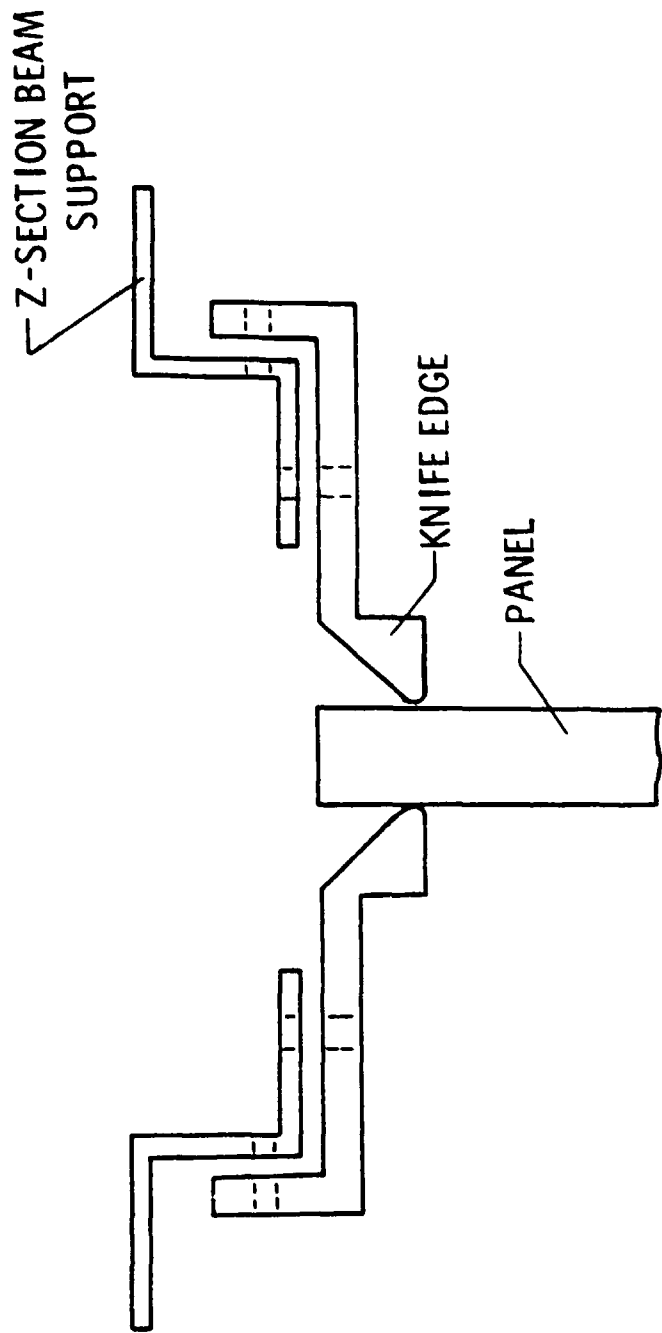
PANEL

(b) Side supports.

Figure 19.- Concluded.

89
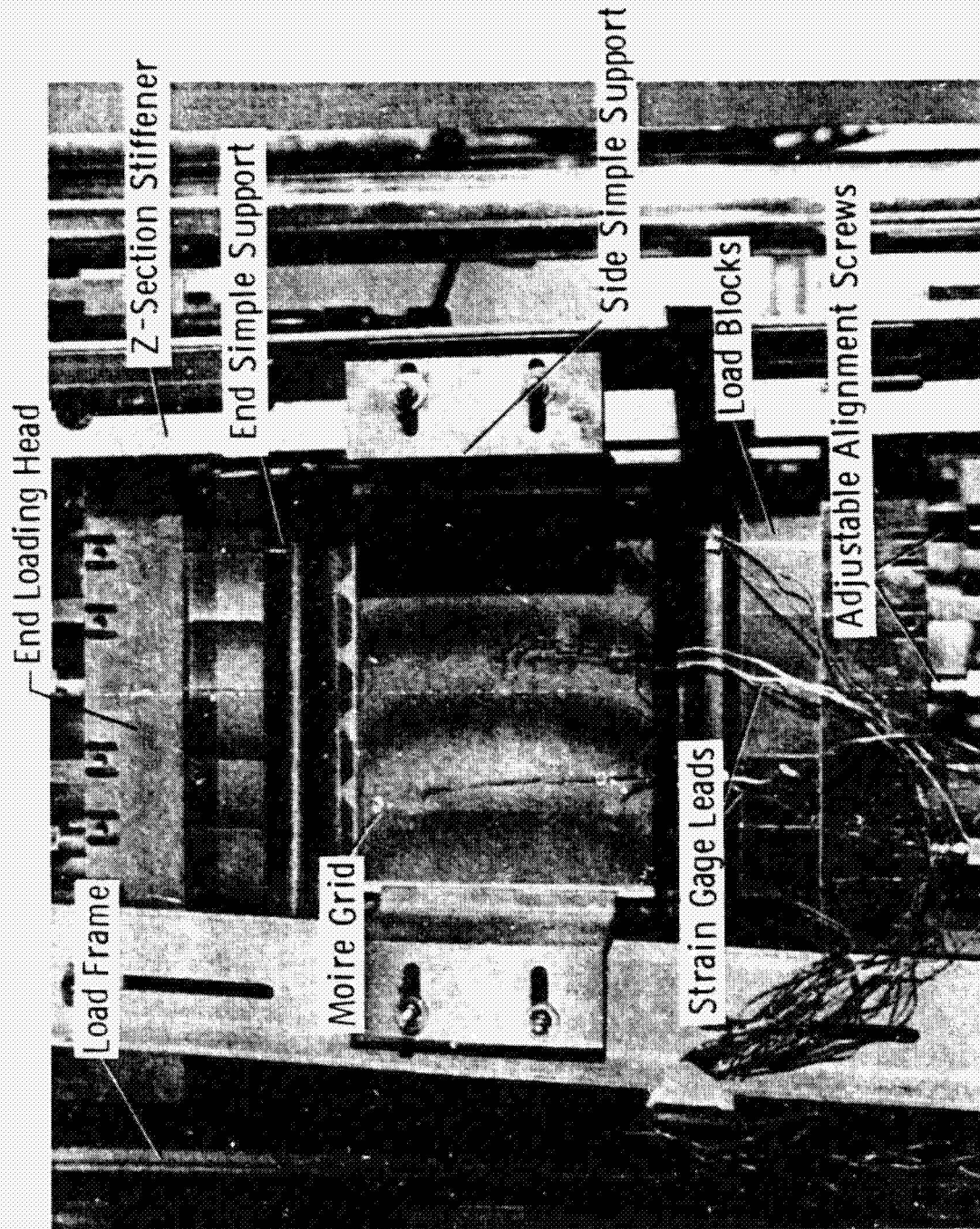
Figure 20. - Buckling specimen in test fixture.

90
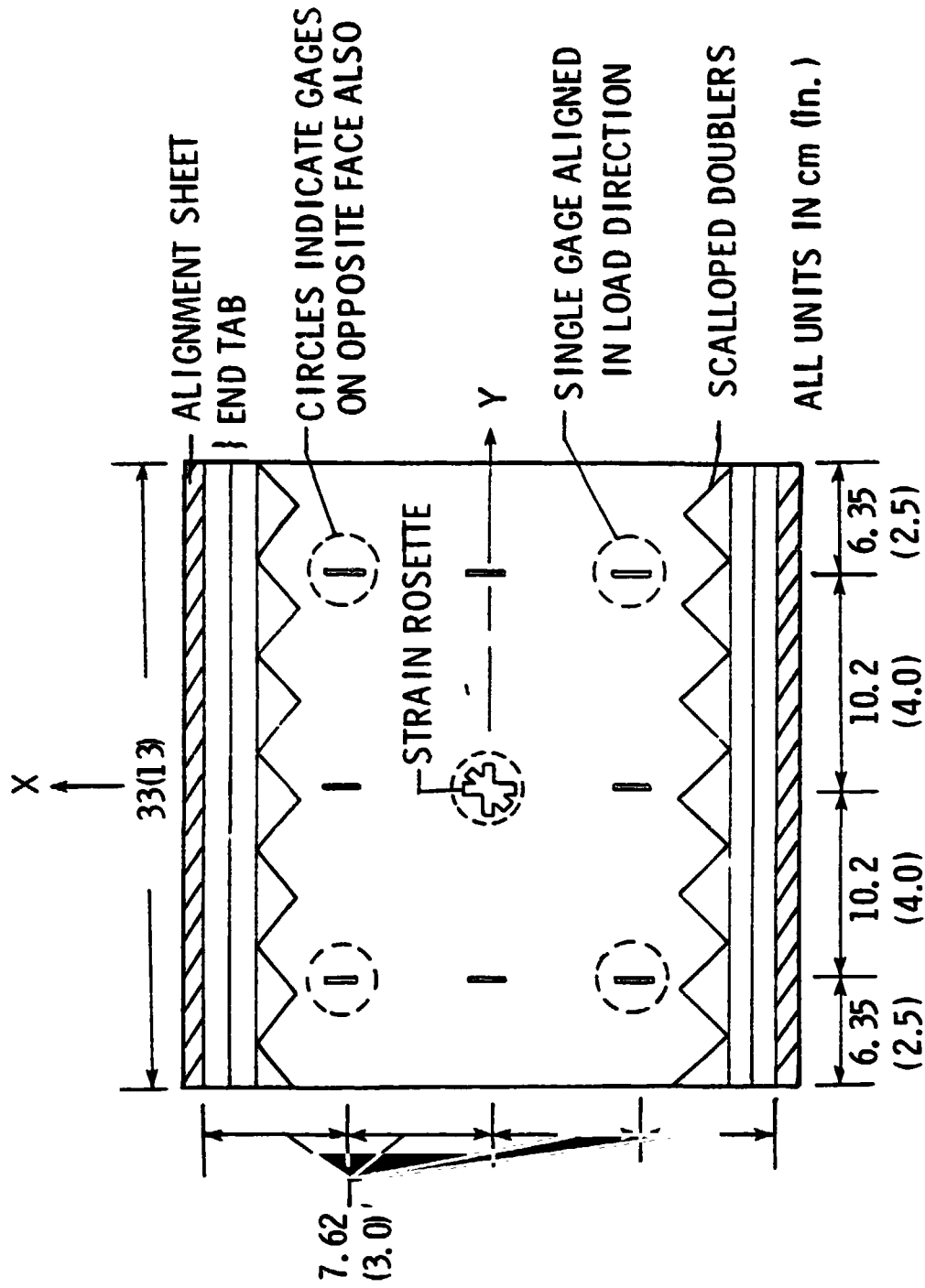
Figure 21.- Schematic diagram of strain gage locations on buckling specimens.

91
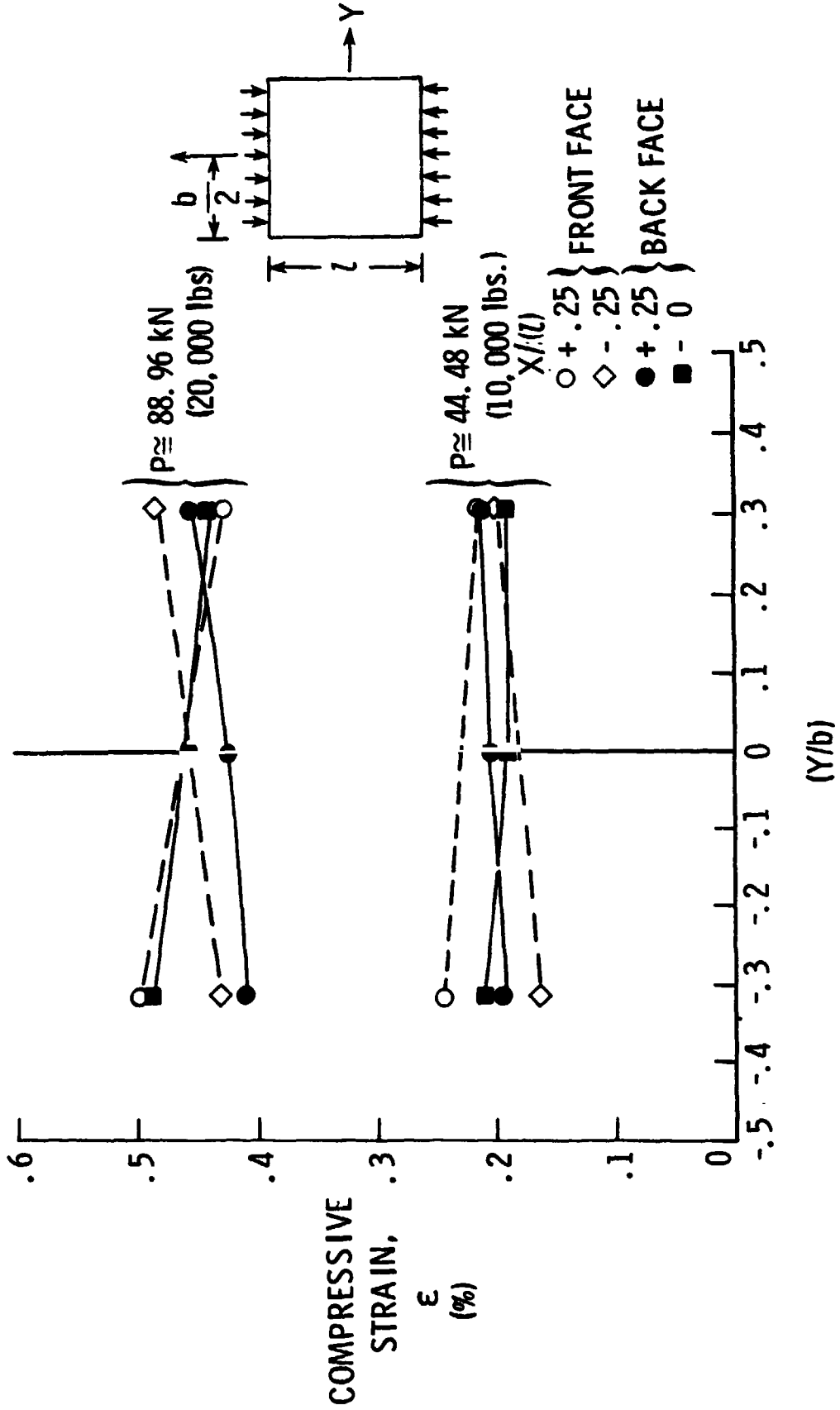
(a) Panel number 77518

Figure 22.- Strain variation across panel width during loading.
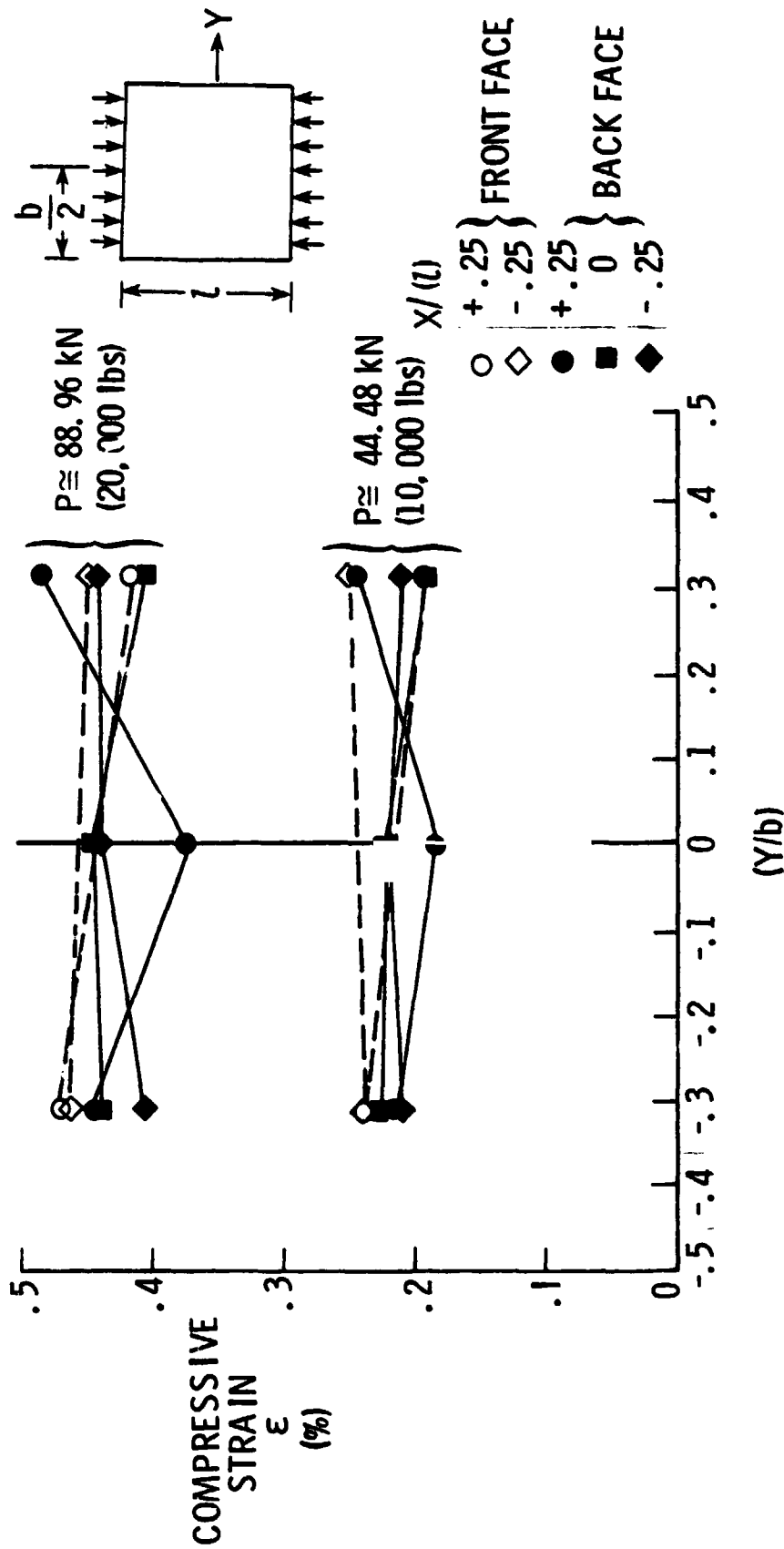
(b) Panel number 77517

Figure 22. - Concluded.

93
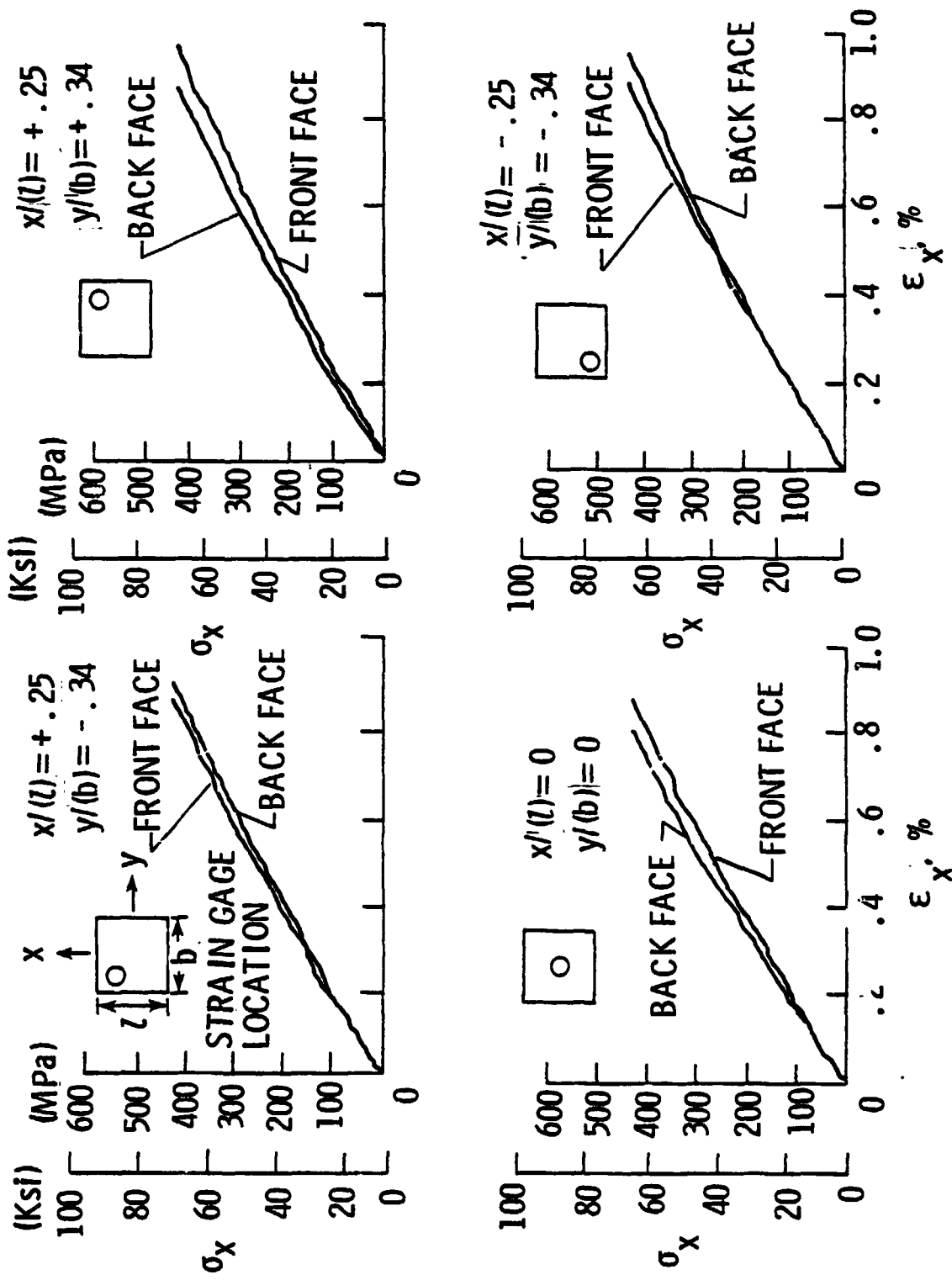
Figure 23.- Back-to-back stress-vs.-strain results at four locations on the wrinkling specimens.

(a) Panel number 75010

94

PANEL NO. 75012
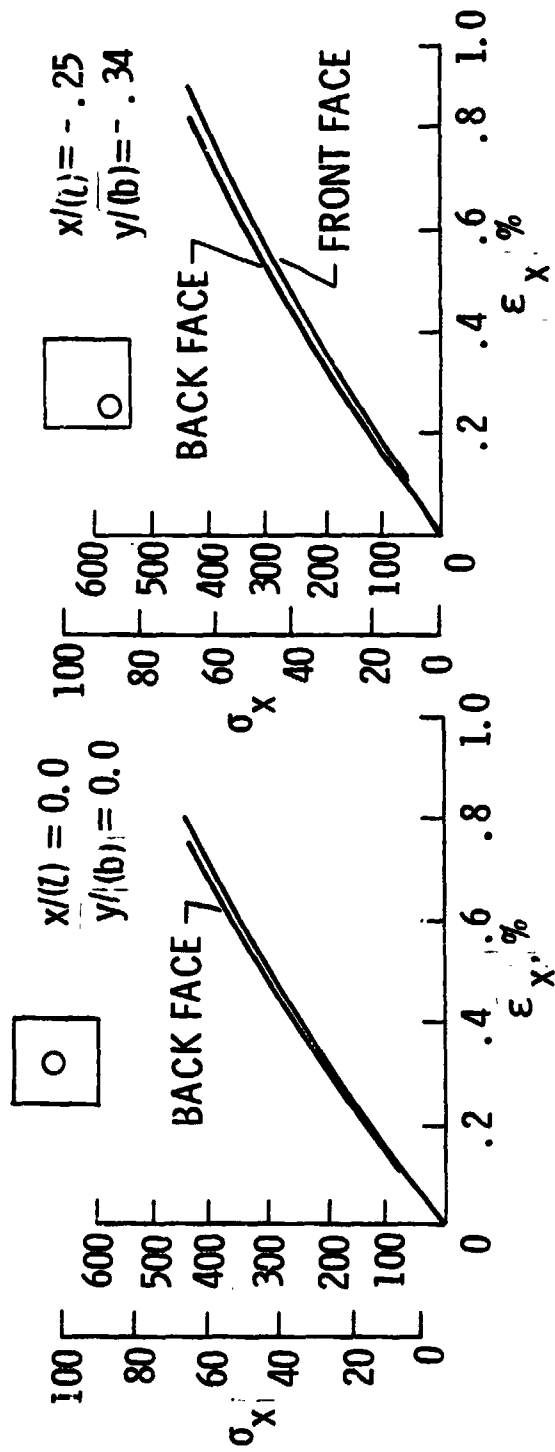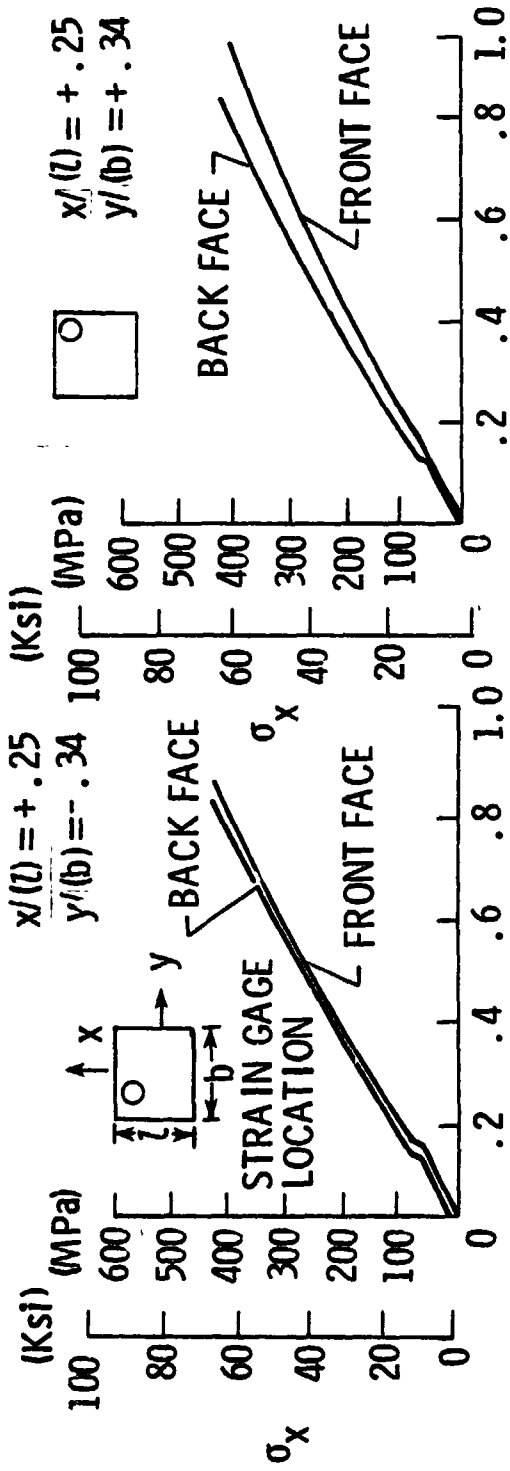
(b) Panel number 75012

Figure 23.- Concluded.
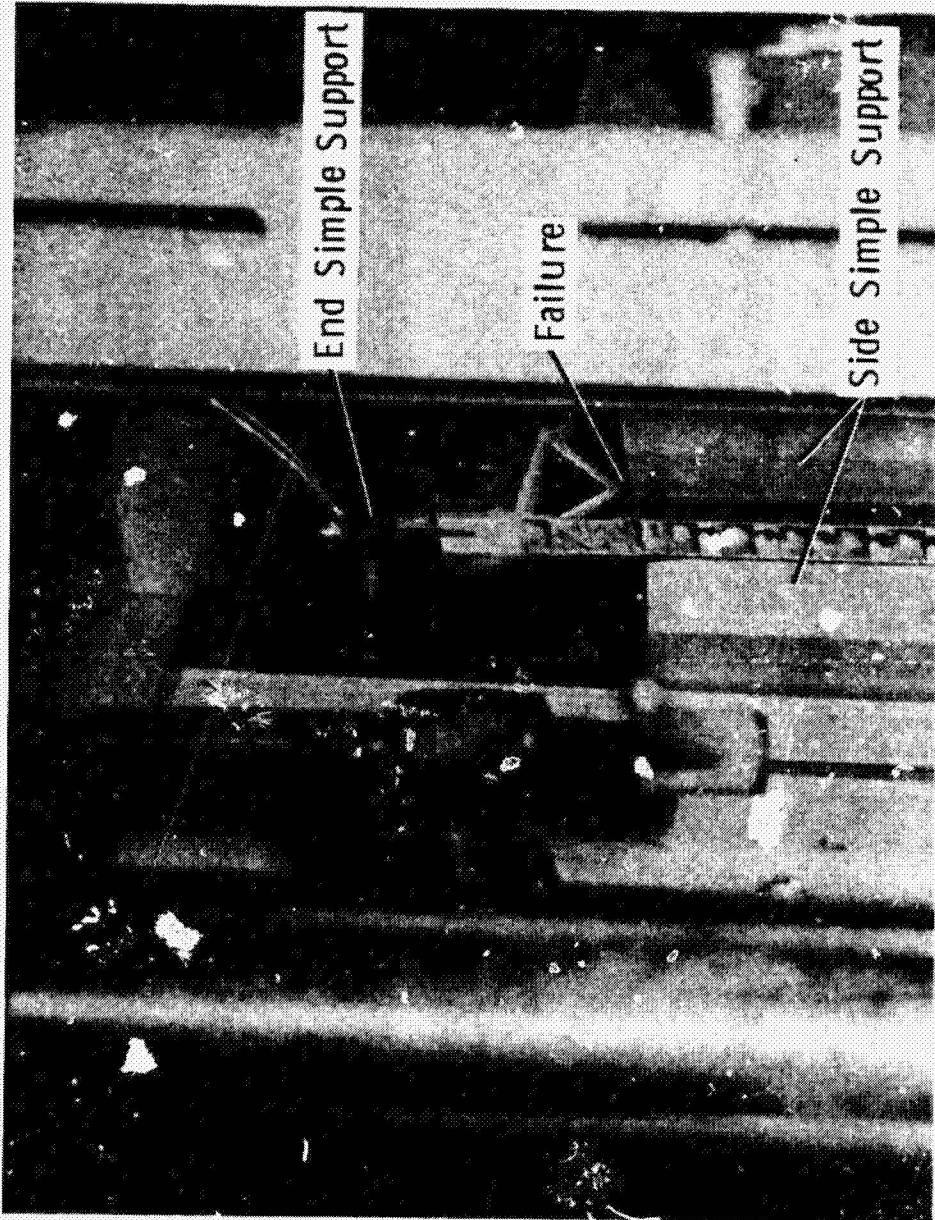
(a) Side view

Figure 24.- Failure near simple support. (wrinkling specimen, $t_c = 1.27$ cm (0.50 in.)).
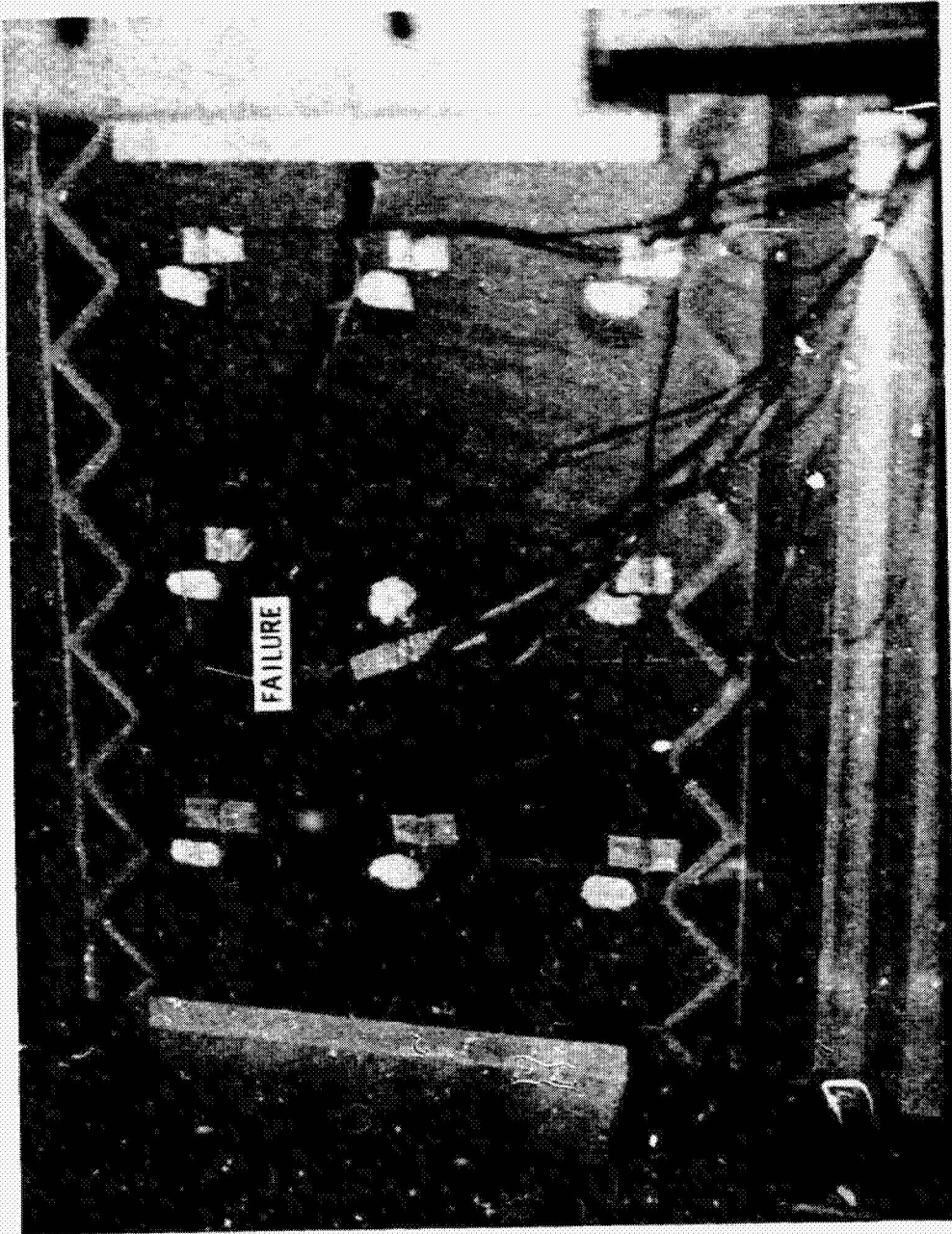
(b) Rear view.

Figure 24.- Concluded.
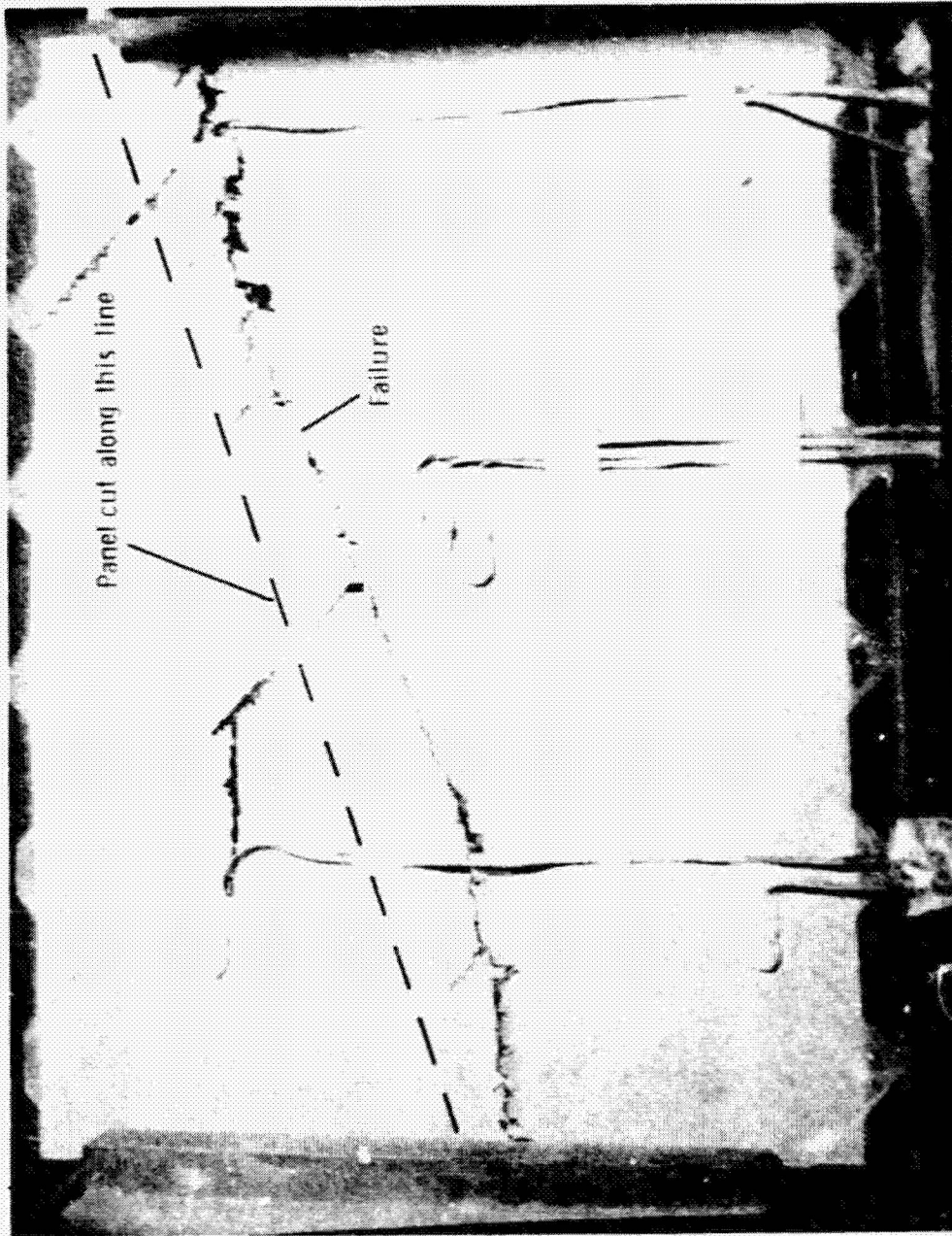
(a) Front view.

Figure 25.- Failed wrinkling specimen (Panel number 7508).

Core-facing debond precipitated by wrinkling
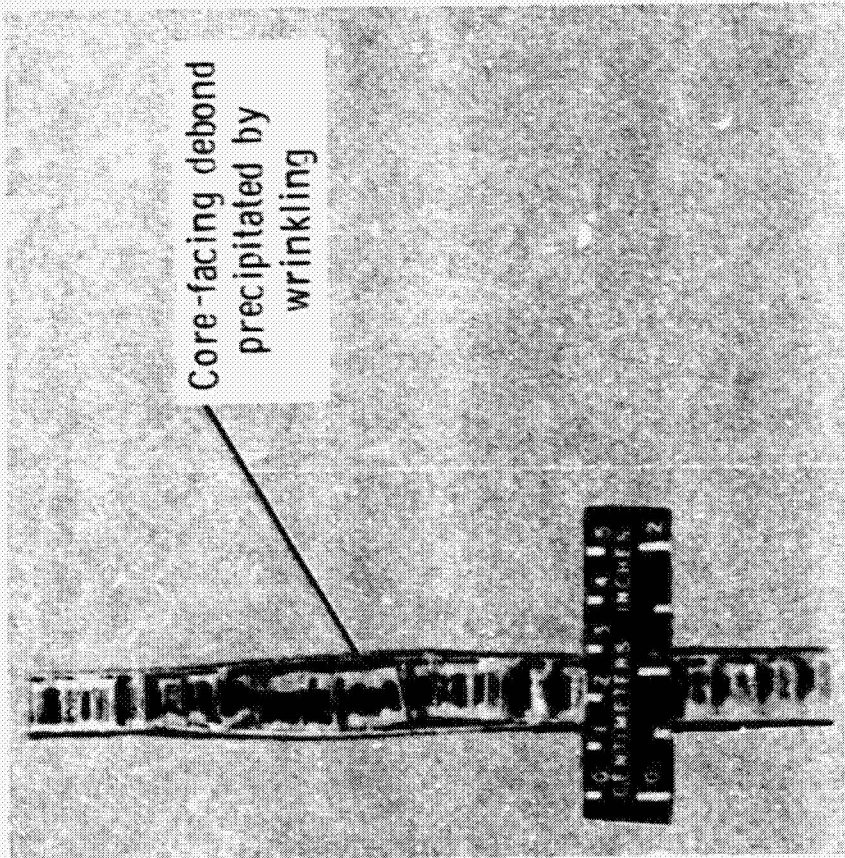
(b) Cutaway view of buckled region.

Figure 25. - Concluded.

Regions of failure
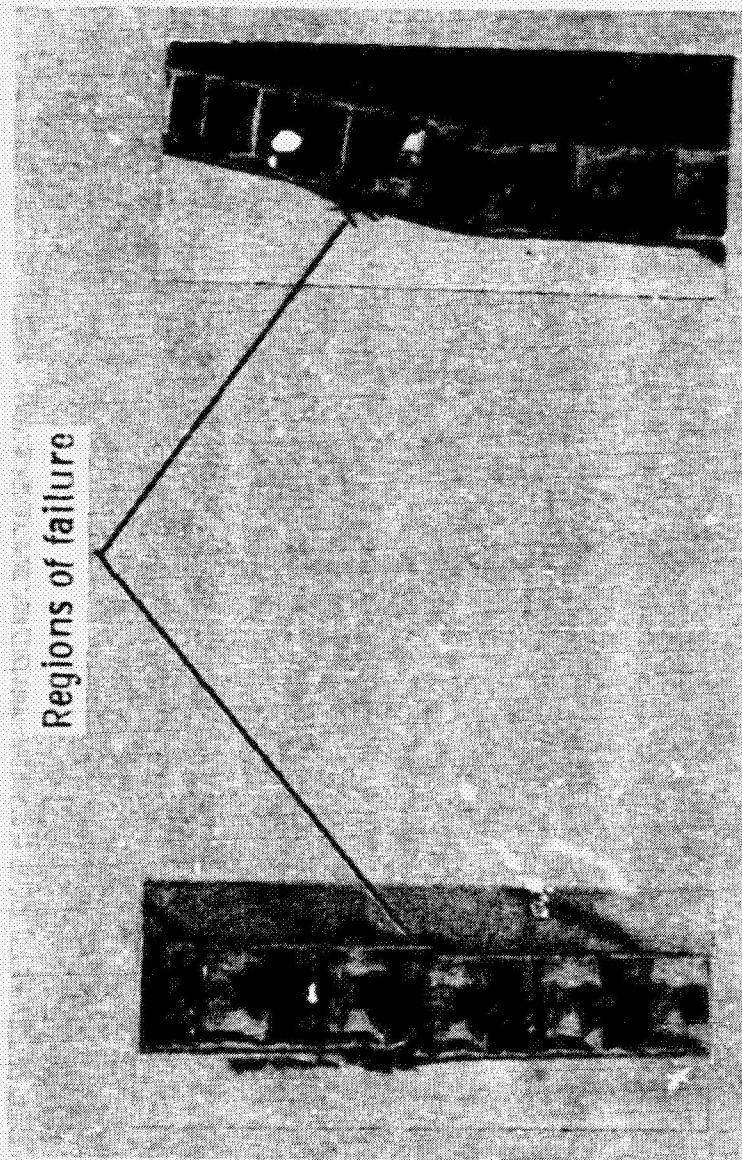
Figure 26.- Side view of two failed wrinkling specimens
(t_c 1.27 cm (0.50 in.))
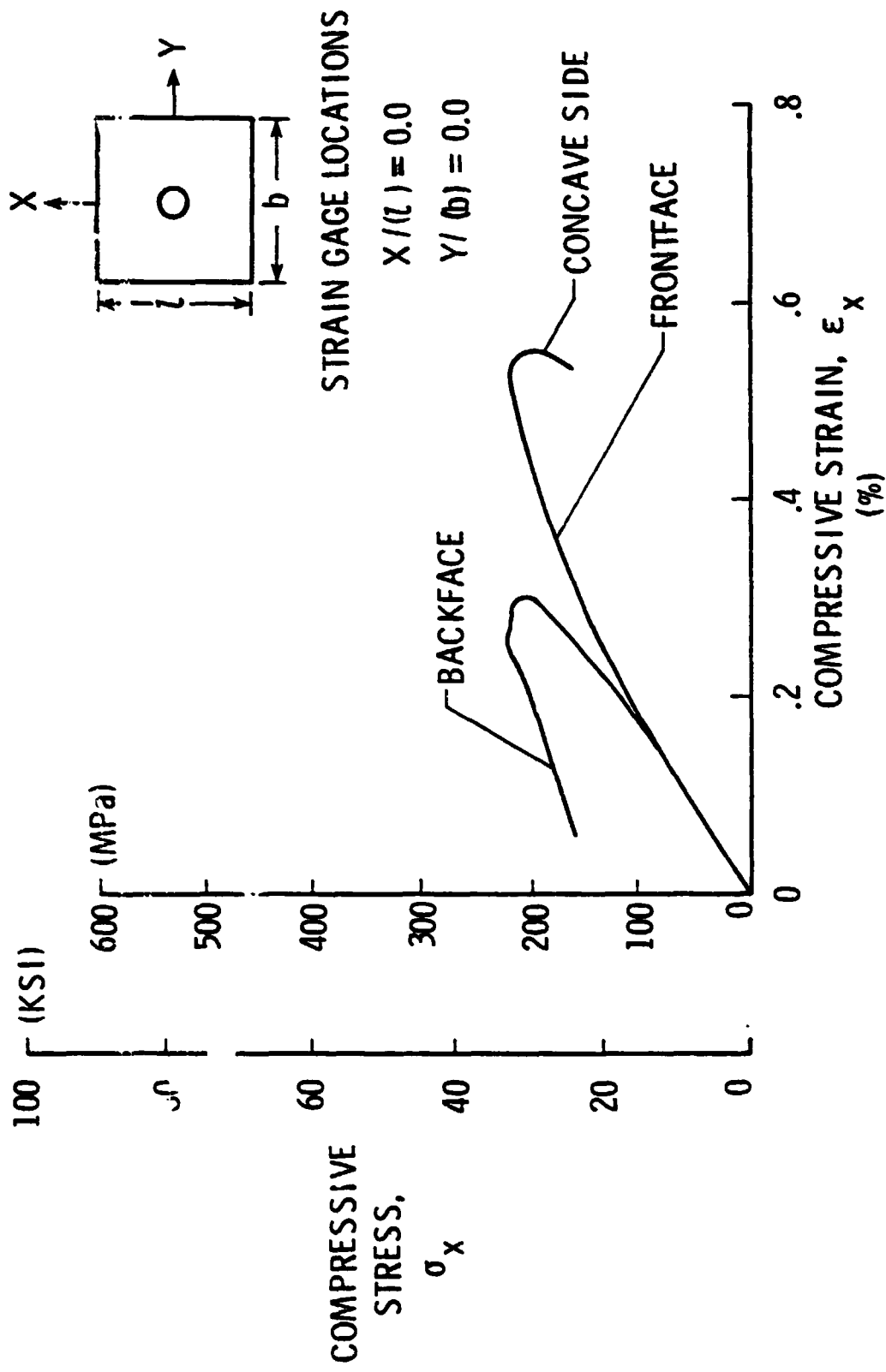
(a) Panel number 7251.

Figure 27.- Back-to-back stress - vs. - strain results of overall buckling specimens.

STRAIN GAGE LOCATIONS
$X/(\ell) = 0.0$
$Y/(b) = 0.0$
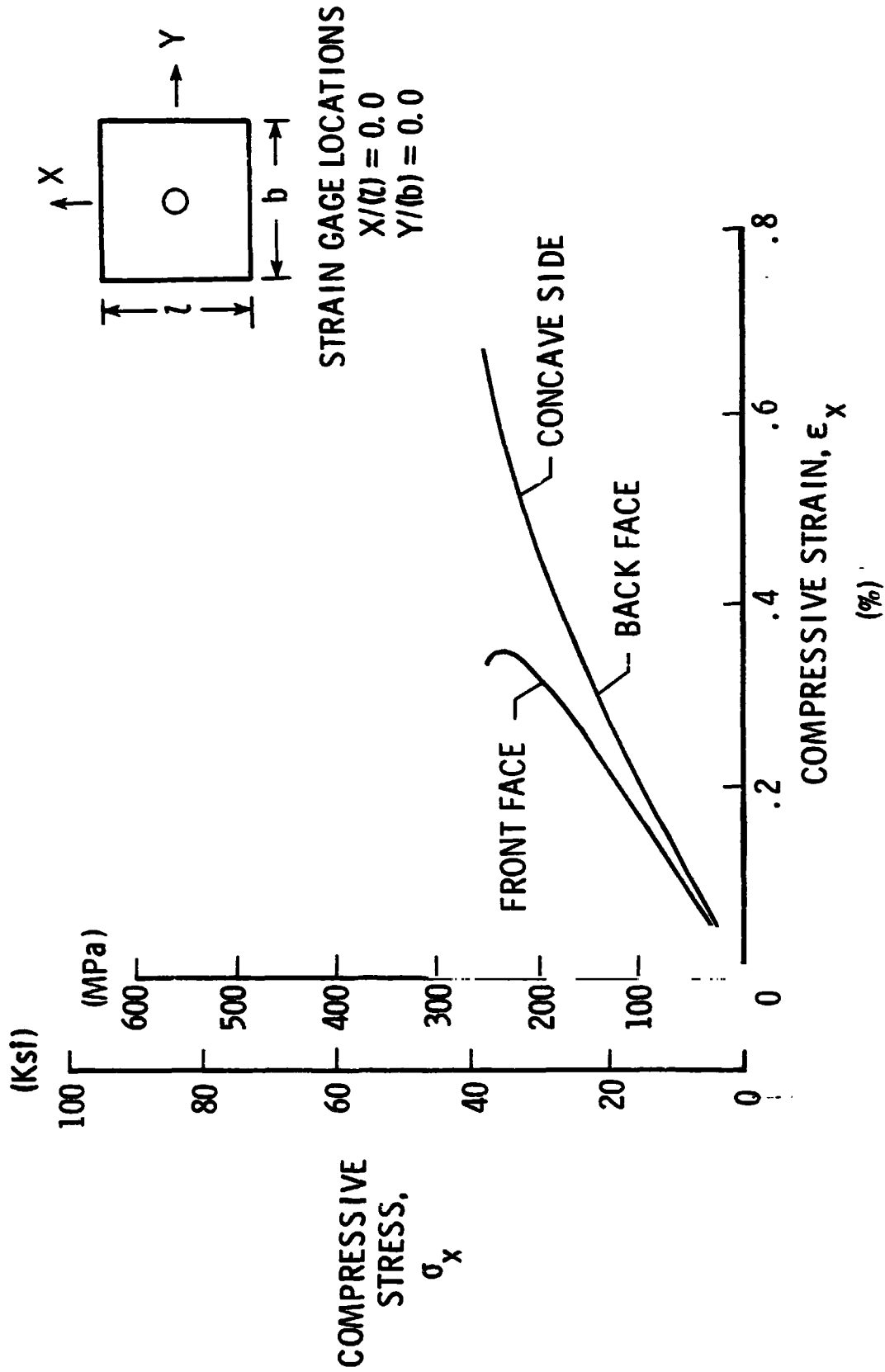
(b) Panel number 7254.

Figure 27.- Continued.

102

STRAIN GAGE LOCATIONS

$|X/(\ell)| = 0.0$

$Y/(b) = 0.0$

CONCAVE SIDE

BACK FACE

FRONT FACE

COMPRESSIVE STRAIN, ε_x

(%)

COMPRESSIVE STRESS, σ_x
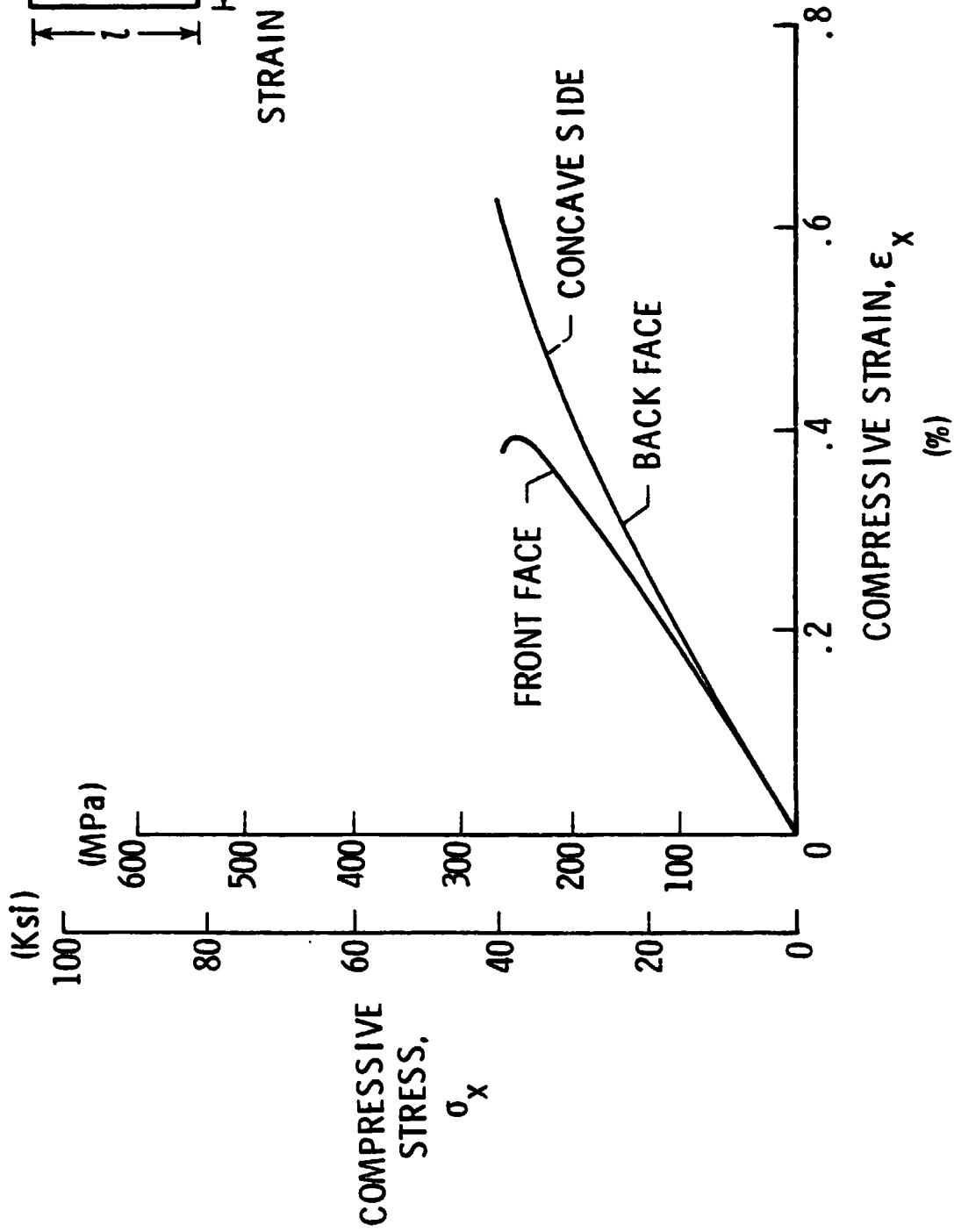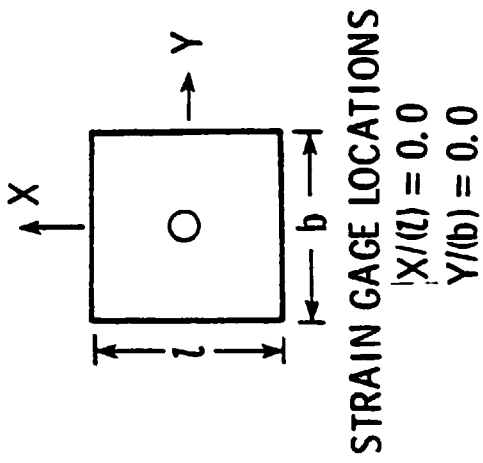
(c) Panel number 7255.

Figure 27.- Continued.

STRAIN GAGE LOCATIONS
X/(ℓ) = 0.0
Y/(b) = 0.0
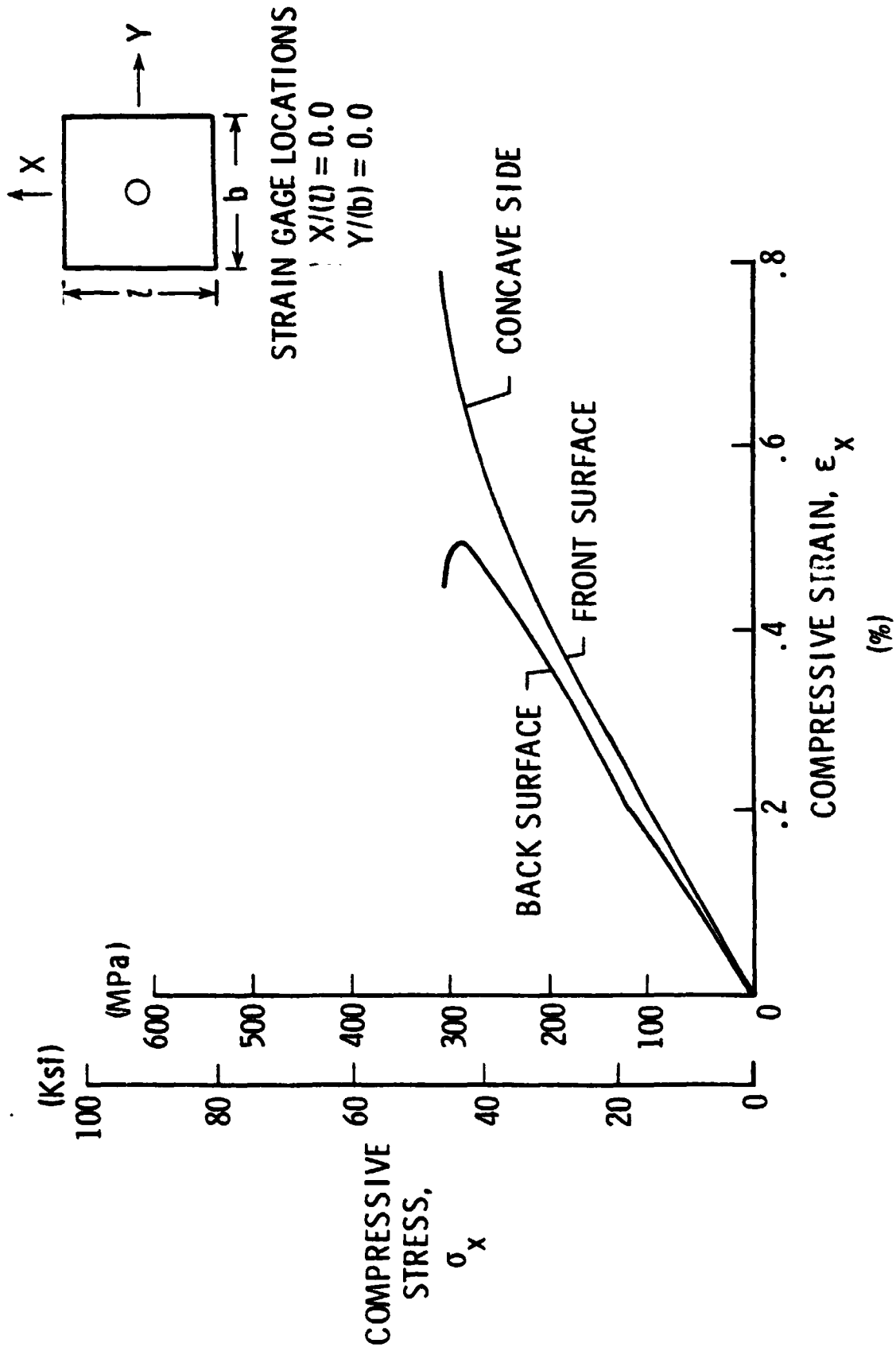
(d) Panel number 7256.

Figure 27.- Concluded.
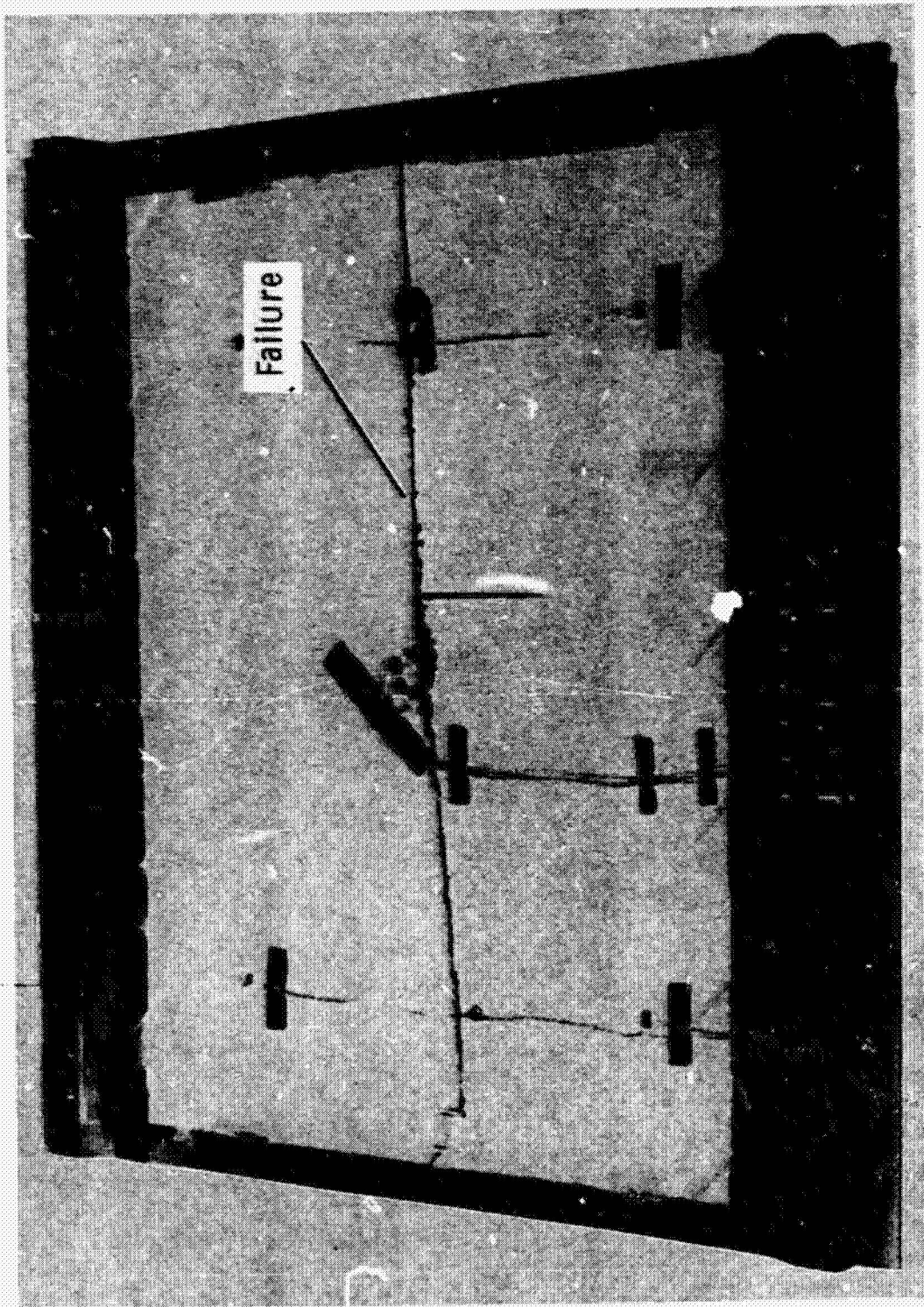
Figure 28.- Failed overall buckling specimen (Panel number 7251).

105
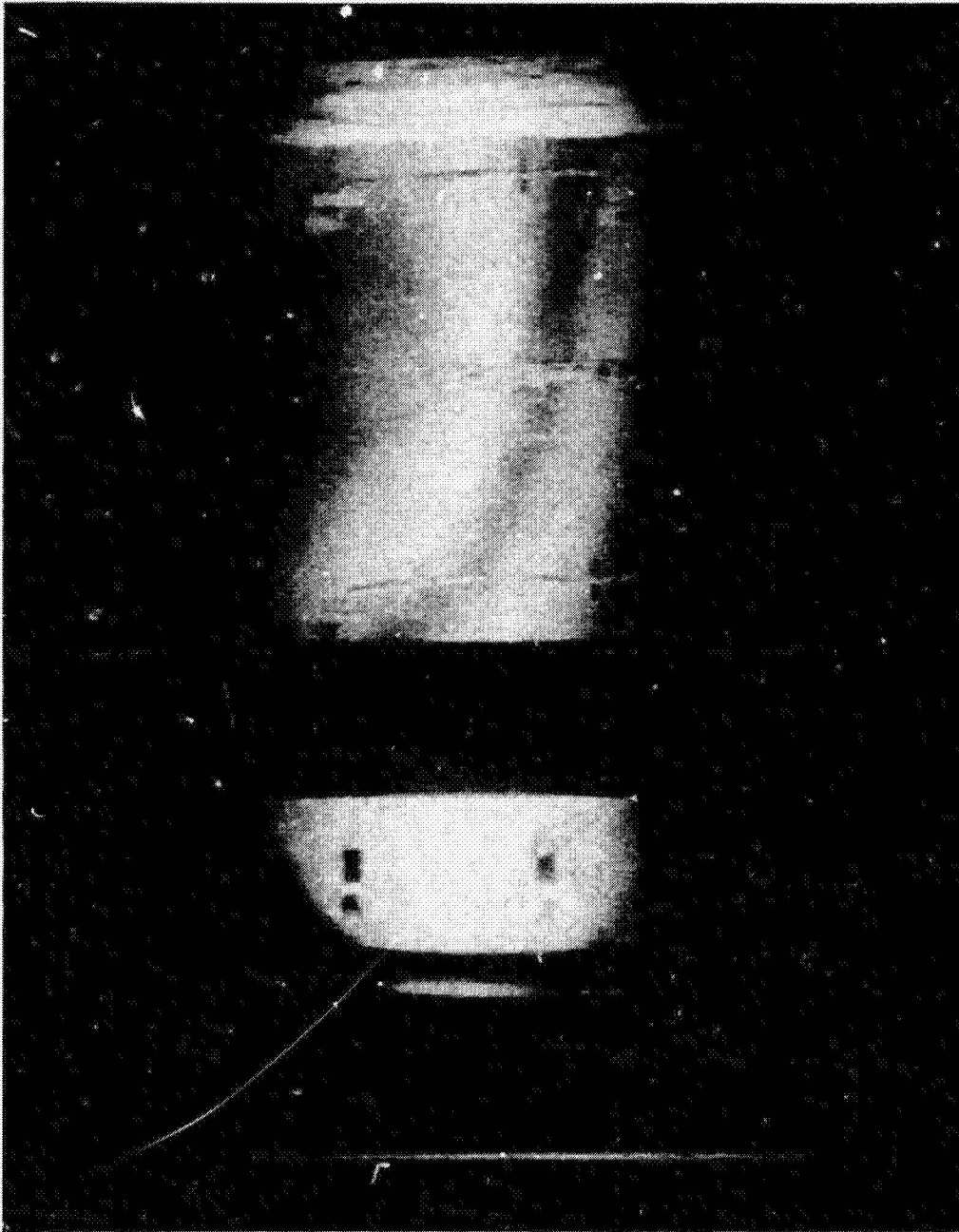
(a) $P/P_{ult} = 0.89$

Figure 29.- Moiré fringe patterns of overall buckling specimen (Panel number 7256).

106
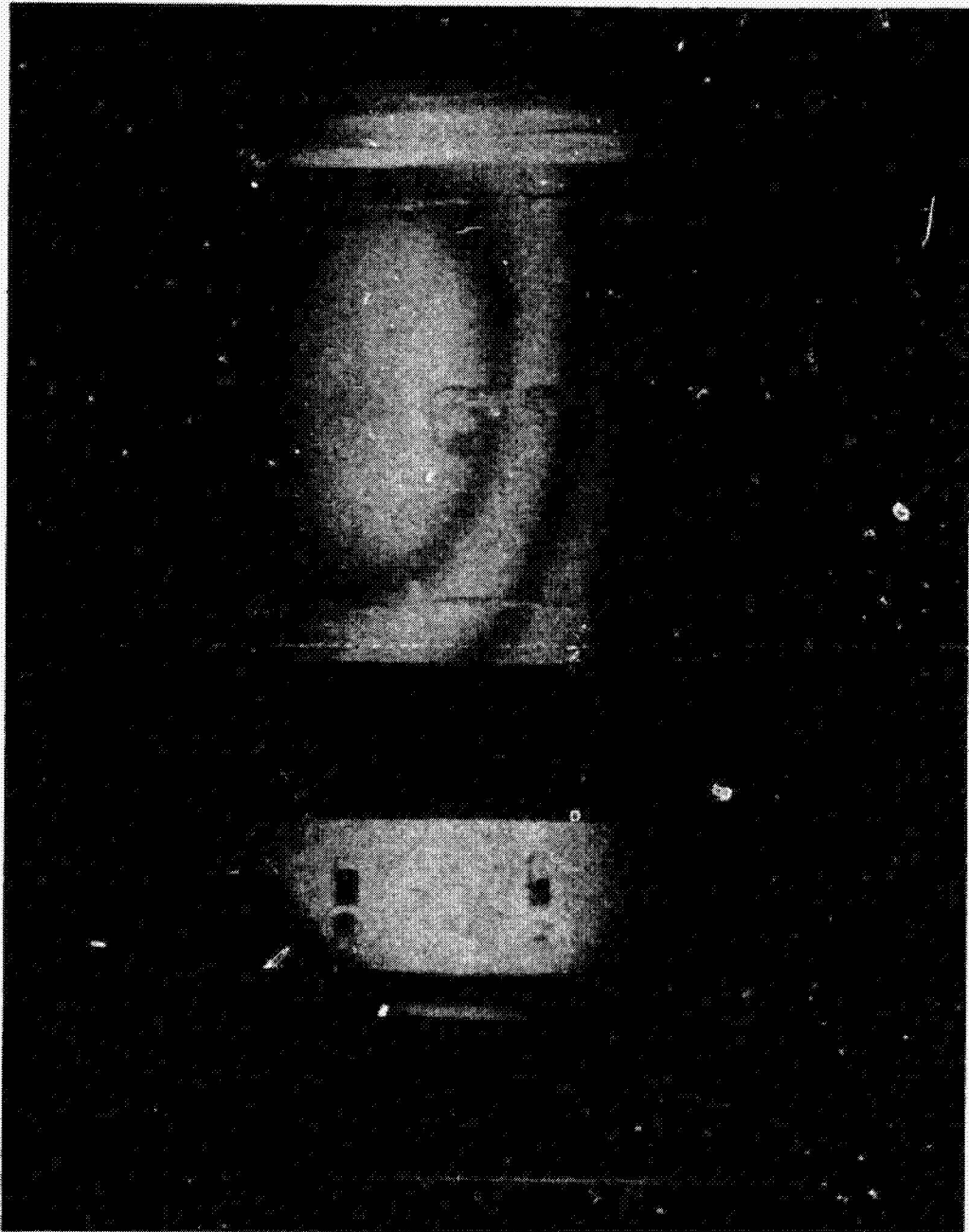
(b) $P/P_{ult} = 0.94$

Figure 29.- Continued.

107
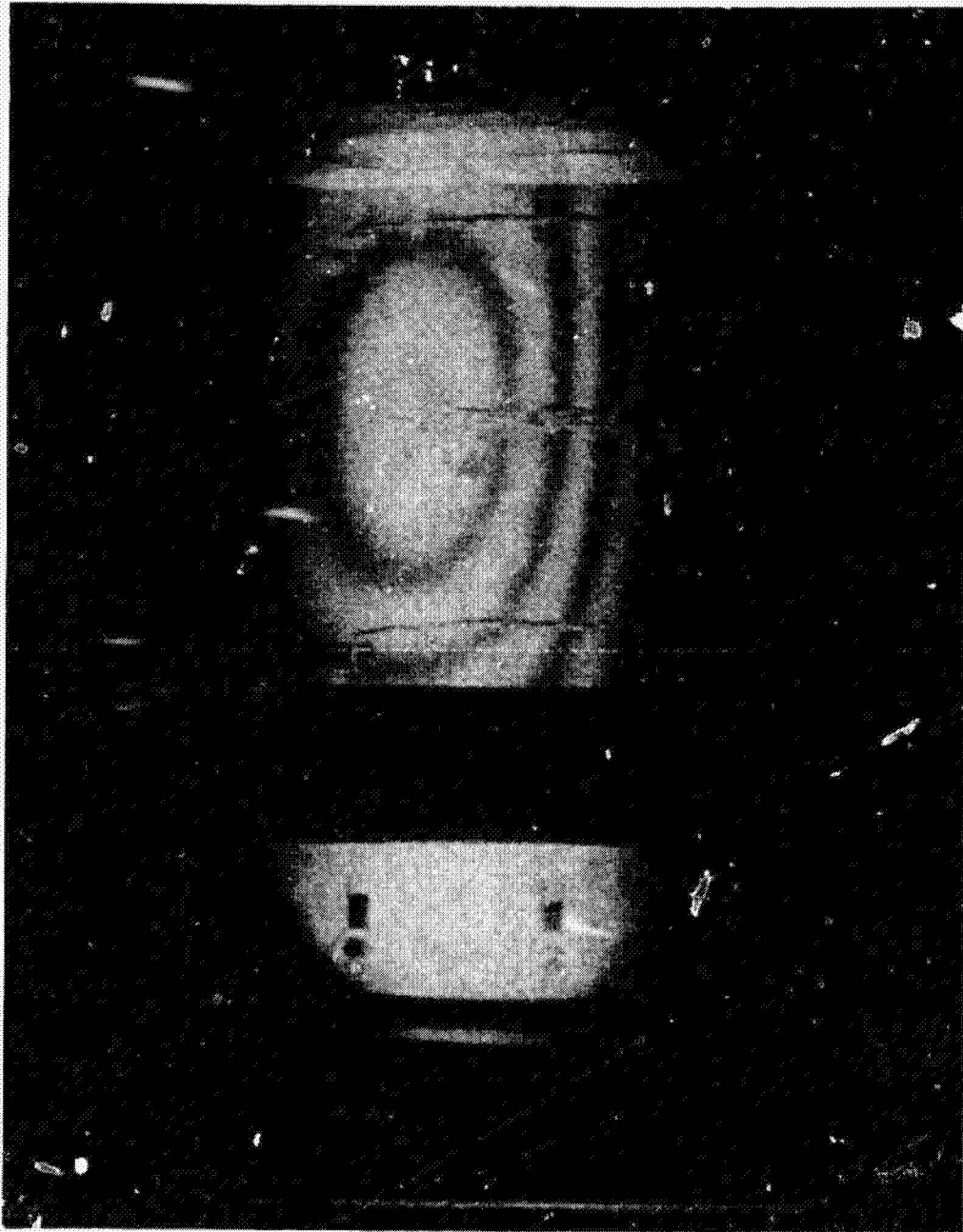
(c) $P/P_{ult} = 1.0$

Figure 29. - Continued.

108
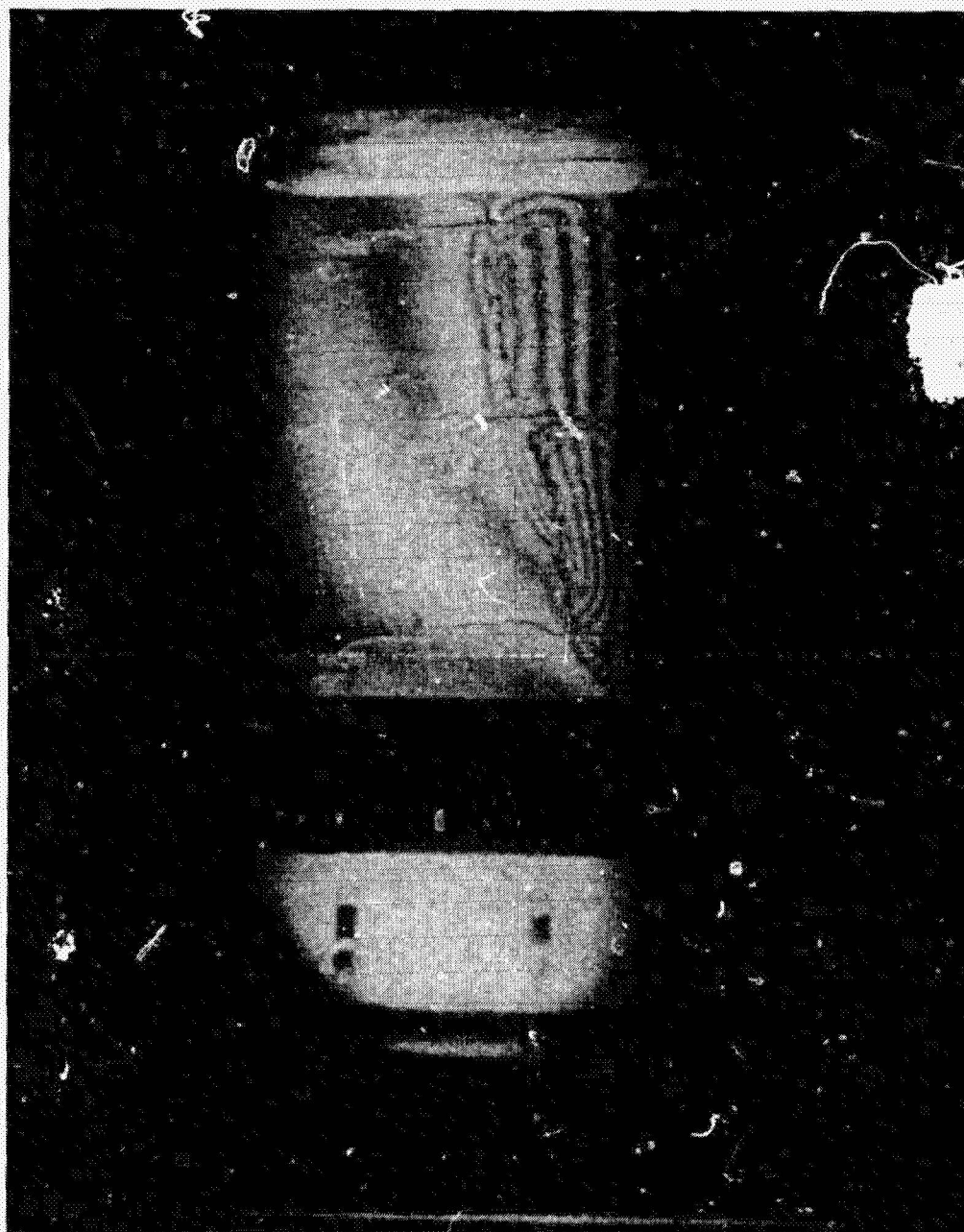
(d) Failure

Figure 29. - Concluded.

(a) P/P_{ult} = 0.72

Figure 30.- Moiré fringe patterns of overall buckling specimen
(Panel number 7251).

(b) $P/P_{ult} = 0.99$

Figure 30.- Continued.
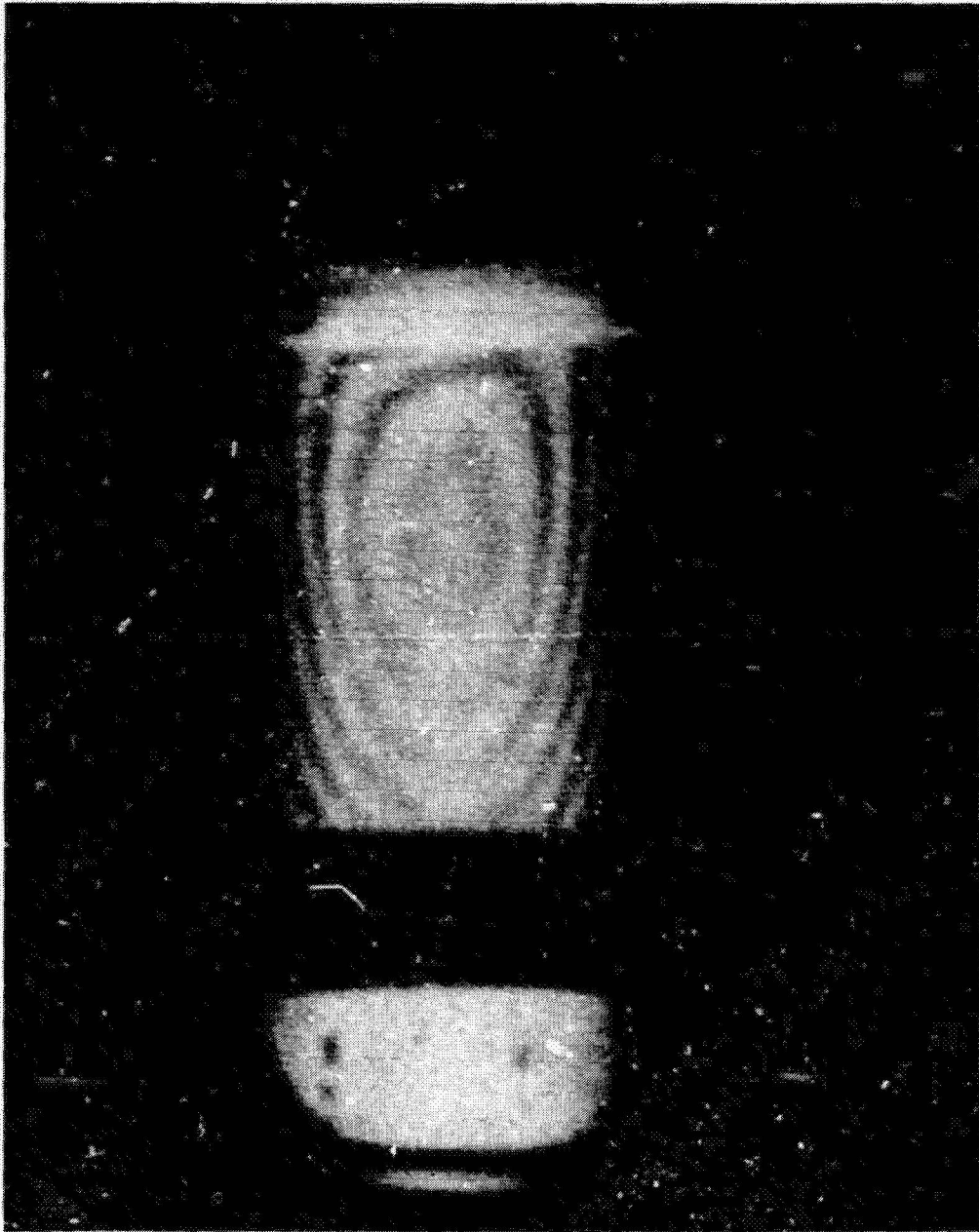
(c) P/P_{ult} = 1.0

Figure 30. - Continued.
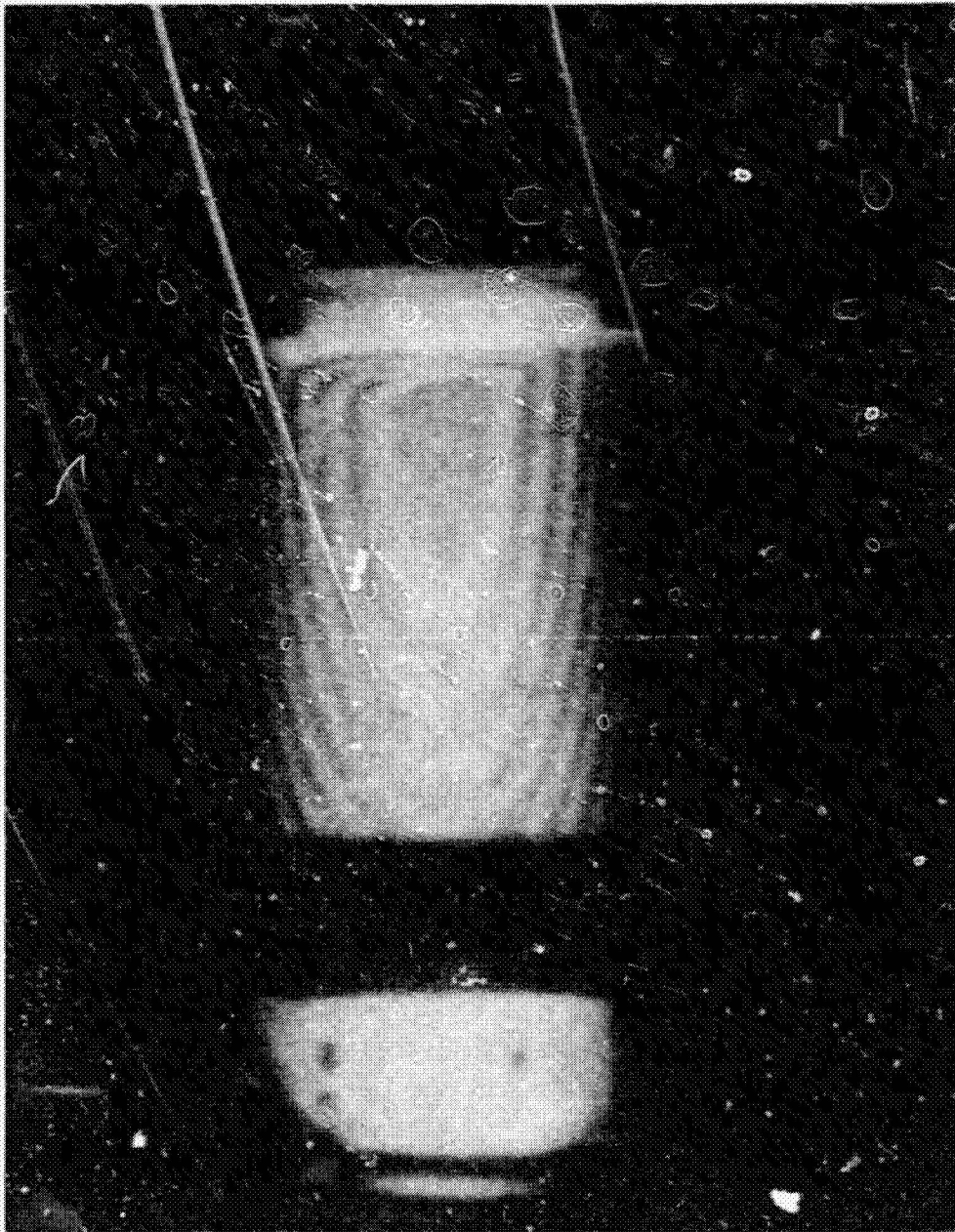
(d) P/P_{ult} = 0.99 (Post buckling)

Figure 30.- Concluded.
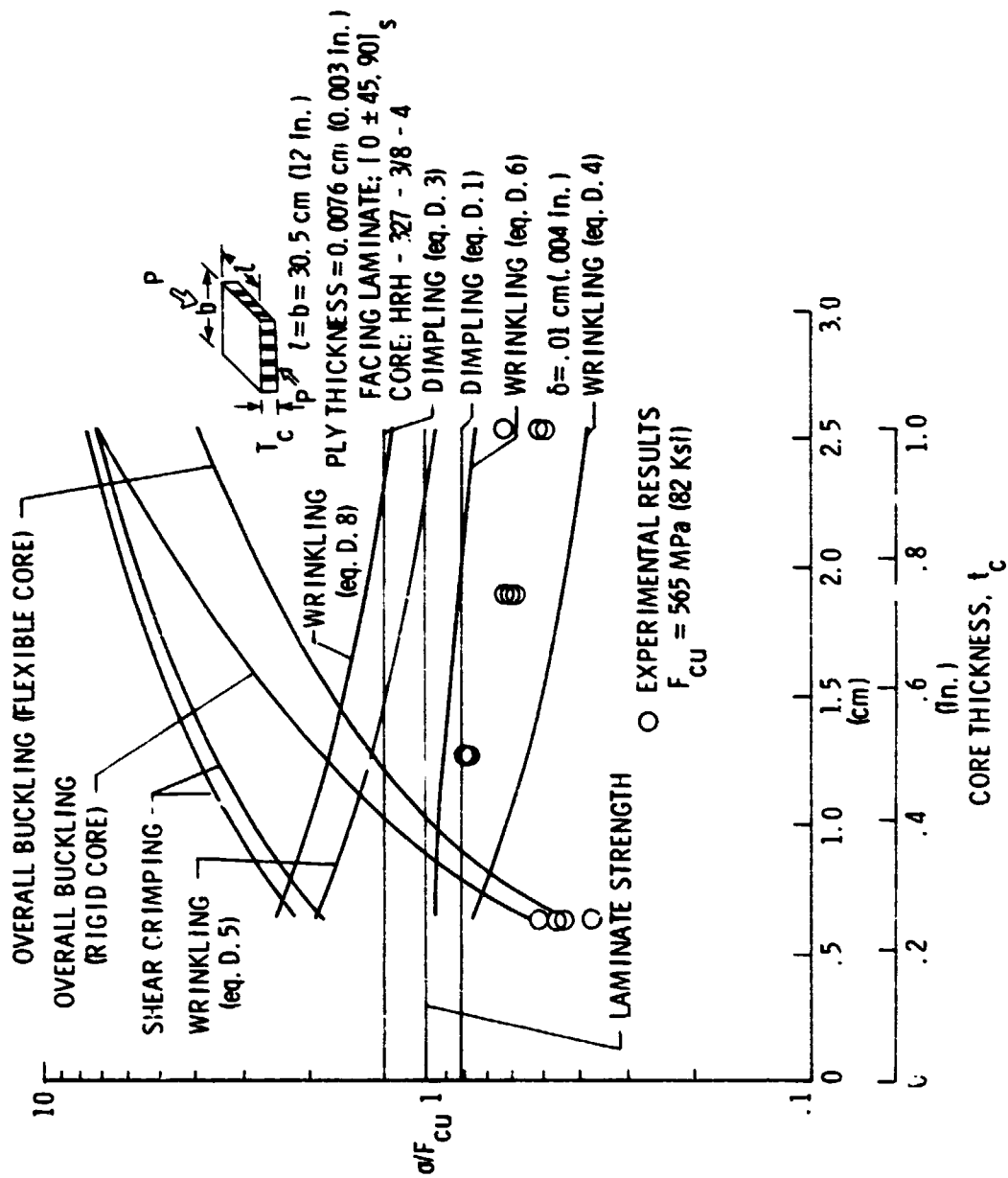
Figure 31.- Comparison of analytical and experimental results.
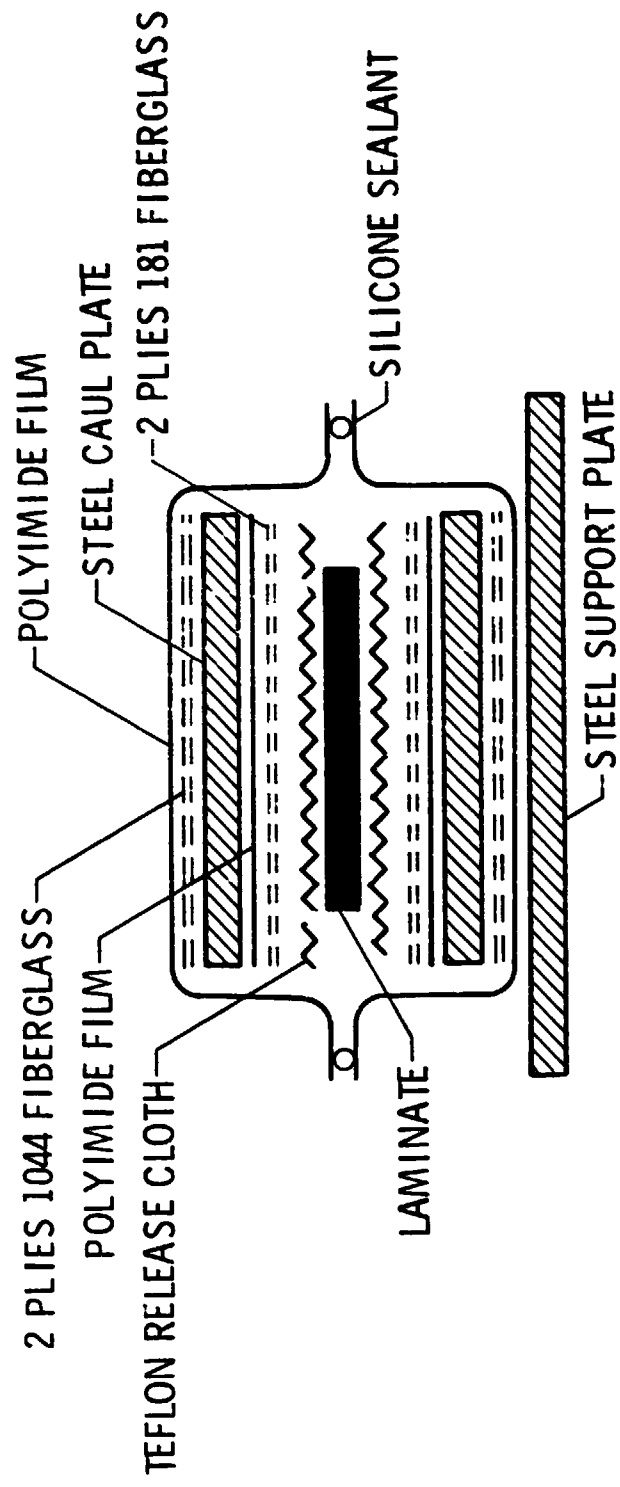
Figure 32.- Vacuum bag schematic for curing PMR-15 laminates used to fabricate flatwise tensile and sandwich beam specimens.

Labels: 2 PLIES 1044 FIBERGLASS; POLYIMIDE FILM; TEFLON RELEASE CLOTH; POLYIMIDE FILM; STEEL CAUL PLATE; 2 PLIES 181 FIBERGLASS; SILICONE SEALANT; STEEL SUPPORT PLATE; LAMINATE
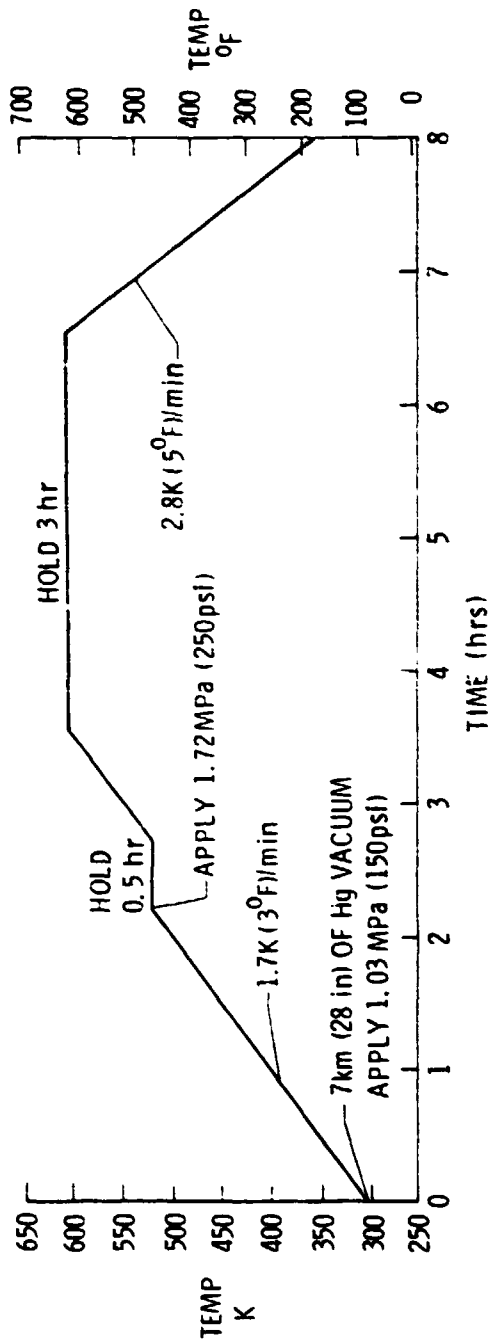
Figure 33.- Cure cycle of PMR-15 laminates used to fabricate flatwise tensile and sandwich beam specimens.

116

0.0076 cm (0.003 in) KAPTON BAG
2 PLIES OF 160 FIBERGLASS CLOTH
2 PLIES OF 120 FIBERGLASS CLOTH
3 TLL

LAMINATE 2
0.159cm (1/16 in.) PERFORATED CAUL PLATE
LAMINATE 1
HEAVY KAPTON

A-800 SEALANT
STEEL BASE PLATE

PERFORATED CAUL PLATE

LAMINATE 1
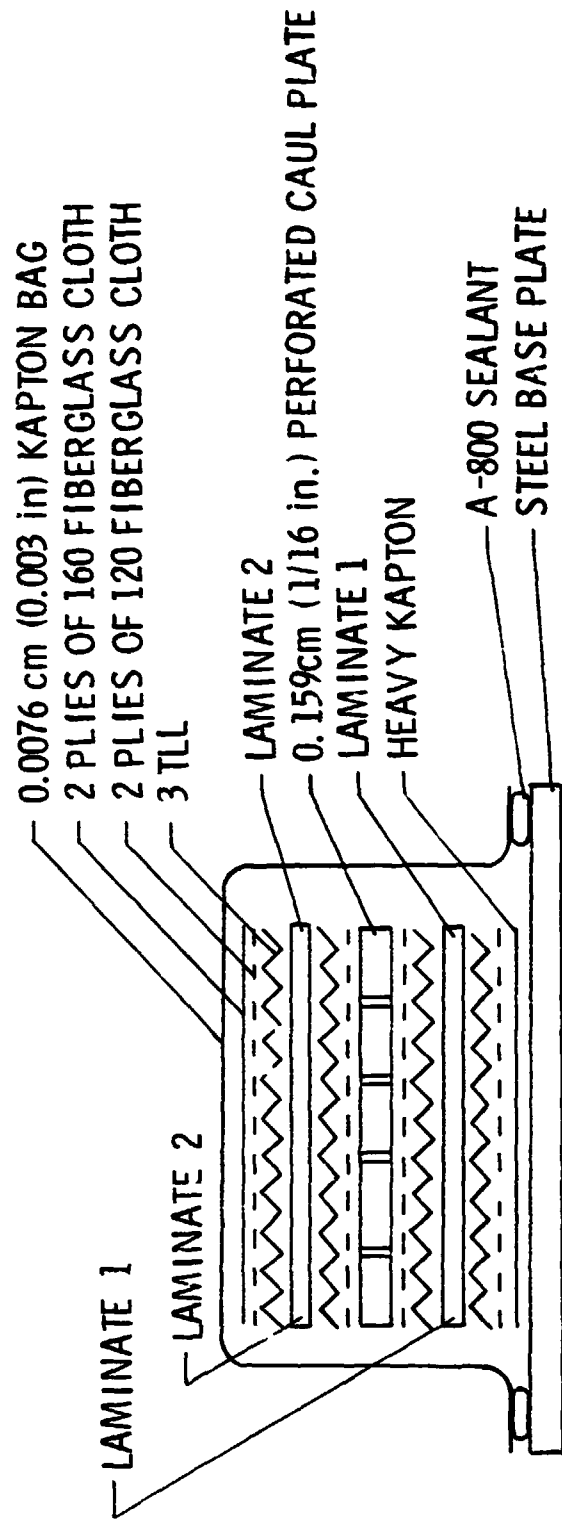
LAMINATE 2

Figure 34.- Vacuum bag schematic for curing PMR-15 laminates used to fabricate buckling specimens.

117
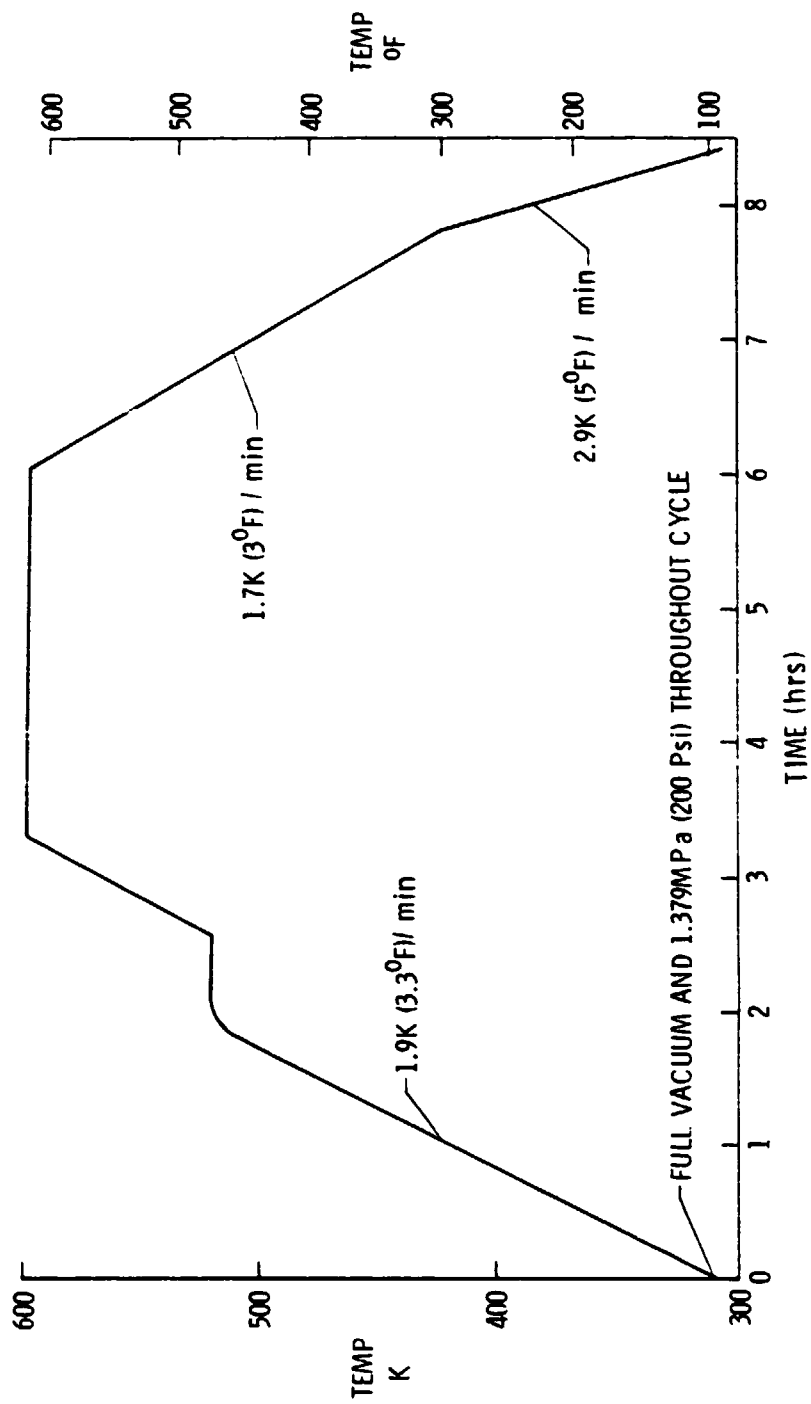
Figure 35.- Cure cycle of Celion 3000/PMR-15 laminates.

118

Figure 36.- Perforating honeycomb core at cell node points.

119

Figure 37.- Potting ends of honeycomb core with Br-34 polyimide adhesive.
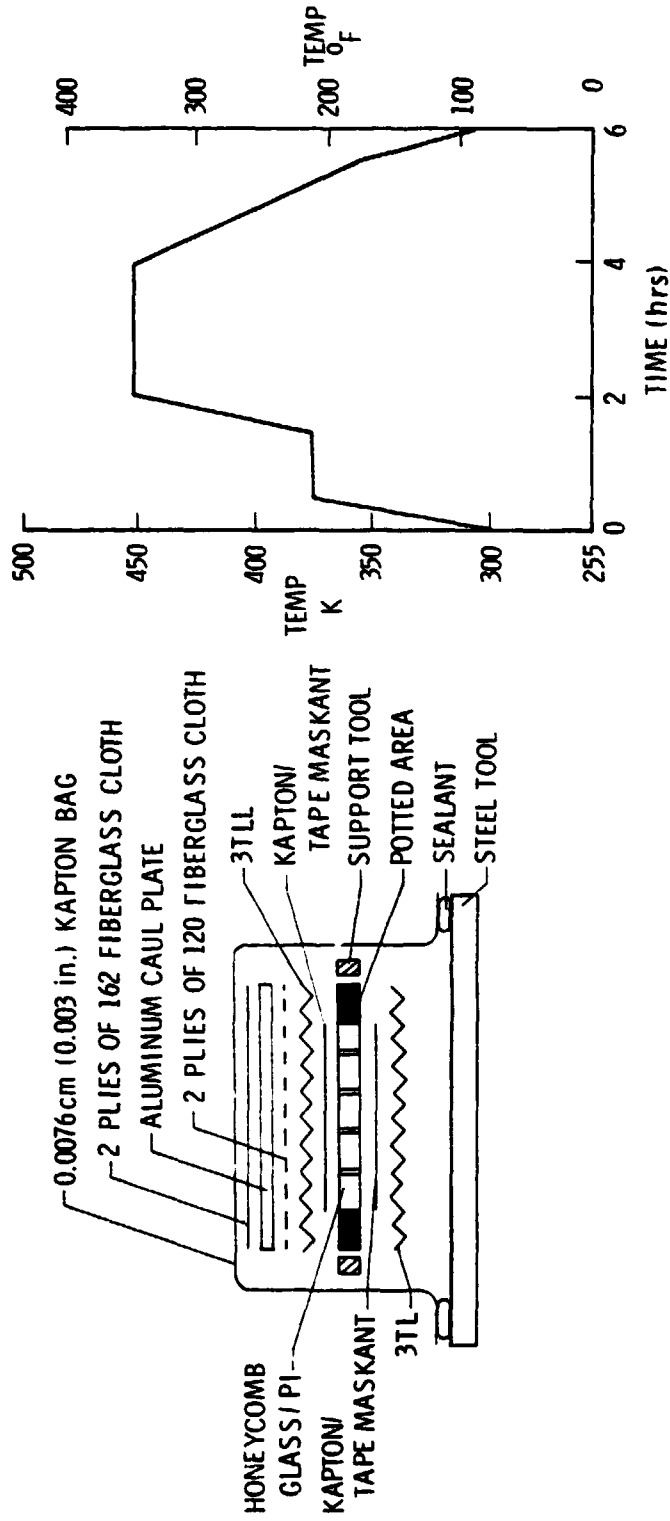
Figure 38.- Vacuum bag schematic and cure cycle for Br-34 potting of Honeycomb core.

121
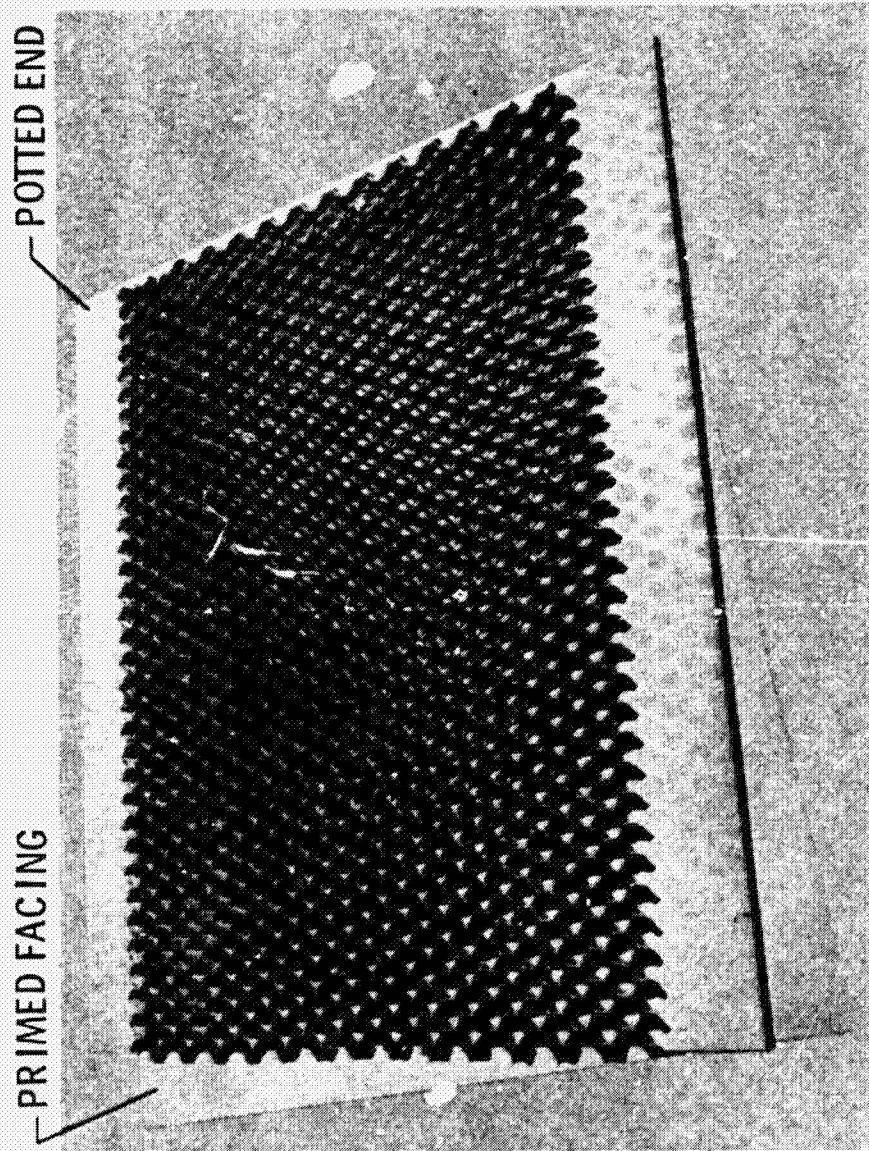
Figure 39.- Ends of panel potted and machined flat and parallel.

ALIGNMENT SHEET

GLASS/PI
TAPERED END TABS

GLASS/PI
SCALLOPED
DOUBLER

[0, ±45, 90]s
Gr/PI
FACING

GLASS/PI
HONEYCOMB
CORE
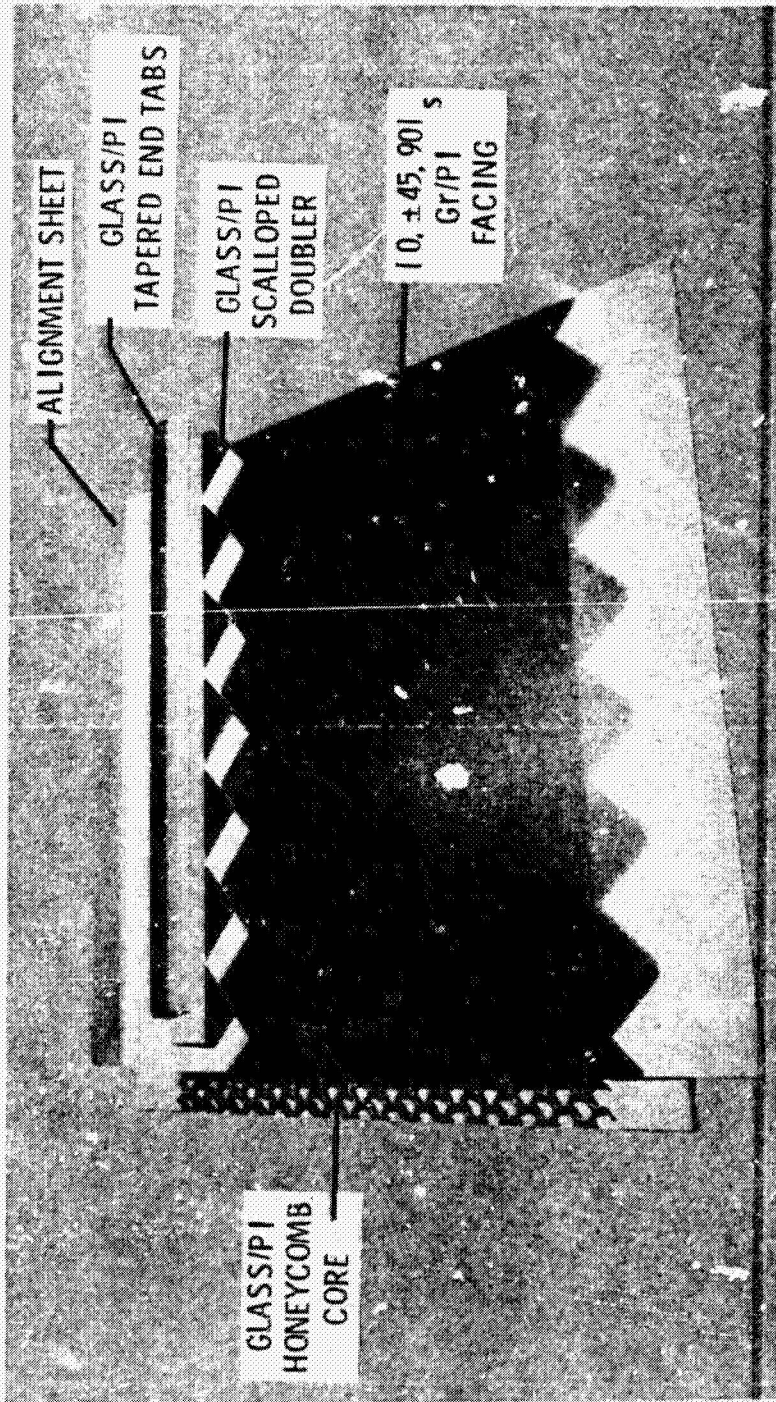
Figure 40.- View of honeycomb core, scalloped doublers, tapered end tabs,
stainless-steel alignment sheet, and Gr/PI facing.

123
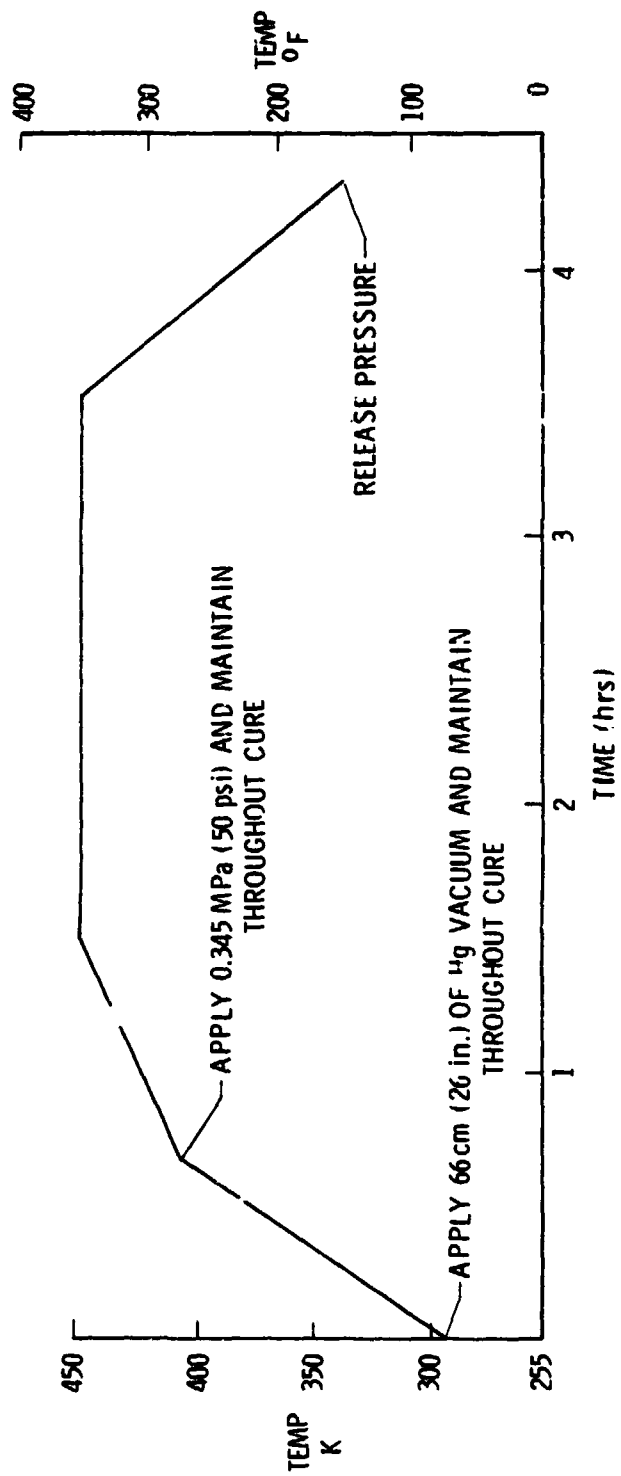
Figure 41.- FM-34 cure cycle.

124
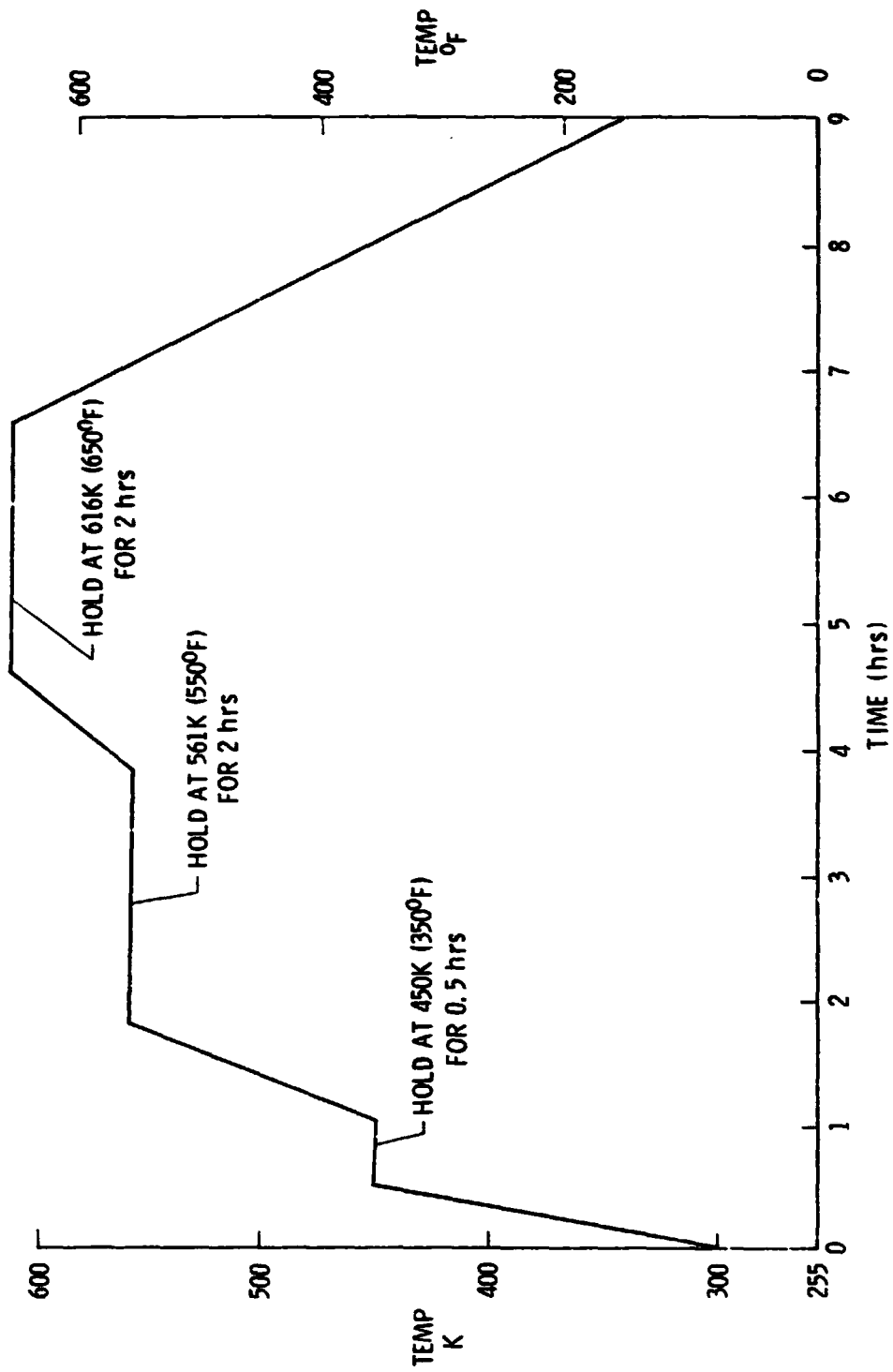
Figure 42.- FM-34 postcure cycle.

125
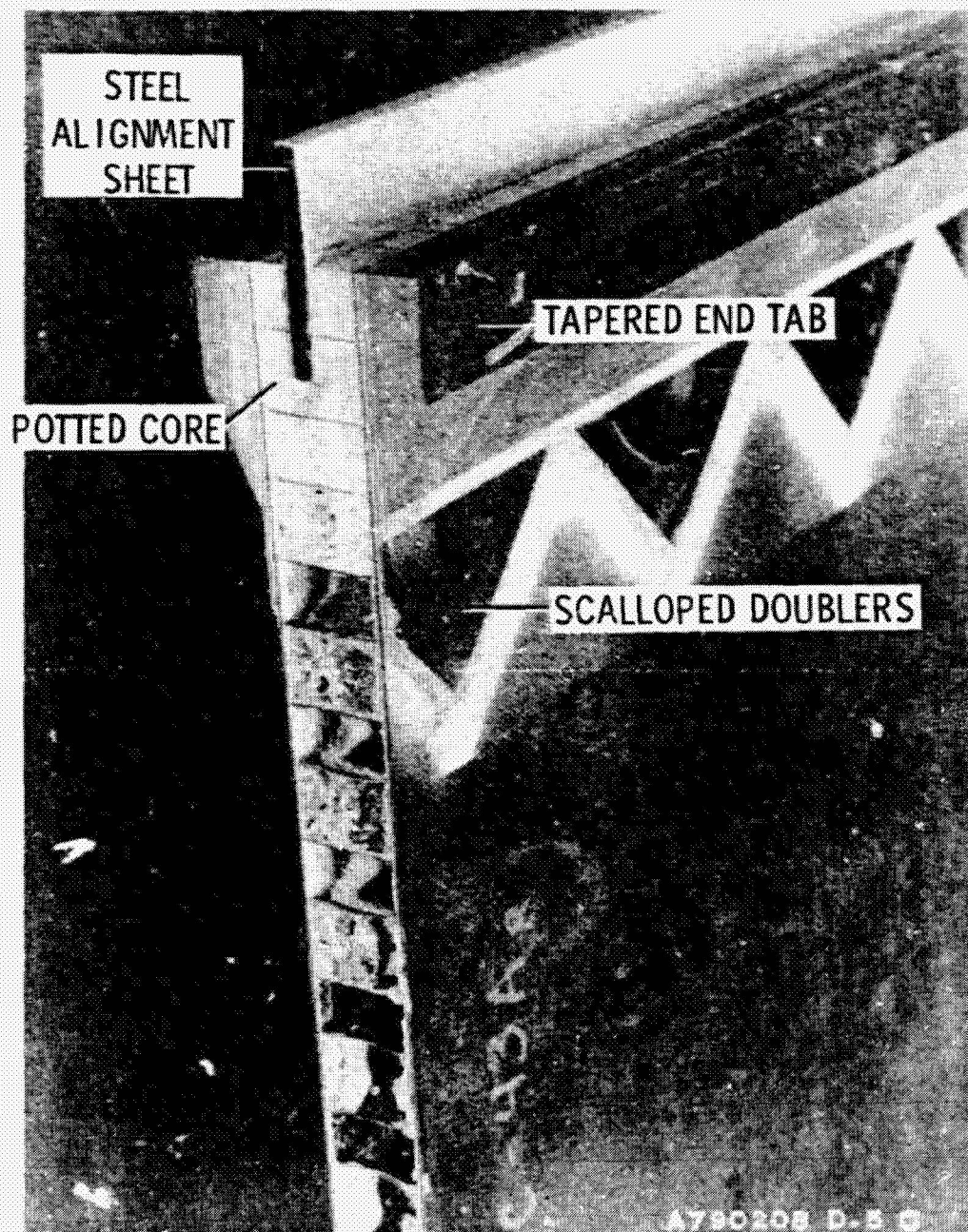
Figure 43.- End view of buckling specimen.
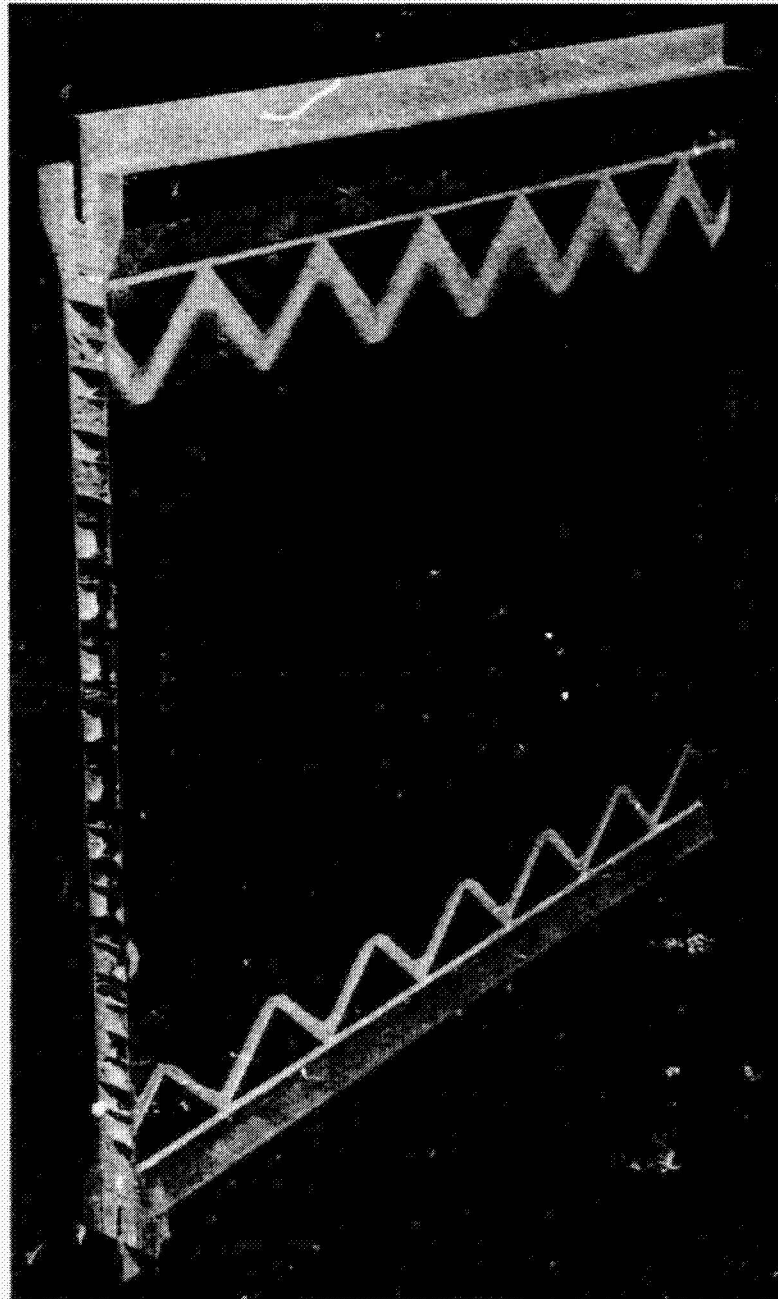
Figure 44.- Completed Gr/PI honeycomb sandwich
buckling specimen.
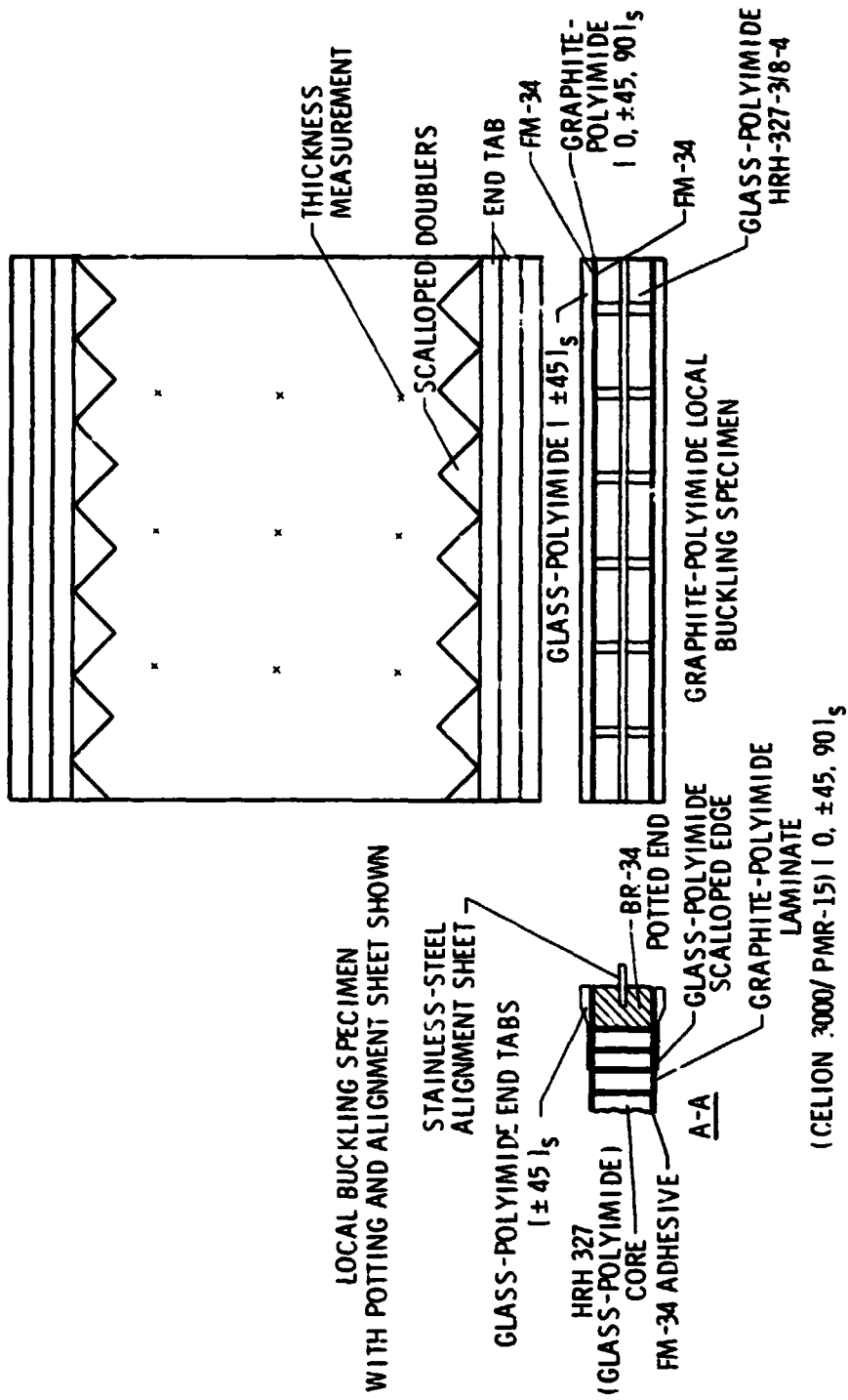
Figure 45.- Schematic diagram of buckling specimen.

128

0.025 cm (0.01 in.)

Y

X
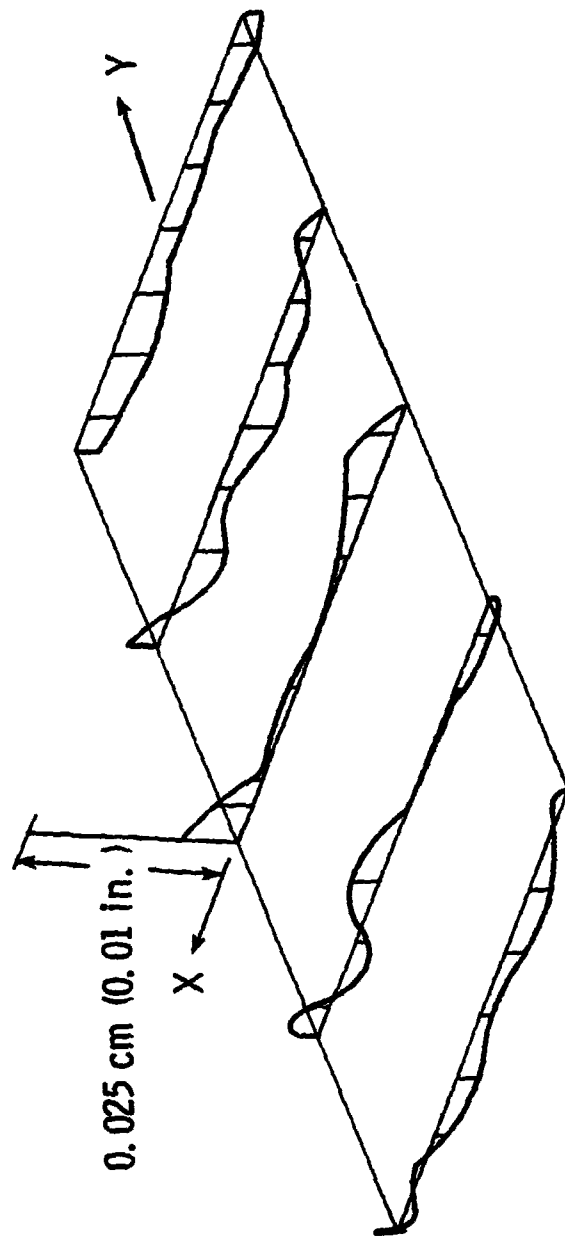
Figure 46.- Typical plot used to determine maximum waviness, δ_{max}, of each panel. (Panel number 7508 lower surface).
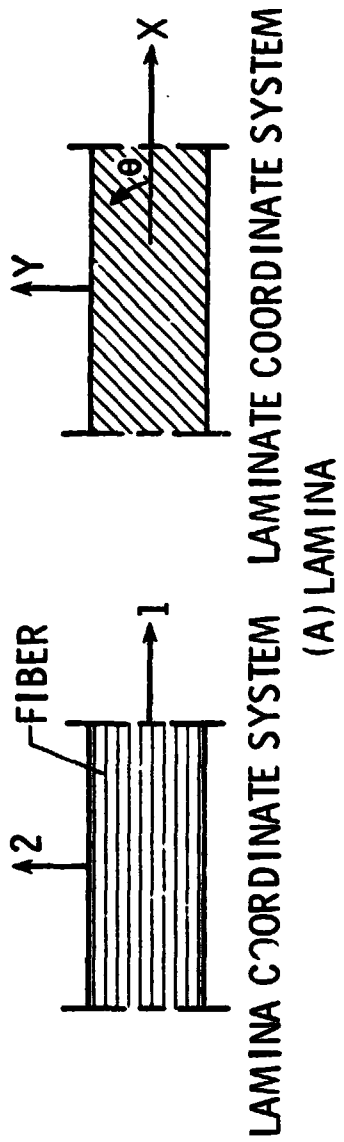
129
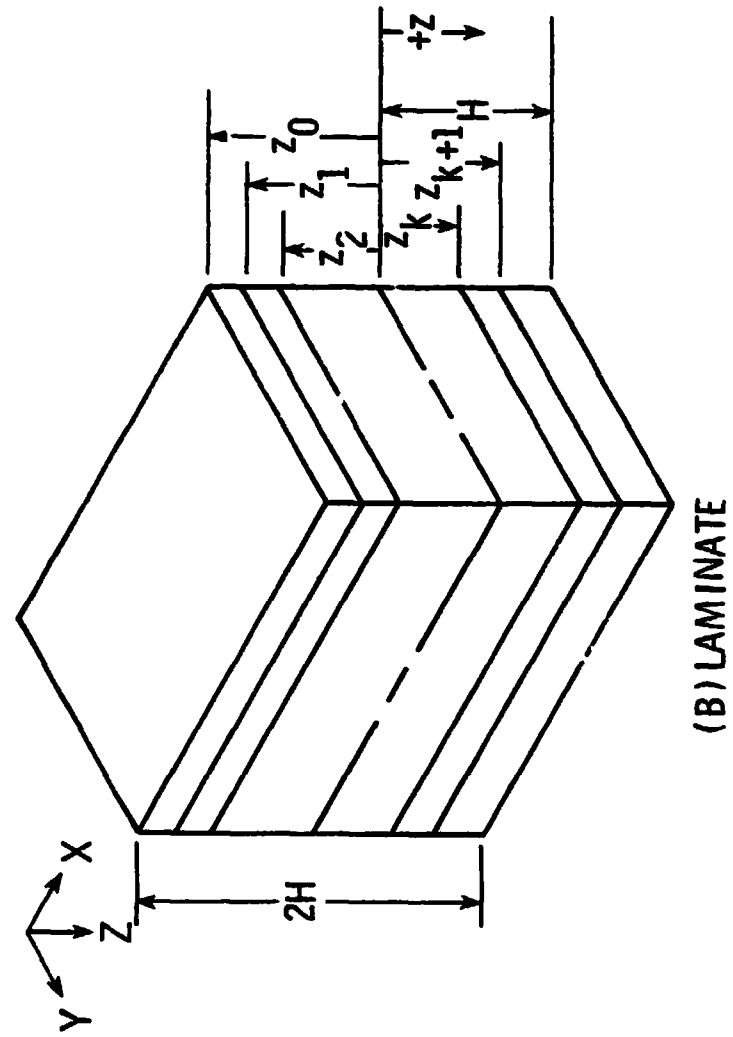
Figure 47. - Lamina and laminate geometry.

130
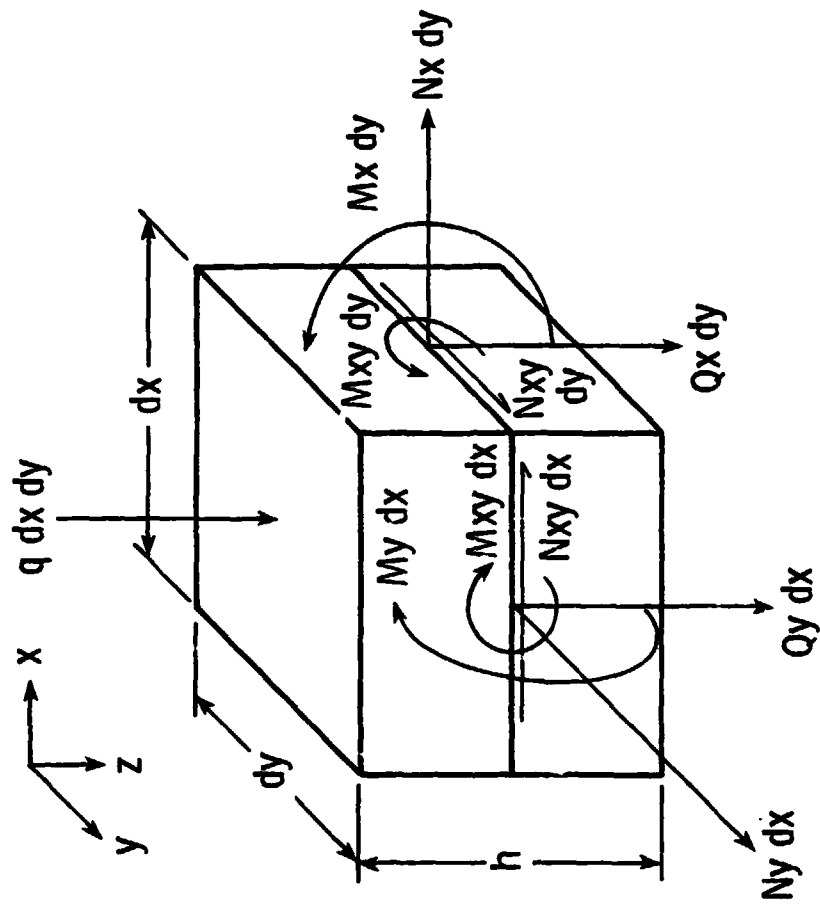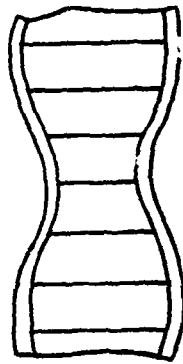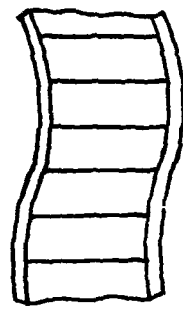
Figure 8.- Forces and moments acting on differential element dx dy.

131

INTRACELLULAR BUCKLING
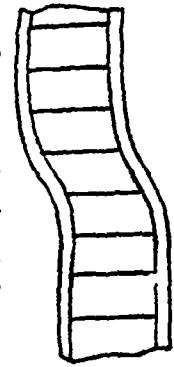
SYMMETRIC
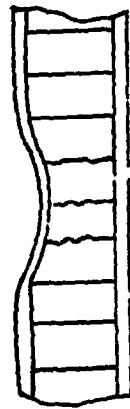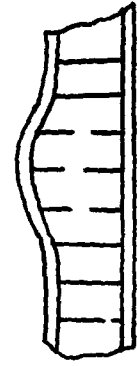
ANTISYMMETRIC

FACE WRINKLING

SHEAR CRIMPING

Figure 49.- Local instability modes of failure of honeycomb sandwich structures.

CORE CRUSHING

TENSILE CORE RUPTURE

TENSILE BOND RUPTURE

Figure 50.- Ultimate failures precipitated by face wrinkling of sandwich structures.

133